

Faculty of Science and Engineering

Western Australian School of Mines

Department of Mining Engineering

**Integration of Synthetic Aperture Radar Interferometry
(InSAR) and Geographical Information Systems (GIS) for
Monitoring Mining Induced Surface Deformations**

Hani Zahiri

This thesis is presented for the Degree of

Doctor of Philosophy

of

Curtin University

September 2012

This thesis is dedicated to my wife *Azadeh*, for her great forbearance, devotion, understanding and love.

Declaration

I, Hani Zahiri, declare that this thesis, submitted in fulfilment of the requirements for the award of Doctor of Philosophy, in the Western Australian School of Mines, Faculty of Science and Engineering, Curtin University of Technology, is wholly my own work unless otherwise referenced or acknowledged. The thesis was completed under the supervision of Dr A. Jarosz and has not been submitted for qualification at any other academic institution.

Signed: 

Date: 22/10/2012

The following publications co-authored by the candidate present issues covered in this thesis:

- Jarosz A., **Zahiri H.** and Sowter A., (2010), Utilisation of InSAR for monitoring of caving zone subsidence over perseverance mine in Western Australia, XIV Congress of the International Society for Mine Surveying, Sun City, South Africa, September 2010.
- Jarosz A. and **Zahiri H.**, (2008), Interferometric Synthetic Aperture Radar (InSAR) and its potential to monitor subsidence over caving zones induced by underground mining, First International Future Mining Conference, Sydney, Australia, November 2008.
- Jarosz A., **Zahiri H.**, Warren M. and Sowter A., (2007), Utilisation of InSAR for subsidence monitoring over the caving zone of underground metalliferous mine, Fifth International Workshop on ERS SAR Interferometry (Fringe), Frascati, Italy, November 2007.
- Jarosz A. and **Zahiri H.**, (2007), Integration of InSAR and GIS for monitoring of subsidence induced by block-cave Mining, International Federation of Surveyors (FIG) Working Week, Hong Kong, May 2007.

Acknowledgments

The author would like to express his sincere gratitude to Dr Andrew Jarosz for his invaluable supervision, support and encouragement provided during the course of this research. I also wish to specially thank Dr Andrew Sowter for his guidance and inspiration, in particular for his support during my stay in IESSG of University of Nottingham.

My thanks go to all of the staff and research students of the Western Australian School of Mines for their kind assistance. I am grateful to the BHP Billiton-Nickel West, Rio Tinto-Argyle Diamond Mines, European Space Agency, Australian National Earth Observation Group and Apogee Imaging International for providing data and technical support for this research.

I wish to express my appreciation to Mr. Shamim Babaii, Mr. Luis Machuca, Dr. Kelly Fleetwood, Mr. Dietrich Wanke and Dr. Mark Warren for their helpful assistance.

I also wish to thank my mom, dad, my sister and my grandmothers for all their love and supports.

Hani Zahiri

September 2012

Abstract

Surface subsidence induced by mining is a source of risk to people, equipment and environment. It may also disrupt mining schedules and increase the cost of mine safety. To provide accurate assessment of the surface subsidence and its level of impact on mine production and environment, it is necessary to develop and introduce comprehensive subsidence monitoring systems. Current techniques for monitoring of surface deformation are usually based on classical survey principles. In general these techniques have disadvantages that limit their applicability: they follow point-by-point data collection techniques, they are relatively time-consuming and costly, they usually cover only a small area, they are not applicable for the monitoring of inaccessible areas and they are not able to collect data continuously.

As a complementary or alternative technique, the thesis discusses the applicability of SAR interferometry for monitoring mining induced deformations. InSAR is a remote sensing technique that makes use of Synthetic Aperture Radar (SAR) observations to acquire change in terrain topography. In spite of the widespread application of the technique for monitoring large-scale deformations of the Earth crust, specific modifications are necessary for utilising the technology within a mining context. Limitations, such as difficulty to resolve deformation for a high gradient slope, difficulty to retrieve subsidence for localised highly dynamic ground movements and the unavailability of SAR images with the desired specifications restrict the potential to monitor high rate, localised mine subsidence on day-to-day basis.

The secondary aim of the thesis is to present integration of InSAR and GIS in order to propose an optimum methodology for processing of InSAR data to determine mine subsidence. The presented research also involves detailed analysis of InSAR limitations. This in consequence has led to suggestions on how to improve current InSAR capability with respect to the mining needs.

The thesis introduces a set of new GIS-based tools and methodologies that are integrated into a conventional InSAR processing technique, to further improve and

facilitate application of InSAR in mining. The developed tools and techniques cover the three main stages of data processing (pre-processing, processing and post-processing). The researcher tried to address InSAR's limitations associated with mining related applications and also to provide practical solutions to resolve these issues.

Table of Contents

Declaration	I
Acknowledgments	II
Abstract	III
Table of Contents	V
List of Figures	VIII
List of Tables	XIII
List of Abbreviations	XIV

Chapter 1 : General Introduction **1**

1.1. Underground Mining and Subsidence	1
1.1.1. Type of Subsidence Induced by Underground Mining	1
1.1.2. Longwall Underground Mining Method and Subsidence	3
1.1.3. Caving Underground Mining Methods and Subsidence	5
1.1.3.1 Block Caving Underground Mining Method	5
1.1.3.2. Sublevel Caving Underground Mining Method	7
1.1.3.3 Subsidence Prediction of Caving Underground Mining Methods	9
1.2. Subsidence Monitoring Techniques	10
1.3. Applicability of Interferometric Synthetic Aperture Radar (InSAR) and GIS for Monitoring Mining Induced Subsidence	11
1.4. Thesis Aims and Objectives	12

Chapter 2 : Subsidence Monitoring Techniques **17**

2.1. Total Station Surveys and Levelling	18
2.2. Global Positioning System (GPS) and Global Navigation Satellite System (GNSS)	19
2.3. Laser Techniques	21
2.4. Airborne Laser Scanning (ALS)	23
2.5. Photogrammetry	23
2.6. Slope Stability Radar (SSR)	24
2.7. Chapter Summary	25

Chapter 3 : SAR Interferometry Background **27**

3.1. History of Synthetic Aperture Radar Interferometry (InSAR)	27
3.1.1. Radar	27
3.1.2. Synthetic Aperture Radar	28
3.1.3. SAR Interferometry	31
3.1.4. Examples of InSAR Applications	33
3.1.4.1 Earthquake	33
3.1.4.2 Volcanic Activities	33
3.1.4.3 DEM Generation	34
3.1.4.4 Land Subsidence	34
3.1.4.5. Glacier and Ice Monitoring	35
3.1.5. InSAR and Mining	37
3.2. Principles of SAR Interferometry	40
3.2.1. What is SAR Imagery?	40
3.2.2. SAR Interferometry	44

3.3. InSAR Limitations	48
3.3.1. Limitations due to Phase Noise and Errors	48
3.3.1.1. Atmospheric Effects	48
3.3.1.2. Temporal Decorrelation	49
3.3.1.3. Phase Noise due to Different Look Angle	49
3.3.1.4. Phase Noise due to Volume Scattering	50
3.3.2. Geometry Related Limitations	50
3.3.2.1. Geometric Distortions (Layover, Shadow and Foreshortening)	50
3.3.2.2. Ambiguous Height	51
3.4. General InSAR Processing Steps	52
3.4.1. Data Selection	53
3.4.2. Coregistration	54
3.4.3. Interferogram Generation	54
3.4.4. Complex Multilooking	55
3.4.5. Generating Coherence Map	56
3.4.6. Phase Unwrapping	57
3.4.7. Phase to Height	57
3.4.8. Georeferencing	57
3.5. Chapter Summary	57
<u>Chapter 4 : Geographical Information Systems Background</u>	<u>59</u>
4.1. What is GIS?	59
4.2. What is Spatial Data?	60
4.3. GIS and Spatial Analysis	62
4.4. GIS, InSAR and Geoprocessing	63
4.5. Chapter Summary	64
<u>Chapter 5 : InSAR Toolbox for Mine Subsidence Monitoring</u>	<u>65</u>
5.1. What is InSAR Toolbox?	65
5.2. Pre-processing stage, considerations and tools	70
5.2.1. Layover Analysis	70
5.2.2. Effects of Using Current and Accurate DEM	74
5.2.3. Deformation Rate Analysis	76
5.2.4. Optimum Acquisitions Selection and Planning	79
5.2.5. Cartesian (XY) Coordinate to Pixel and Line Tool	84
5.3. Data Processing Stage	85
5.3.1. Data Input and Processing Steps Windows	88
5.3.2. Reading Master and Slave images	90
5.3.3. Extract Complex Data from Images	91
5.3.4. Create Multilooked Amplitude Image	91
5.3.5. Preparing DEM and Calculate Reference Phase	92
5.3.6. Coarse Co-registration	93
5.3.7. Fine Coregistration	94
5.3.8. Slave Image Resampling	94
5.3.9. Complex Interferogram Creation	94
5.3.10. Differential Interferogram Creation	95
5.3.11. Phase Unwrapping	96
5.3.12. Results Preparation	97
5.4. Post-processing Stage	98
5.4.1. Phase Trend Removal	99

5.4.2. Result Interpolation	100
5.4.3. Precise Georeferencing and Coordination Transformation	101
5.5. Chapter Summary	103
<u>Chapter 6 : Case Studies</u>	<u>105</u>
6.1. Perseverance- Leinster Nickel Mining Operation	105
6.1.1. Case Study Overview	105
6.1.1.1. Previous WASM Research Experience in Mining Application of InSAR	109
6.1.2. Deformation Rate	110
6.1.3. Data Selection	112
6.1.4. Layover Mask	114
6.1.5. Data Processing and Results	115
6.1.6. Comparison with Subsidence Analysis Using Classical Surveys	118
6.1.7. Mine Specific Deformation Analysis	120
6.1.7.1 Apparent Heave	120
6.1.7.2 Deformation Rates and the Issue of Ambiguity	121
6.2. Argyle Diamond Mines	127
6.2.1. Case Study Overview	127
6.2.2. Data Selection	128
6.2.3. Layover Analysis	130
6.2.4. Data Processing and Result	131
6.3. Ridgeway Underground Gold Mine – ALOS	133
6.3.1. Case Study Overview	133
6.3.2. Data Selection	135
6.3.3. Data Processing and Results	136
6.4. Ridgeway Underground Gold Mine – TerraSAR-X	141
6.5. Discussion and Summary	143
6.6. Chapter Summary	146
<u>Chapter 7 : Conclusions and Recommendations</u>	<u>147</u>
7.1. Summary	147
7.2. Results and Developed Tools	153
7.2.1. InSAR and Mining	153
7.2.2. InSAR Toolbox	157
7.3. Recommendations for Future Research Projects	159
<u>Chapter 8: References</u>	<u>161</u>

List of Figures

Figure 1.1: Classification of underground mining methods.....	2
Figure 1.2: Types of subsidence.....	2
Figure 1.3: Schematic of a typical longwall mine.....	3
Figure 1.4: Cross-section of longwall mine subsidence	4
Figure 1.5: Ground movements around a longwall extraction	4
Figure 1.6: Block caving mining	6
Figure 1.7: Ground movement induced by block caving	7
Figure 1.8: Sublevel caving mining	8
Figure 1.9: Ground movement induced by sublevel caving mining	8
Figure 1.10: Progressive failure sequence with increasing mining depth; (a) mining from outcrop; (b) failure of overhanging wedge; (c) formation of steep face; (d) development of tension crack and failure surface; (e) development of second tension crack and failure surface; (f) initial open pit; (g) formation of tension crack and failure surface; (h) second tension crack and failure surface; (i) progressive failure with increase in mining depth	9
Figure 2.1: a) Simple illustration of levelling , b) Levels	19
Figure 2.2: Rover and base station receivers for RTK	21
Figure 2.3: Laser scanning results for La Coipa mine open pit mine, Chile.....	22
Figure 2.4: SSR equipments	24
Figure 3.1: Interferogram from Lander earthquake	32
Figure 3.2: SAR Imagery System	41
Figure 3.3: Target location in a SAR image, intersection of the range sphere, Doppler cone and phase cone	42
Figure 3.4: Sample of a SLC-SAR image acquired from Argyle Diamond Mine, WA, Australia.....	43
Figure 3.5: Geometry of acquisitions for InSAR processing. S1 and S2 are the 2 satellite positions, B the baseline, R1 and R2 the ranges to target T and $B \perp$ the perpendicular baseline.....	44
Figure 3.6: Geometry of InSAR with non-zero baseline	46
Figure 3.7: Geometric distortions, foreshortening (A), layover (B) and shadow (C)	50
Figure 3.8: Layover points (A, B and C) will fall into the same cell of the SAR image	51

Figure 3.9: Wrapped phase (a) and unwrapped phase (b).....	52
Figure 3.10: General procedure for InSAR implementation.....	53
Figure 3.11: Sample of a phase interferogram resulted from differential SAR interferometry for Perseverance Mine, WA, Australia	55
Figure 3.12: Coherence map over Ridgeway gold mine, NSW, Australia, generated from two ALOS images with temporal baseline of 44 days	56
Figure 4.1: Positional data in raster and vector format	61
Figure 4.2: Raster and vector format	62
Figure 5.1: Snapshot of InSAR Toolbox in ArcGIS Desktop.....	67
Figure 5.2: Snapshot of PythonWin IDE and necessary imported bindings.....	69
Figure 5.3: Height profile across the pit indicating the layover scenario.....	71
Figure 5.4: Estimating the layover from the DEM postings	72
Figure 5.5: Input data window for distortion tool	73
Figure 5.6: A slant range SAR image of Perseverance mine (left) and with layover area highlighted in red (right).....	73
Figure 5.7: DEM modification tool.....	75
Figure 5.8: The results of Terrain Correction (left) and Layover Masking (right) using the SRTM DEM for the Argyle Diamond Mines.....	76
Figure 5.9: A georeferenced SAR image of Argyle Diamond Mines (left) and with layover area highlighted in red (right) using current DEM.....	76
Figure 5.10: Reference grid used in deformation rate analysis tool.....	78
Figure 5.11: Input window for deformation rate tool.....	79
Figure 5.12: Deformation rate analysis result for Perseverance mine generated by deformation rate tool.....	79
Figure 5.13: Data input window for XYtoPL tool	85
Figure 5.14: Snapshot of result window of XYtoPL_ALOS tool.....	85
Figure 5.15: Interferometry processing chain	87
Figure 5.16: InSAR data input windows for ALOS data	89
Figure 5.17: Processing steps selection window	89
Figure 5.18: Simple illustration of a SAR image data file	91

Figure 5.19: Multilooked amplitude image created for Ridgeway Gold Mine, NSW, Australia	92
Figure 5.20: Multilooked coherence images generated from two TerraSAR-X spotlights images with 11 days temporal baseline, over the Cadia hill pit, NSW, Australia	95
Figure 5.21: Multilooked differential interferogram generated from two TerraSAR-X spotlights images with 11 days temporal baseline, over the Cadia hill pit, NSW, Australia	96
Figure 5.22: Subsidence detected by InSAR for two ALOS PALSAR images with almost one year (368 days) temporal baseline, Ridgeway Gold Mine, NSW, Australia.....	98
Figure 5.23: Unwrapped phase image generated using two ERS2 SAR images over the Leinster area, WA, Australia, a) before trend removal b) after trend removal	100
Figure 5.24: Snapshots of Geostatistical analyst performing local polynomial interpolation of sample InSAR results.....	101
Figure 5.25: Project raster tool.....	102
Figure 5.26: Sample InSAR result georeferencing process performed using georeferencing toolbar	103
Figure 6.1: Location of Leinster Mining Operation and Perseverance open pit and underground operations	106
Figure 6.2: Surface deformation over Perseverance open pit between 1995 and 2006 (Black dash line: boundary of the pit in 1995) and caving profile in 2000	107
Figure 6.3: Deformation detected by InSAR generated by previous study over the perseverance open pit	109
Figure 6.4: Deformation rate analysis results for Perseverance mine generated by deformation rate tool in case using ERS (C-band).....	110
Figure 6.5: Deformation rate analysis results for Perseverance mine generated by deformation rate tool in case using ALOS-PALSAR data (L-band).....	111
Figure 6.6: Deformation rate analysis results for Perseverance mine generated by deformation rate tool in case using TerraSAR-X data (X-band).....	111
Figure 6.7: A slant range SAR image of Perseverance mine (left) and with layover area highlighted in red (right).....	115
Figure 6.8: A geocoded SAR image of Perseverance mine (left) and with layover area highlighted in red (right).....	115
Figure 6.9: Subsidence detected by InSAR over Perseverance mine for pair 41554-40552 with 70 days temporal baseline	117
Figure 6.10: Slope stability monitoring stations over the area of study.....	119
Figure 6.11: Vertical movement detected by classical surveys between the dates of processed SAR acquisitions (41554-40552).....	119

Figure 6.12: Set of GPS monitoring stations used for comparative analysis	120
Figure 6.13: Apparent heave of the ground.....	121
Figure 6.14: Location of reference areas over 1995 DTM.....	123
Figure 6.15: Subsidence between 2001-2003 derived from topo surveys for Perseverance mine.....	124
Figure 6.16: Subsidence between 2001-2006 derived from topo surveys for Perseverance mine.....	124
Figure 6.17: Subsidence along A-B cross-section referenced to 2001 DTM.....	125
Figure 6.18: Development of subsidence between 2001 and 2006 calculated based on available DTMs,.....	126
Figure 6.19: Equivalent subsidence rate in the period 2003-2004 along the profile A-B calculated based on available DTMs (from the point A to the edge of pit's crest; temporal baseline of 318 days).....	126
Figure 6.20: Location of Argyle Diamond Mines	127
Figure 6.21: Height profile across the pit indicating the layover scenario.....	130
Figure 6.22: A slant range SAR image of Argyle (left) and with layover areas highlighted in red (right)	131
Figure 6.23: A geocoded SAR image of Argyle (left) and with layover area highlighted in red (right)	131
Figure 6.24: Deformation detected by InSAR for pairs with temporal baseline 35 days	132
Figure 6.25: Interpolated contour map of deformation (subsidence) detected by InSAR....	132
Figure 6.26: Location of Ridgeway underground operation	134
Figure 6.27: Ridgeway and Cadia hill operations and location of subsidence cater above caving zone	134
Figure 6.28: Amplitude images generated for the first processed pair, describing subsidence crater and surrounding area.....	136
Figure 6.29: a) Deformation detected by InSAR over Ridgeway operation for period of 46 days between 02/11/07 and 18/12/07, b) Coherence image for subsidence crater.....	137
Figure 6.30: Amplitude images generated for images 18/12/07 and 02/02/08, describing subsidence crater and surrounding area	137
Figure 6.31: a) Deformation detected by InSAR over Ridgeway operation for period of 92 days between 18/12/07 and 02/02/08, b) Coherence image for subsidence crater.....	138
Figure 6.32: Amplitude images generated for images 02/11/07 and 02/02/08, describing subsidence crater and surrounding area	138
Figure 6.33: a) Deformation detected by InSAR over Ridgeway operation for period of 46 days between 02/11/07 and 02/02/08, b) Coherence image for subsidence crater.....	139

Figure 6.34: Coherence and deformation images produced by InSAR toolbox over Ridgeway and Cadia hill operations for period of 46 days between 21/05/06 and 06/07/08.....	140
Figure 6.35: Coherence and deformation images produced by InSAR toolbox over Ridgeway and Cadia hill operations for period of 368 days between 01/01/07 and 04/01/08.....	140
Figure 6.36: Coherence and deformation images produced by InSAR toolbox over Ridgeway and Cadia hill operations for period of 46 days between 04/01/08 and 19/02/08.....	140
Figure 6.37: Amplitude images generated for TerraSAR-X image 03/10/08	141
Figure 6.38: Coherence and deformation images produced by InSAR toolbox using TerraSAR-X data over Ridgeway and Cadia hill operations for period of 11 days between 03/10/08 and 14/10/08	142
Figure 6.39: Coherence and deformation images produced by InSAR toolbox using TerraSAR-X data over Ridgeway and Cadia hill operations for period of 11 days between 14/10/08 and 25/10/08	142

List of Tables

Table 2.1: Overview of methods used in measuring surface displacements	17
Table 3.1: Wavelengths of the signals in the microwave spectrum	27
Table 3.2: List of satellite SAR missions and their specifications	31
Table 3.3: InSAR application for mine subsidence monitoring (summary of presented case studies)	40
Table 5.1: Number of SAR images acquired by ERS 1-2 and Envisat missions over Western Australia, New South Wales and Western Europe, till end of Oct. 2008	82
Table 6.1: Available SAR scenes	112
Table 6.2: Orbital baselines of all pairs (m)	113
Table 6.3: Doppler Centroid separations for all pairs (Hz)	113
Table 6.4: Temporal baselines of all pairs (days)	114
Table 6.5: Description of the three acceptable pairs	114
Table 6.6: Monitored deformation by InSAR vs GPS (over 70 days)	120
Table 6.7: Digital terrain models	122
Table 6.8: Average elevations and elevation differences for reference areas (m)	122
Table 6.9: Planned SAR images	129
Table 6.10: Possible pairs for interferogram generation using the available SAR images ..	129
Table 6.11: Geometric and Temporal baseline for selected pairs	135
Table 7.2: Price list for SLC SAR images	156

List of Abbreviations

ALS:	Airborne Laser Scanning
ASAR:	Advanced Synthetic Aperture Radar
ASI:	Agenzia Spaziale Italiana
BEM:	Boundary Element Method
CEOS:	Committee on Earth Observation Satellites
DEM:	Digital Elevation Model
DGPS:	Differential Global Positioning System
DInSAR:	Differential SAR interferometry
DLR:	German Aerospace Centre
DTM:	Digital Terrain Model
DXF:	Drawing Exchange Format
EDM:	Electronic Distance Metres
EOLi:	Earth Observation Link
ESA:	European Space Agency
ESRI:	Environmental Systems Research Institute
FDM:	Finite Difference Method
FEM:	Finite Elements Method
GBAS:	Ground Based Augmentation System
GDAL:	Geospatial Data Abstraction Library
GIS:	Geographical Information Systems
GNSS:	Global Navigation Satellite System
GPS:	Global Positioning System
GUI:	Graphical User Interface
IDE:	Integrated Development Environment
IMU:	Inertial Measurement Unit
InSAR:	Interferometric Synthetic Aperture Radar
IESSG:	Institute of Engineering Surveying and Space Geodesy
JERS:	Japanese Earth-Resources Satellite
JPL:	NASA/Jet Propulsion Laboratory
LiDAR:	Light Detection and Ranging
LOS:	Line of Sight
MRMR:	Mining Rock Mass Rating
mtpa:	Million tons per annum

PSI:	Persistence Scatterers Interferometry
RMS:	Root Mean Square
RTK:	Real Time Kinematic
SAR:	Synthetic Aperture Radar
SLC:	Single Look Complex
SRTM:	Shuttle Radar Topography Mission
SSR:	Slope Stability Radar
UTM:	Universal Traverse Mercator
WASM:	Western Australian School of Mine

Chapter 1

General Introduction

Chapter 1

General Introduction

1.1. Underground Mining and Subsidence

Surface subsidence due to underground mining could be a source of risk for people, equipment and environment. It may also disrupt mining production, increasing its cost and impact on mine safety; therefore it is always of major concern to the mining industry. As defined by Soliman (1998), subsidence is “a natural and man-made phenomenon associated with a variety of processes including compaction of natural sediments, ground water dewatering, wetting, melting of permafrost, liquefaction and crustal deformation, withdrawal of petroleum and geothermal fluids, and the mining of coal, limestone, salt, sulphur and metallic ores”. Subsidence is an inevitable consequence of underground mining that may be small and localized or extended over large areas; also, it may be immediate or delayed for many years (Hartman, 1992).

The first formal studies of subsidence in 19th century were mostly focused on the coal mining and its impacts on overlying infrastructures or railways. These early attempts provided the main foundation of extensive future studies (Villegas, 2008). Today, studies of subsidence include structural geology, geomechanics, surveying, mining and property law and also mining engineering (Hartman, 1992).

1.1.1. Type of Subsidence Induced by Underground Mining

Different forms of underground mining (Figure 1.1) may produce different shapes and extent of surface subsidence (Figure 1.2), however as a general classification, subsidence can be categorised into two types of continuous and discontinuous subsidence. Continuous subsidence is characterised by lowering of the surface producing a smooth subsidence profile. In contrast, discontinuous type of subsidence may result in large vertical surface subsidence, discontinuities or even surface collapse over the affected zone (Brown, 2003).

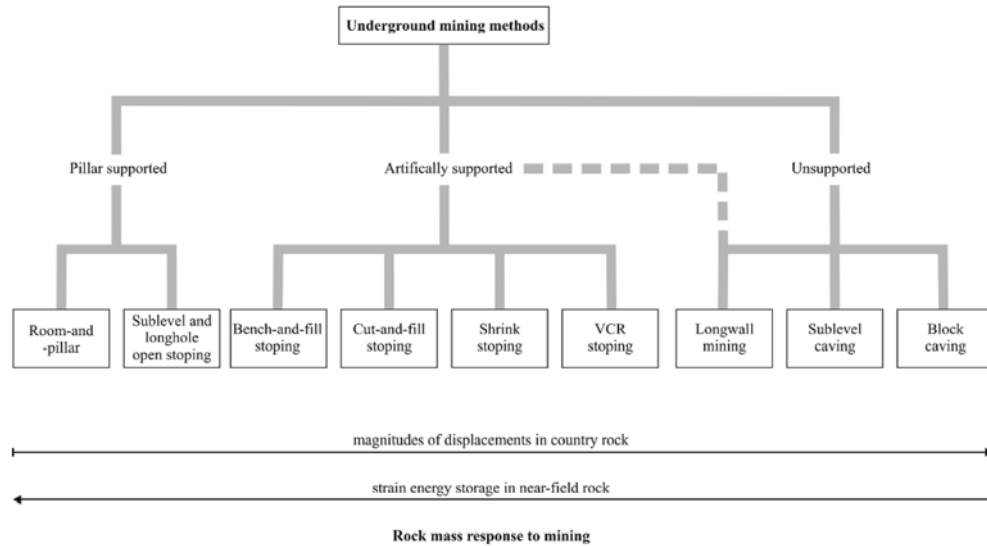


Figure 1.1: Classification of underground mining methods (Brady and Brown, 1993)

In case of continuous subsidence, ground displacement usually follows a trough shape pattern. Continuous subsidence is the most common type of subsidence induced by longwall underground mining method. Discontinuous subsidence, which is more associated with caving underground mining methods, can be seen as cracks, steps, chimney or sinkholes (Villegas, 2008). Furthermore and in the case of presence of a pre-existing open cut, the progression of subsidence may cause instability of pit slopes (Owen, 1981).

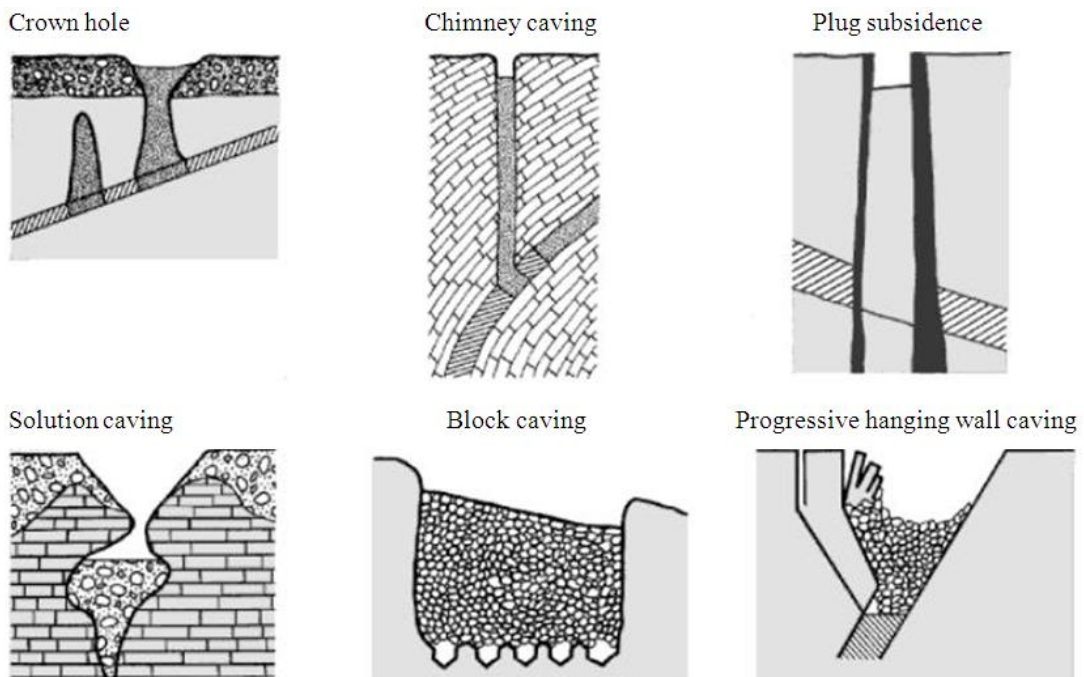


Figure 1.2: Types of subsidence (Brady and Brown, 1993)

1.1.2. Longwall Underground Mining Method and Subsidence

Longwall mining is most suitable for seam type of deposits with large horizontal extent and almost uniform thickness; coal seams or potash layers for instance. As shown in Figure 1.3, development of longwall mines usually results in dividing the deposit into rectangular panels that involves the excavation of a network of haulage drifts for access to ore body and transport of ore to main. The method extracts ore along a straight front having a large longitudinal extension. When working face advances the goaf behind the working face may be allowed to cave at some distance that results in surface subsidence (Hamrin, 2001). Long working front, the large area worked at the time and the rapid extraction are main characteristics of longwall mining (Kratzsch, 1983).

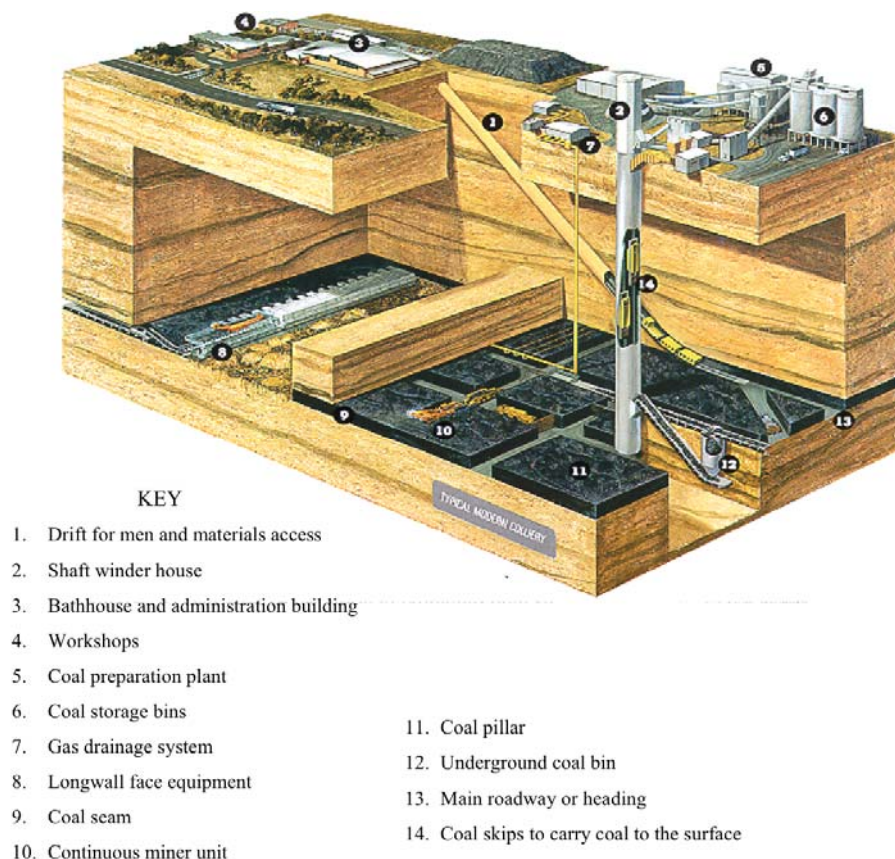


Figure 1.3: Schematic of a typical longwall mine (MSE, 2007)

As mentioned before, ground displacement in longwall mining usually follows a trough shape pattern, which is the result of redistribution of strata pressure around the longwall panels ahead of an advancing mine face (Figure 1.4). Based on Nesbitt

(2003), different factors can affect size and geometry of continuous subsidence induced by longwall underground mining including: depth of cover, overlying strata properties, seam thickness, panel width, chain pillar size, and surface topography.

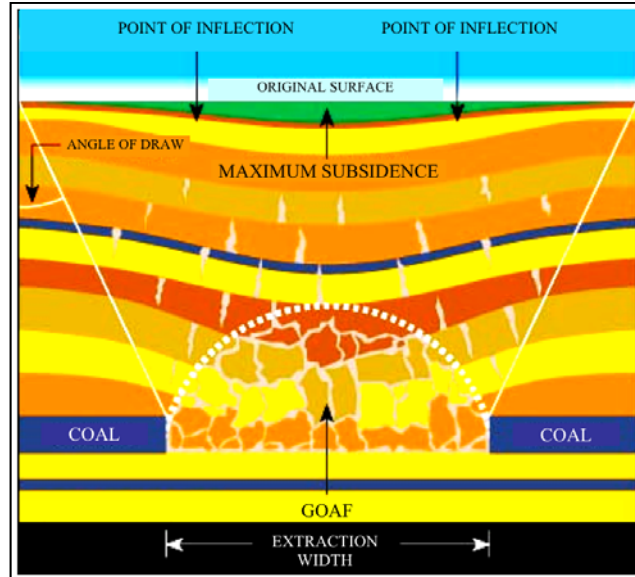


Figure 1.4: Cross-section of longwall mine subsidence (Ecological Australia, 2004)

As illustrated in Figure 1.5, the basic indexes that define a surface subsidence trough are:

- vertical displacement,
- horizontal displacement,
- tilt or slope (differential subsidence),
- horizontal strain (extension and compression) and
- vertical curvature (differential tilt) (Villegas, 2008).

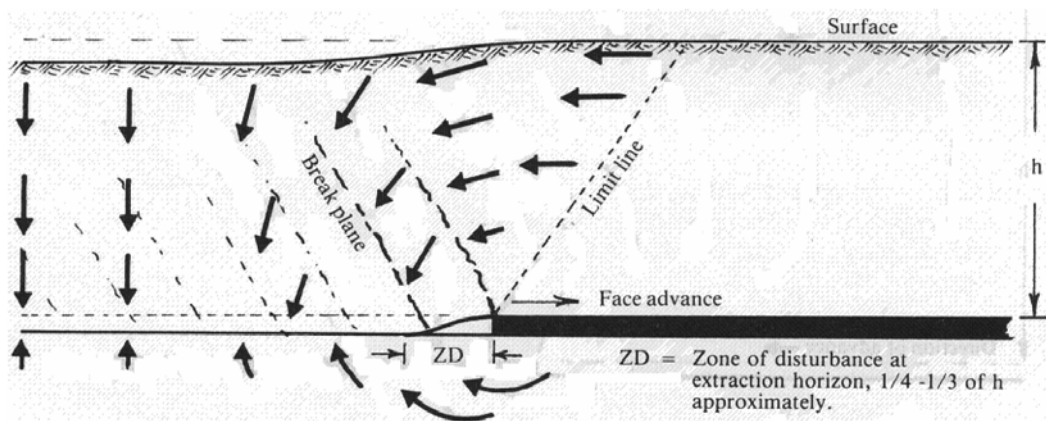


Figure 1.5: Ground movements around a longwall extraction (Whittaker and Reddish, 1989)

Trough subsidence is characterized by its high degree of predictability of movements perpendicular and parallel to the direction of face advance (Bell and Donnelly, 2006). Most conventional methods used for subsidence prediction induced by longwall mining can be listed as following (Villegas, 2008):

- Empirical methods that use existing surface movement data and fit them to subsidence functions in order to predict future subsidence effects.
- Semi-empirical methods:
 - ✓ Profile functions method that uses mathematical expression of subsidence profile.
 - ✓ Influence functions method that uses influence functions based on the principle of superposition.
- Analytical methods such as the Finite Elements Method (FEM), the Finite Difference Method (FDM) and the Boundary Element Method (BEM).

1.1.3. Caving Underground Mining Methods and Subsidence

The trend seen recently is that numerous mines are transferring from surface mining to underground mining within Western Australia and around the world. Mining companies intending to increase life time of their mines and caving methods, such as block caving or sublevel caving, can offer less costly and more efficient mining options; consequently, caving underground mining methods are becoming more and more popular. Considering this fact, subsidence resulting from caving underground mining methods was decided to be the primary focus of this thesis.

1.1.3.1 Block Caving Underground Mining Method

Block caving is a large-scale production underground mining method, which is most suitable for low-grade, massive ore bodies with large vertical and horizontal dimensions. The main objective in this method is to use internal rock stresses with the help of gravity to fracture and break the ore body into pieces. The broken ore, then, is handled out from designed drawpoints while the overlying rock caves in progressively (Hamrin, 2001). As shown in Figure 1.6, the method requires intensive

preparation that involves excavating shafts, haulage tunnel, access drifts that divide ore body into large sections (blocks) and the development of several drawpoints; however block caving method has the lowest mining costs of all underground mining methods.

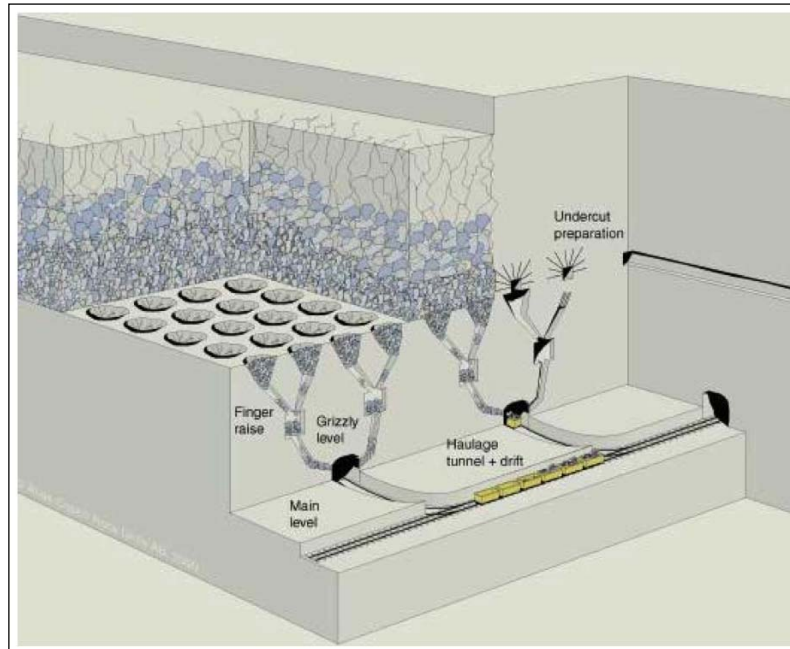


Figure 1.6: Block caving mining (Hamrin, 2001)

Block caving produces discontinuous type of subsidence. Well-defined geological cut-off between ore body and the host rock is one of the main conditions that makes the block caving method applicable to the deposit. This results in propagation of the cave vertically to surface with inclined surface slopes forming in surface layers (Brown, 2003). Considering the above, chimneys and tension cracks are the most common type of surface deformation associated with block caving. As described by Figure 1.7, three main zones are visible in subsidence induced by block caving (Gilbride et al, 2005):

- Primary subsidence zone characterised by massive movement, ten to hundreds of meters. This zone is usually visible as a crater.
- Transition zone characterised by vertical scarps or steps and tension cracks.
- Continuous deformation zone characterised by continuous, moderate ground movement.

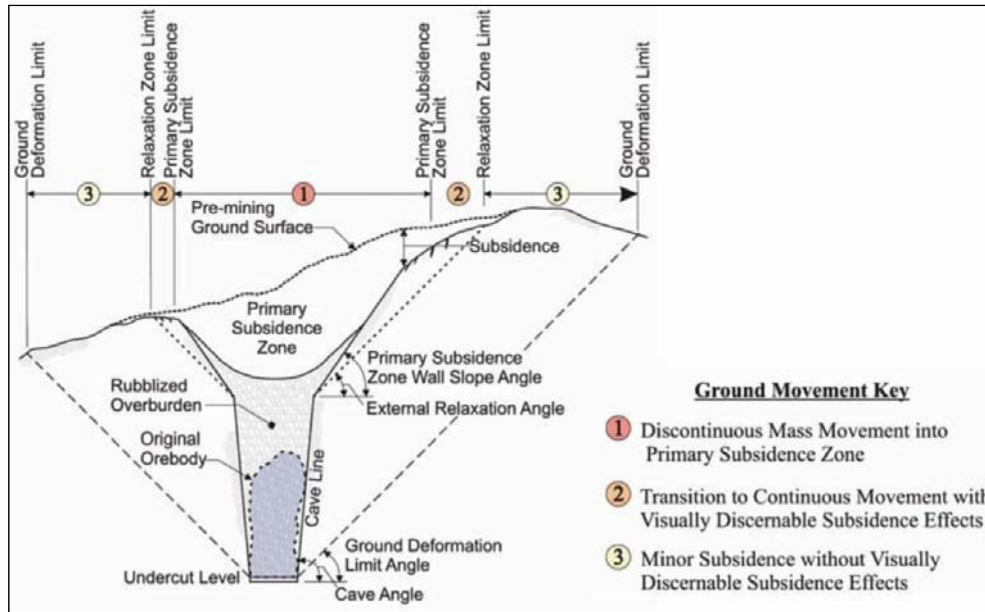


Figure 1.7: Ground movement induced by block caving (Gilbride et al, 2005)

According to Brown (2003), a number of factors that may influence the shape and extent of the ground deformation resulting from block caving can be summarised as following:

- The dip of the ore body,
- the shape of the ore body in plan,
- the depth of mining and associated in situ stress field,
- the strengths of both the caving rock mass and different rock and soil layers above it,
- the slope of the ground surface,
- major geological features such as faults and dykes,
- prior surface mining,
- the placement of fill in a pre-existing or newly produced crater, and
- existing underground or open cut mining.

1.1.3.2. Sublevel Caving Underground Mining Method

Sublevel caving method (SLC) is a bulk mining method most suitable for large, steeply dipping ore bodies (Hamrin, 2001). The method involves the development of several drifts and cross-cuts, parallel and perpendicular to the ore body, at regular spacing. The broken ore is drawn at the brow of the cross-cut by the effect of gravity and hauled to the haulage level where it is transported to the surface (Figure 1.8).

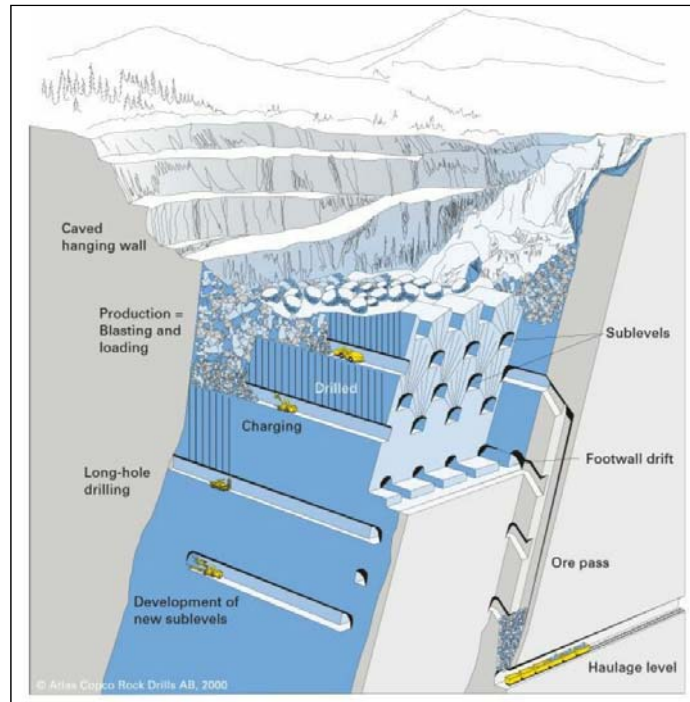


Figure 1.8: Sublevel caving mining (Hamrin, 2001)

Sublevel caving develops a large-scale surface subsidence over hangingwall, and also footwall (Figure 1.9). Subsidence over hangingwall can be described in three different zones (Villegas, 2008):

- The caved zone characterised by massive downward movement formed by collapse of the sidewalls.
- The fractured zone characterised by tension cracks, fractures, steps and scattered pits near to the caved zone.
- The zone of continuous deformation.

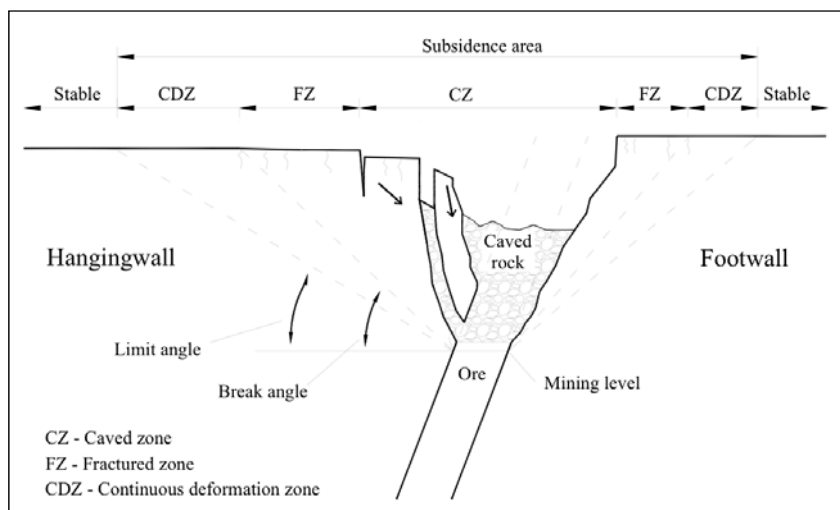


Figure 1.9: Ground movement induced by sublevel caving mining (Villegas, 2008)

1.1.3.3 Subsidence Prediction of Caving Underground Mining Methods

Different methodologies, almost similar in block caving or sublevel caving, are used for prediction of subsidence resulting from these methods. Current approaches for assessing surface subsidence include empirical, analytical or numerical methods. An example for an empirical method is Laubscher's method. This method is based on a design chart that relates the predicted cave angle to the MRMR (Mining Rock Mass Rating), density of the caved rock, height of the caved rock and mine geometry (Laubscher, 2000). As an example of an analytical method, limit equilibrium is the most commonly used technique which is based on analysis of surface cracking associated with sublevel caving of an inclined ore body (Figure 1.10, (Hoek, 1974)). Numerical methods involve modelling of the ground strains and tilts using two or three-dimensional codes such as ABACUS or FLAC.

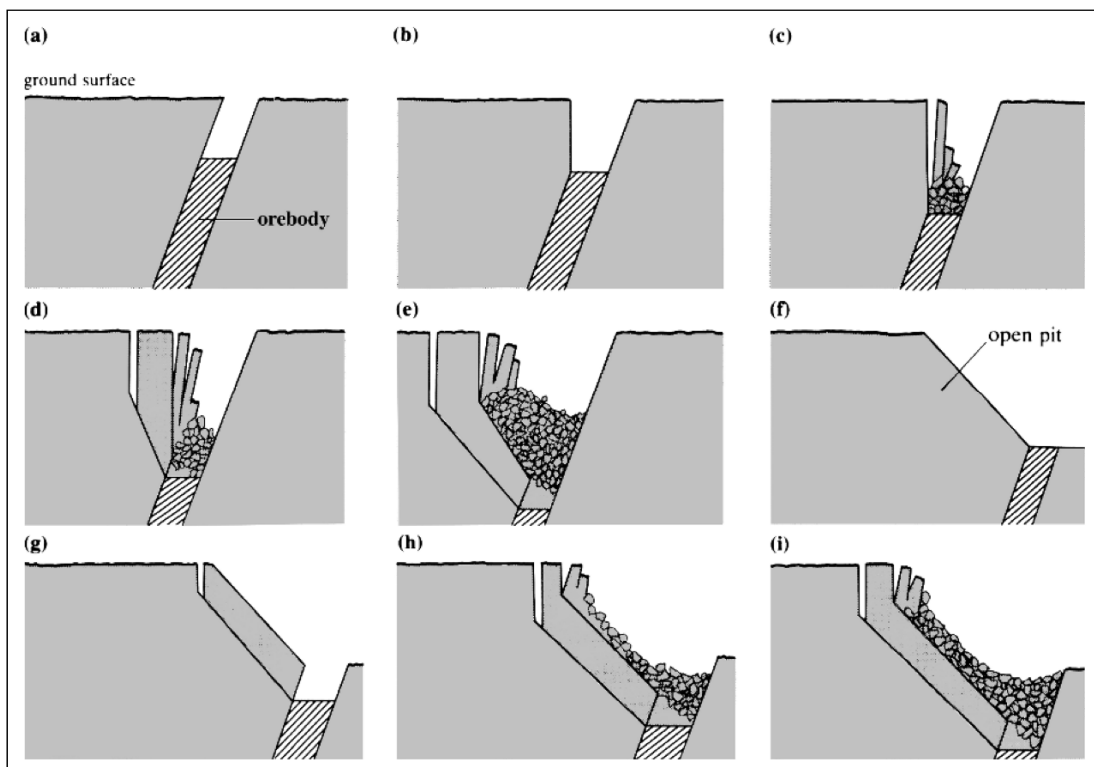


Figure 1.10: Progressive failure sequence with increasing mining depth; (a) mining from outcrop; (b) failure of overhanging wedge; (c) formation of steep face; (d) development of tension crack and failure surface; (e) development of second tension crack and failure surface; (f) initial open pit; (g) formation of tension crack and failure surface; (h) second tension crack and failure surface; (i) progressive failure with increase in mining depth (Hoek, 1974)

1.2. Subsidence Monitoring Techniques

A comprehensive knowledge of the mechanisms associated with rock strata deformation is crucial for any mining activity. Despite the considerable efforts to improve current techniques or development of new techniques and methodologies, it is almost impossible to achieve an advance accurate assessment of location, development rate, final extent of the surface subsidence and in particular the level of its impact on mine production and environment. Therefore, the development and installation of comprehensive subsidence monitoring systems, capable of collecting accurate displacement data over the area affected by mining and the development of deformation models as excavation progresses is vital for any underground operation. This is of particular importance for planning, as the impact of induced subsidence on the surface and surrounding infrastructure needs to be understood, to allow for a management program (and risk mitigation) to be developed and implemented. Furthermore, this monitoring information is also necessary for other reasons such as (Brown, 2003):

- Definition of exclusion zones above and around the subsidence zone both on the surface and underground due to safety regulations,
- Giving warning of the potential impact of subsidence on surface installations and infrastructure, and
- Monitoring the stability of overlying or nearby open pit slopes.

Current techniques for monitoring surface deformation are usually based on classical surveying principles. Automatic or digital levels (levelling), total stations and GPS receivers are the most widely used instruments for monitoring subsidence in both open cut or underground mining operations (Schofield and Breach, 2007). For monitoring surface deformation, mining companies also use techniques such as photogrammetry and Airborne Laser Scanning (ALS). Current techniques can deliver different level of accuracy and coverage, which will be discussed in Chapter 2.

In general, the current techniques have notable disadvantages that limit their applicability, particularly in terms of coverage, repeatability, risk and accuracy. They follow point-by-point data collection techniques and therefore are relatively time-

consuming and costly. Surveys usually cover only a small area and produce much localised information. Furthermore, classical techniques are not applicable for the monitoring of inaccessible areas and since monitoring points are not close enough, they are not able to provide a reliable interpolation of data (Ge et al., 2004). Considering this, there is increasing demand to design and utilise cost-efficient supplementary or alternative techniques with the capability to deliver continuous coverage and accuracies, comparable or exceeding that of classical surveys. Recent extensive developments of remote sensing technologies and improvement of Geographical Information Systems (GIS) may suggest practical individual and integrated solutions to this demand.

1.3. Applicability of Interferometric Synthetic Aperture Radar (InSAR) and GIS for Monitoring Mining Induced Subsidence

As an almost new remote sensing technology, basically developed for detecting large-scale surface deformation, Interferometric Synthetic Aperture Radar (InSAR) can also be used for the monitoring of mine subsidence. By using this technique a localised surface subsidence may be monitored up to sub-centimetre accuracy. InSAR does not require any field instrumentation and consequently allows for monitoring of hazardous and inaccessible areas. InSAR uses radar signals and so it is able to work under different atmospheric conditions. A Geographical Information System (GIS) or any other spatial processing software can further process the InSAR results, which can be utilised to provide a valuable calibration tool for rock strata deformation models. Taking the above into consideration, utilisation of the InSAR technique significantly reduces the costs of the monitoring and interpretation process (Jarosz and Wanke, 2004b).

In spite of the wide application of the InSAR technique for monitoring of large-scale deformations of the Earth's crust, specific modifications are necessary to utilise the technology in a mining context. Limitations, such as difficulty to resolve deformation for a high gradient slope, difficulty to retrieve subsidence for localised highly dynamic ground movements and the unavailability of SAR images with the

desired specifications, restrict the potential to monitor high rate, localised mine subsidence on day-to-day basis (Wegmüller et al., 2005).

GIS functionalities can be used to develop a wide range of tools to enhance InSAR capabilities. It can be utilised to pre-examine mining area in order to assess applicability of InSAR, as well as, providing tools for development of an optimum methodology for data acquisitions and processing. GIS can be also used for post-process, interpreting and assimilating disparate InSAR results. GIS also has the ability to combine different spatial datasets and to uncover and estimate the spatial relationships between them by providing a range of models (Zahiri and Baafi, 2008); this capability will be used for validating InSAR results and integrating them with other available collected data from the mine, such as classical surveying, geology and mining progress data. It may reveal and model possible relationships between different data sets and lead to better understanding of subsidence mechanism.

1.4. Thesis Aims and Objectives

The primary aim of the presented research is to propose an optimum methodology for the application of InSAR to monitor mine subsidence. The research also involved detailed analysis of InSAR limitations that led to suggestions to improve current InSAR capability with respect to the mining needs and the characteristics of mining induced deformation.

GIS functionalities were integrated to InSAR processing steps and used in different parts of the proposed methodology. GIS capabilities can be used to analyse geometry of the mine site, review the available historical data and to provide better assessment of InSAR applicability for each case study including optimum planning for data acquisitions. The proposed methodology also utilises GIS as a powerful environment to develop a set of tools easing the data processing steps and also allowing for InSAR result validation, management and presentation. The key objectives of the research can be summarised as follows:

- To improve current InSAR capability and provide insights about application of InSAR remote sensing techniques for monitoring of mining induced surface subsidence.
- To propose guidelines for mining related InSAR applications, in particular in areas with existing open pit mine characterised by deep and steep slopes; and
- To link the InSAR process with GIS and use GIS capability for InSAR feasibility studies. GIS could be used during and after InSAR processing in order to post-process, validate and interpret InSAR results.

Still there is a long way to go before finding a proper answer to the critical question “If InSAR can practically be used in mining? Where? and How?”; however this research along with other studies, carried out around the world, aims to address InSAR limitations associated with mining related applications and provide practical solutions to deal with them. Some of these studies attempt to modify the technique, taking specifications of mining-induced deformations into account; and some studies focus on dealing with InSAR limitations. This current attempt takes both of these approaches into consideration. Using GIS functionalities, InSAR process can be facilitated; result validation can be improved; integration with other methods can be eased and also more practical results can be generated. In addition, new GIS-based tools can be developed in order to detect InSAR limitations and to determine their level of influence on the produced results. The objectives of producing such tools can be summarized into three main aspects:

1. Providing a mining-oriented methodology for InSAR:

All InSAR applications must follow almost the same processing steps, however each case calls for special care considering different types of input data, data validation or expected outputs. Taking the needs of a mining-related InSAR application into account and also InSAR limitations itself, the research tried to address these issues, provide practical solutions to deal with them and implement them into InSAR processing steps. It suggests a set of advices or practical tools to select

generate or improve quality of input data as well as generating value-added output data in any given format.

2. Proving a simple and user-friendly environment to run InSAR processing steps:

The SAR interferometry by itself is complicated and consequently InSAR processing software has a high level of complexity that requires a relatively long time in order to be understood and mastered. Several open-source or commercial software dedicated to the SAR interferometry are available and offer different levels of complexity. This was one of the objectives of the thesis: to create an environment capable of performing SAR interferometry with a reasonable level of complexity suitable for ordinary users. Using a GIS environment makes it possible to easily manage and run InSAR processing steps by using tools developed in the geoprocessing framework and also employing GIS functionalities before, during and after processing.

3. Integrating InSAR and GIS in order to propose an optimum data processing methodology:

Integrating GIS capabilities into interferometry data processing can be very advantageous; however none of the previous InSAR studies highly involved GIS or were directly performed using a GIS-based approach. Many valuable tools can be generated using geoprocessing to ease the interferometry process. GIS can be involved in feasibility and data selection studies. It can also be used as a value-adding tool and its functionalities will be employed to post-process, interpret and assimilate disparate InSAR results. GIS provides a powerful environment for comparing and integrating InSAR results with other available data at the mine, including: classical surveying, geology and mining progress data. Despite the variety of InSAR processing software, only a few of them include options or provide tools to conveniently integrate the InSAR process and its results with a GIS environment. The thesis introduced a set of new GIS-based tools and methodologies for InSAR application in mining, covering three main stages of pre-processing, data processing

and post-processing. For the first time and through this research, it was possible to implement all InSAR data processing steps inside the ArcGIS Desktop environment. The InSAR module was developed as a tool inside ArcToolbox of ArcGIS desktop as one of the most popular GIS software used by the mining industry.

Chapter 2

Subsidence Monitoring Techniques

Chapter 2

Subsidence Monitoring Techniques

The main objective of any subsidence monitoring system is to detect surface movement, its magnitude and extent. Data collected using such systems is also crucial as it can be used in order to define the relationship between vertical and horizontal movements, determination of influence of time and also to monitor and predict surface damage induced by surface subsidence (Forrester and Aston, 1987).

Historically, a variety of surveying techniques have been used to monitor mine subsidence. Tapes and wire devices have been used to measure changes in distance between points or crack walls (Gulla et al., 1988). Levels, theodolites, electronic distance metres (EDM) and total station made it possible to measure both the coordinates and changes of target and control points together (Ashkenazi et al., 1980). Aerial or terrestrial photogrammetry is used to determine point coordinates, contour maps, cross-sections of the deformation and also the movement vectors (Chandler and Moore, 1989; Oka, 1998). Table 2.1 provides an overview of methods used in measuring surface displacements and their precision.

Table 2.1: Overview of methods used in measuring surface displacements (modified after Gili et al., 2000)

Method	Results	Typical range	Typical precision
Precision tape	Δ distance	< 30 m	0.5 mm/30 m
Fixed wire extensometer	Δ distance	< 10-80 m	0.3 mm/30 m
Rod for crack opening	Δ distance	< 5 m	0.5 mm
Offsets from baseline	$\Delta H, \Delta V$	< 100 m	0.5-3 mm
Surveying triangulation	$\Delta X, \Delta Y, \Delta Z$	< 300-1000 m	5-10 mm
Surveying traverses	$\Delta X, \Delta Y, \Delta Z$	Variable	5-10 mm
Geometrical levelling	ΔZ	Variable	2-5 mm/km
Precise geometrical levelling	ΔZ	Variable	0.2-1 mm/km
Electronic distance measurement (EDM)	Δ distance	Variable (usual 1-14 km)	1-5 mm + 1-5 ppm
Terrestrial photogrammetry	$\Delta X, \Delta Y, \Delta Z$	Ideally < 100 m	20 mm from 100m
Arial photogrammetry	$\Delta X, \Delta Y, \Delta Z$	$H_{\text{flight}} < 500$ m	10 cm
Clinometers	$\Delta \alpha$	$\pm 10'$	0.01-0.1°
GPS	$\Delta X, \Delta Y, \Delta Z$	Variable (usual < 20 km)	5-10 mm + 1-2 ppm
Slope stability radar (SSR)	Δ distance	Variable	< 1 cm

1 ppm (part per million) = one additional millimetre per kilometre of measured line

Extensive research programs in recent years, involving both academic and commercial concerns resulted in improvements of existing methods, as well as, development of new techniques. There is also rapid progress in design new precise geodetic survey instruments. The most significant change was to develop advances in automatic data collection, storage and transfer. Today, the equipments used for conventional mine subsidence monitoring usually include EDM devices, total station or precise levels. New remote sensing and satellite based techniques are also widely introduced and used as alternative or complementary methods to conventional surveys.

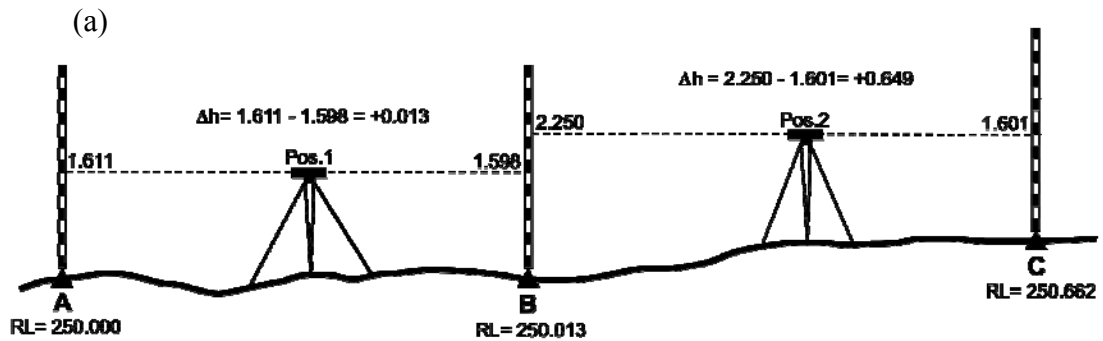
Techniques for monitoring mine subsidence are usually based on determination of relative ground movement between a network of survey stations. The conventional methods include total station surveys and levelling, GPS surveys, photogrammetry aerial mapping, and laser scanning.

2.1. Total Station Surveys and Levelling

Total station surveying and levelling techniques used for mine subsidence monitoring involves one or more of following methods (Jarosz, 2009):

1. **3-D Triangulation:** The technique uses a system of triangles or quadrilaterals between the surveying stations. Quadrilaterals are the preferred structure, as it provides a much stronger geometrical network. Triangulation technique is mostly replaced by high accuracy techniques such as Global Navigation Satellite System (GNSS) surveying. However, the technique is still used to establish the mine's primary control network and also to validate the positioning provided by the GNSS method.
 2. **3-D Trilateration:** The technique is similar to triangulation only the angular measurements are replaced by distance measurements between vertices of triangles or quadrilaterals.
 3. **Levelling:** As illustrated in Figure 2.1, the technique focused only on vertical positioning of survey points (levelling benchmarks):
 - a. Differential levelling: The vertical distances are determined between horizontal plane and surveyed benchmarks.
-

- b. Trigonometric levelling: The vertical distances are determined as a function of a slope (or horizontal) distance and a vertical angle.
- c. Precise levelling: A highly accurate method of differential levelling that uses highly accurate instruments (levels) and with a more complicated observing procedure than general levelling. It can deliver high orders of accuracy such as 1 mm per 1 km traverse.



(b)



Figure 2.1: a) Simple illustration of levelling (Jarosz, 2009), b) Levels (Trimble, 2009)

2.2. Global Positioning System (GPS) and Global Navigation Satellite System (GNSS)

Global Positioning System (GPS) was started with eight satellites launched and controlled by the US Department of Defence for purposes of precise navigation. GPS functions based on timing of how long it takes a radio signal, transmitted by satellites with known positions, to reach an antenna at a point on earth (Ikehara, 1994). Then coordinates for an unknown point can be calculated by trilateration, using the satellites as reference points (Leick, 1990). At least four satellites are necessary to

compute three-dimensional coordinates of a point. The GPS equipment include a tripod-mounted antenna, a radio signal processing receiver, and some type of data recorder.

Global Navigation Satellite System (GNSS) is the term for satellite navigation systems that provide autonomous geo-spatial positioning with global coverage. The GNSS systems use satellite transmitting signals, which contain information about the positions and the times the signals were transmitted. The receiver makes a comparison between the times of broadcast encoded in the transmission with the time of reception measured by receiver's internal clock. The result would be pseudo-range to the satellite. Assuming several such measurements made at the same time and to different satellites, a real time position of receiver can be determined. After 2009, the United States NAVSTAR Global Positioning System (GPS) is the only fully operational GNSS. The Russian GLONASS is still in the process of being restored to its full operation. China is planning to expand its regional BEIDOU navigation system into the global COMPASS navigation system by 2015. The European Union's Galileo positioning system is a new GNSS which is in initial deployment phase and scheduled to be operational in 2013 (Jarosz, 2009).

Accuracy of position or availability and reliability of the signal in GPS systems can be improved using enhancement techniques such as Differential Global Positioning System (DGPS), Ground Based Augmentation System (GBAS) and The Real Time Kinematic (RTK):

- **Differential Global Positioning System (DGPS):** In this technique the corrections of position are calculated using a network of fixed, ground-based reference stations and based on the difference between the positions indicated by the satellite systems and the known fixed positions.
 - **Ground Based Augmentation System (GBAS):** Considering the topographical characteristics of open pit mines (deep pits with steep slopes), there are difficulties with obtaining GPS satellite signal or with satellite coverage. These difficulties can be solved using the Ground Based Augmentation System (GBAS). GBAS uses accurately positioned
-

radio transmitters that transmit pseudo-satellite signals directly to receivers.

- **Real Time Kinematic (RTK):** This enhancement technique utilises the carrier-phase enhancement. RTK systems use a single base station receiver and a number of mobile units (rovers). The base station measures and re-broadcasts the phase of the carrier GPS signal, and the mobile units compare their own phase measurements with the ones received from the base station. Using this technique the mobile units are able to calculate their relative position with millimetre accuracy; however the accuracy of their absolute position is similar to the accuracy of position of the base station (Figure 2.2).



Figure 2.2: Rover and base station receivers for RTK (Trimble, 2009)

The typical nominal accuracy for these dual-frequency systems is 1 centimetre \pm 2 parts-per-million (ppm) horizontally and 2 centimetres \pm 2 ppm vertically. In mining applications DGPS is usually used for vehicle positioning in mine fleet management systems and the RTK is utilised by mine surveyors as a replacement of total-stations (Jarosz, 2009).

2.3. Laser Techniques

The 3D laser scanners use laser beams to determine vectors between the position of scanner head and sample points, which are usually placed on a regular grid, on the surface of target object (Jarosz, 2009). The main parameter determined by laser scanners is the time-of-flight laser rangefinder which is defined as the distance

between the scanner head and object. A laser emits a pulse of light and an accurate clock measures the amount of time before the reflected light is detected. Then via a reconstruction process, the collected data will be used to extrapolate the shape of the scanned object. In general, 3D scanners work the same as a photographic camera and it can only collect data from unobstructed surfaces; however it usually provides wider field of view (conical or spherical in shape).

In the past few years, laser scanners developed very quickly and become a fast, reliable and accurate option for surveyors. On the other hand, the significant progress in software development allows processing of large amount of data collected by laser scanners. Today, data can be quickly downloaded, combined and converted into a solid representation of the scanned objects. Considering the above, laser scanners are widely used in mining applications as they do not require positioning of reflector which means no staff at a mining site, making whole surveying operations significantly safer (Jarosz, 2009). The available laser scanners are able to deliver accuracy at a level of $\pm(5-15)\text{mm}+20\text{ppm}$ @ 100m range (from data sheets of Riegl scanners). Figure 2.3 shows an example of laser scans obtained from an open pit mine.

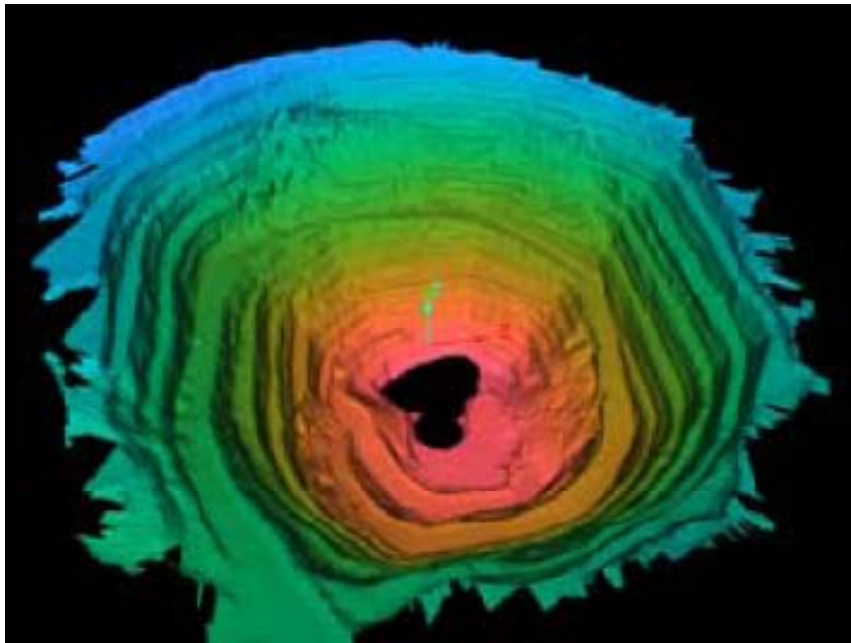


Figure 2.3: Laser scanning results for La Coipa mine open pit mine, Chile (Maptek, 2009)

2.4. Airborne Laser Scanning (ALS)

Airborne Laser Scanning (ALS) is a member of the “Light Detection and Ranging” (LiDAR) group. LiDAR is defined as technology that utilises laser pulses to collect large amounts of data from the physical layout of terrains or landscapes (CSIRO, 2008). Along with Photogrammetry and InSAR, ALS is considered as a technique to generate DEM (Digital Elevation Model). The term “digital elevation model” (DEM) is used generically for the digital cartographic representation of the elevation of the surface.

In ALS, data is collected by a laser scanner mounted on an airplane as a stream of discrete reflected laser points from the ground. Same as ordinary laser scanners, ALS measures the height of the objects based on the distance between the objects and the laser scanner. Therefore, recording the precise location and orientation of the scanner is very crucial. ALS uses GPS, and also an inertial measurement unit (IMU) that enables it to accurately record the position, attitude and acceleration of the aircraft (Chang, 2008). ALS accuracy is dependent on the characteristics of the terrain. Its height accuracy is 0.1-0.5m, and horizontal accuracies of 0.3-1.5m (Turton and Jonas 2003).

2.5. Photogrammetry

Aerial mapping utilising photogrammetry is widely used for mapping large open pit mines. This method is especially useful for mines with large elevation differences, difficult to access or with high traffic areas (Jarosz, 2009). The main advantages of the method are:

- a) Registration of details are real and not generalised which allows registration to be revised at any future time;
- b) It provides remote and safe collection of data; and
- c) Relatively fast survey of a large area.

In spite of its advantages, the method is not economically feasible for small operations as it involves significant mobilisation costs. It also requires significant

preparation activities, including marking and surveying of control points. The positional accuracy of details defined by this method is in the range of $\pm(0.1-0.2)$ m.

2.6. Slope Stability Radar (SSR)

Slope stability radar is a relatively new technology based on differential interferometry that uses radar waves for monitoring mine walls. The methodology of the technique is identical to other phase interferometry techniques including SAR interferometry; it scans a region of the wall at two different times and then uses the phase difference to determine the amount of movement of the slope. According to Harries and Roberts (2007) the main advantages of the technique are:

- Capability to provide full area coverage of a rock slope without the need for reflectors mounted on the rock face;
- Capability to deliver up to sub-millimetre precision of wall movements without being adversely affected by rain, fog, dust, smoke, and haze; However as for any interferometry techniques, the accuracy of the technique diminishes in areas with vegetative cover.
- The equipment can be housed in a self-contained trailer that can be easily and quickly moved around the site; it can be placed in the excavation, or on top of a wall or on a bench to maximize slope coverage whilst not interfering with operations.



Figure 2.4: SSR equipment (Groundprobe, 2009)

2.7. Chapter Summary

The main objective of any subsidence monitoring system is to detect surface movement, its magnitude and extent. A variety of surveying techniques have been used to monitor mine subsidence. Techniques for monitoring mine subsidence are usually based on determination of relative ground movement between a network of survey stations. The conventional methods include total station surveys and levelling, GPS surveys, photogrammetry aerial mapping, and laser scanning. This chapter provided an overview of methods used in measuring surface displacements and their precision.

Chapter 3

SAR Interferometry Background

Chapter 3

SAR Interferometry Background

3.1. History of Synthetic Aperture Radar Interferometry (InSAR)

In general, InSAR can be defined as an integrated technique resulting from the integration of three pre-existing techniques, Radio detection and ranging (radar), Synthetic Aperture Radar (SAR) and Interferometric SAR (InSAR). Providing a review of development of these techniques and stages of their evolution would illustrate the path of InSAR, its birth and development.

3.1.1. Radar

Radar is a detection system that uses electromagnetic waves to identify the range, altitude, direction, or speed of moving and fixed objects such as aircraft, ships, motor vehicles, weather formations, and terrain. The radar emits microwaves or radio signals and records the backscatter signals from objects in its line of sight. Travel time of the emitted signal and intensity of the reflected signal can provide a determination of the range to the object and also its physical properties (Table 3.1).

Table 3.1: Wavelengths of the signals in the microwave spectrum (IEEE, 2009)

Band	Wavelength (cm)
K	1.1 – 1.7
X	2.4 – 3.8
C	3.8 – 7.5
S	7.5 – 15
L	15 – 30
P	30 – 100

The development of radar goes back to the 17th Century and starts with the definition of Maxwell's equations of electromagnetics in 1873 and Hertz's studies in 1886. Nonetheless, the first radar systems were used in 1903 for ship tracking and preventing ship collisions (Buderi, 1996; Thumm, 2009). Despite the fact that in

early years of radar (in particular in 1930s and 40s) the technology was mainly focused on military applications, other radar applications including astronomical applications were also quickly developed. The first radar observation of the Moon was done in 1946 (Buder, 1996); Venus and Mars were observed using radar in 1961 and 1963 (Goldstein and Gillmore, 1963; Goldstein and Carpenter, 1963); attempts to send radar to space, started from 1962, became successful by lunar radar observation from Apollo 17 in 1972 and first global mapping focusing on Venus was performed with an accuracy of about 300m and a spatial resolution of about 50km (Curlander and McDonough, 1991; Henderson and Lewis, 1998).

3.1.2. Synthetic Aperture Radar

Synthetic Aperture Radar belongs to a specific class of radar systems which are called imaging radars. Imaging radar systems usually use side-looking antenna mounted on an aircraft or satellite. The objective is to provide range, while ambiguous reflections should be avoided. The first Side-Looking Air-borne Radars (SLR or SLAR) were only able to provide range information and the phase information of the emitted and reflected signal was not recorded. Moreover, they used a physically long antenna; therefore the system was named Real Aperture Radar (RAR) (Hanssen, 2001).

The concept of using phase information in the radar signals was first introduced by Carl Wiley (Wiley, 1965). During 50s and 60s, further development of this concept by universities of Illinois and Michigan lead to the development of Synthetic Aperture Radar (SAR). Availability of coherent radar was critical for the precise process of receiving and preserving phase-amplitude information of a signal. This information must be accurate enough for later comparison and processing. Considering the above and also the necessity of stability of the phase behaviour within the period of sending and receiving the signal, the idea of a long artificial antenna created synthetically by a moving antenna was adopted. This approach combines the information received from many reflected signals within the synthetic antenna length; it was also able to increase the azimuth resolution up to three orders of magnitude (Hanssen, 2001).

Early remote sensing satellites such as the Landsat satellites use optical scanners utilising visible and infrared waves. Although these satellites were able to provide precious information about the planet, their limitations such as not being able to work under cloud cover or their need to solar illumination had restricted their suitability. So, demands for new remote sensing techniques, overcoming limitations of optical scanners, lead to development of satellite SAR missions. The experiences of airborne SAR in the 60s and 70s were used in designing and building an L-band SAR system on-board Seasat. This satellite was launched in 1987 with the objective of ocean studies. Despite the failure of the Seasat mission (A short-circuit ended the operation after only 100 days), SAR imagery was quite successful and later resulted in integration of SAR systems in many upcoming satellite missions (Elachi et al., 1982).

Following the success of Seasat, Shuttle Imaging Radar (SIR) laboratory was built in 1981 as the first SAR instrument to be carried by a space shuttle. SIR-A was an L-band instrument with an incidence angle of 50 degrees that operated for 2.5 days. SIR-B was launched in 1984 and was able to utilise different look angles. Also, for the first time SIR-B used digital data recording equipment. SIR-B was followed by Soviet Union satellites Cosmos-1870 (first S-band satellite) in 1987 and ALMAZ-1 in 1991 (Hanssen, 2001). Magellan, the first SAR mission to another planet (Venus), was launched in 1989 and mapped 98% of Venus with the resolution of 150m (Henderson and Lewis, 1998).

The history of synthetic aperture radar went to the next level when the European Space Agency (ESA) launched its first satellite with SAR onboard in July 1991. Main objective of ERS-1 (European Remote Sensing Satellite) was to monitor polar oceans and ice using C-band radar. It was initially planned to operate for 5 years, however the satellite was in operation until 2000. ERS-1 systematic data acquisitions, the possibility of controlling orbit, and the data distribution policy adopted by ESA, were main contributions of ERS-1 to radar interferometry and a source of major improvement in the lifespan of the technique (Hanssen, 2001). In April 2005, almost an exact copy of ERS-1, ERS-2, was sent to the same orbit as ERS-1. This provides the possibility of performing tandem-mode operations of two

satellites. ERS-1 and 2 work in two modes: image mode for imaging the Earth's surface and wave/wind mode for collecting data over oceans.

In 1992, Japan launched its first SAR satellite, Japanese Earth-Resources satellite (JERS). JERS was equipped with L-band radar with an incidence angle of 35 degrees. SIR-C/X-SAR developed by NASA/Jet Propulsion Laboratory (JPL), German Aerospace Centre (DLR) and Agenzia Spaziale Italiana (ASI), was launched in 1994. SIR-C/X-SAR was able to utilise three different frequency ranges: L-band, C-band and X-band that leads to significant improvement of data interpretation (Lanari et al., 1996; Melsheimer et al., 1996). In 1995, Canadian Space Agency (CSA) joined the league with Radarsat-1 that enables ScanSAR mode and working in wide swaths. Radarsat-1 was followed by Radarsat-2 launched in December 2007.

In 2000, the Shuttle Radar Topography Mission (SRTM) tried to overcome the problem of repeat-pass missions. SRTM mission was performed using a single-pass configuration with a fixed 60m boom that carried two radar antennas to map all land masses in 11 days, between 11 and 23 February 2000. It uses two levels of accuracy, C-band for the whole globe and X-band for tiles of USA (Balmer, 1999).

On the 1st of March 2002, the European Space Agency launched Envisat as the successor to ERS-1 and 2. The Envisat has a similar configuration as ERS-1, 2 and ensuring the continuity of the data measurements of previous satellites. Envisat works in seven modes including Advanced Synthetic Aperture Radar (ASAR). ASAR itself is able to produce five different types of data including: stripmap mode (Image), wave mode, global monitoring, alternating polarisation and wide swath (Eurimage, 2009).

The Japanese launched their second satellite, the Advanced Land Observing Satellite (ALOS), in 2006. ALOS carries two optical sensors, PRISM and AVNIR-2, and one active radar sensor, PALSAR. PALSAR is an L-band, able to combine 18 different off-nadir beams for strip SAR, and provides five observation modes, Fine Beam Single (FBS), Fine Beam Dual (FBD), Direct Transmission (DT), SCANSAR, and polarimetry (Furuta et al., 2005).

The newest SAR related satellite mission, launched in June 2007, is TerraSAR-X, the German national SAR-satellite system which is based on a public-private-partnership agreement between the DLR and EADS Astrium GmbH. TerraSAR-X follows the technology previously used in X-SAR (1994) and SRTM (2000) missions. This satellite provides data in X-band and three operational imaging modes: SpotLight (down to 1m resolution), StripMap (3m resolution), and ScanSAR (18 m resolution). Table 3.2 shows a list of satellite SAR missions and their specifications.

Table 3.2: List of satellite SAR missions and their specifications (Modified after Hanssen (2001))

Mission	Year	Repeat cycle (days)	Satellite altitude (km)	Carrier wavelength	Incidence angle (deg)	Swath (km)
Seasat	1978	3	800	L-band	23	100
SIR-A	1981	-	235	L-band	50	50
SIR-B	1984	-	235	L-band	15-64	10-60
Cosmos 1870	1987-89	var	250	S-band	30-60	20-45
ALMAZ	1991-92	-	300	S-band	30-60	20-45
Magellan	1989-92	var	290	S-band	17-45	20
Lacrosse 1,2,3	1988-97	var	275	S-band	steerable	var
ERS-1	1991-2000	35	790	C-band	23	100
ERS-2	1995	35	790	C-band	23	100
JERS-1	1992-98	44	568	L-band	39	85
SIR-C/X-SAR	1994	-	225	L, C, X-band	15-55	10-70
Radarsat	1995	24	792	C-band	20-49	10-500
Envisat	2001	35	800	C-band	20-50	100-500
ALOS	2006	44	700	L-band	8-60	40-350
Radarsat-2	2007	24	798	C-band	20-60	20-500
TerraSAR-X	2007	11	530	X-band	20-45	10-150

*Bolded missions are capable of interferometry

3.1.3. SAR Interferometry

Radio interferometry was started after WWII with Ryle and Vonberg studies; however, U.S. military was first to use airborne SAR interferometry for topographic

mapping in 1971. They used phase difference images to obtain elevation (Henderson and Lewis, 1998). Nonetheless, Graham (1974) was first to publish results produced by SAR interferometry. Zebker and Goldstein (1986) produced the first set of interferograms which was generated by multiplying amplitudes of two SAR images and their phase subtraction. Result was a topographic map of an area of 10×11 km, with accuracy 10-30m.

The first application of interferometry with satellite data was performed in 1987-1988 using Seasat and SIR-B data and the repeat-pass method (Li and Goldstein 1990; Gabriel and Goldstein, 1988; Gabriel et al., 1989). Massonnet et al., (1993) was the first to introduce differential radar interferometry (DInSAR) for mapping the displacement field of the Landers earthquake (Figure 3.1). They also used a reference elevation model to remove the topographic phase component (Hanssen, 2001).

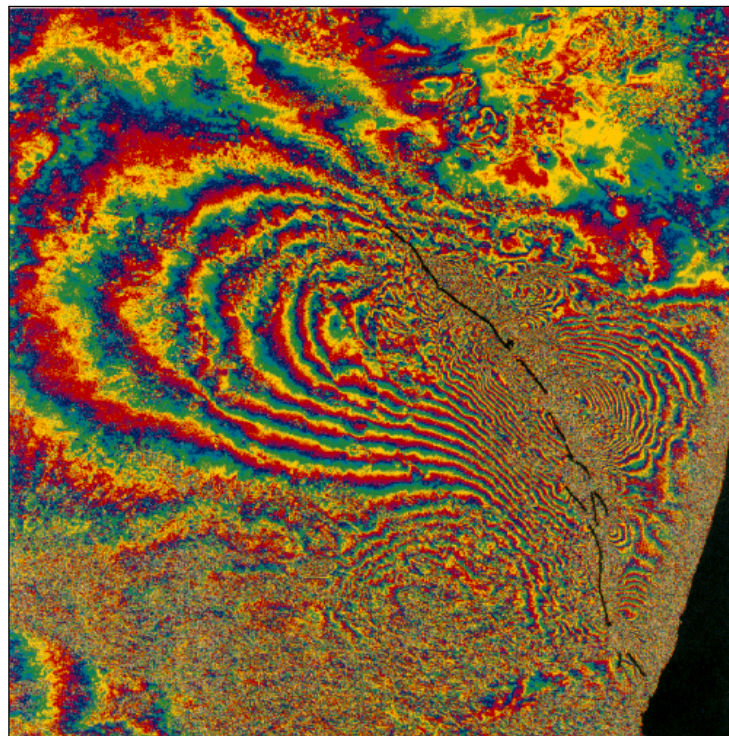


Figure 3.1: Interferogram from Lander earthquake generated by Massonnet et al., (1993)

3.1.4. Examples of InSAR Applications

3.1.4.1 Earthquake

Conventional GPS-based monitoring systems are usually spaced tens of kilometres apart and consequently are not suitable to detect smaller events or details of a larger rupture. In contrast by using InSAR, in case of availability of a SAR image acquired and archived before an earthquake, it is possible to produce an interferogram using post-earthquake images which means the possibility to study earthquakes even in the most remote regions of the world (Bürgmann et al., 2000).

Earthquake mapping using InSAR began with analysis of co-seismic deformation; however in the late 90s, InSAR was also used to map post-seismic deformation (deformations immediately after an earthquake). Surface displacement data produced by InSAR can provide better understanding of dynamic and distribution of an earthquake and also does not need any field surveys. InSAR makes it possible to detect earthquake location, fault geometry and rupture dynamics from the measured co-seismic deformation field (Lu et al., 2007).

3.1.4.2 Volcanic Activities

As opposed to earthquake, a volcanic eruption is a precursory phenomenon that allows an early warning through stages of increasing unrest and characteristic deformation patterns reflecting the ascent of magma through the volcanic edifice. Currently, only a small number of volcanoes can be routinely monitored with GPS or terrestrial methods. Considering the fact that once the eruption takes places, monitoring using classical methods is almost impossible due to safety reasons, routine monitoring of volcanic activity using a remote sensing method like InSAR would be very advantageous (Bürgmann et al., 2000).

The first InSAR application in volcanic activity was used at Mount Etna and Kilauea target (Massonnet et al., 1995; Rosen et al., 1996). After that InSAR has proved its capability in the study of a variety of volcanic activities including volcanic eruptions, inter-eruption strain caused by changes in magma distribution at depth, gravitational spreading of volcanic edifices and volcano-tectonic deformation

(Wadge, 2003). Today, InSAR is mostly used for detecting volcanic deformation, although its application as a monitoring technique for volcano observatories has been limited due to its limitations such as orbital repeat times, lack of archived data, incoherency and atmospheric errors (Stevens and Wadge, 2004).

3.1.4.3 DEM Generation

Topographic maps initially were able to only provide qualitative expressions of hills, valleys, and mountains on general maps which later were followed with topographic contour maps. In early twentieth century, stereo aerial photography made it possible to collect photogrammetric measurements of elevations over substantial areas. This continued by stereo images or photographs taken by satellites (Bürgmann et al., 2000). The first digital elevation models (DEMs) were made by digitizing from topographic maps and interpolating the elevations to form a regular grid.

Today, along with photogrammetry and ALS, InSAR is used to generate elevation models. Much commercial and open-source software provides this possibility, even for non-expert users, to generate DEMs with various specifications using available SAR images. Especially data acquired by ERS-1 and 2 tandem mode were widely used for DEM generation. Though InSAR and optical methods may seem to follow the same basics with respect to the topographic measurements, InSAR has no need to identify homologous features as required by photogrammetry which pose problems in snowy or sandy areas. Furthermore, InSAR does not need illumination by the sun and is able to work at night or dark areas. Necessity of using method like InSAR became more obvious considering the fact that in Europe only 10% of all acquired optical data is useful for topographic mapping due to heavy cloud cover (Hanssen, 2001).

3.1.4.4 Land Subsidence

Natural subsidence usually cover large areas and develop very slowly. In contrast to natural subsidence, human-made subsidence for instance induced by groundwater consumption, petroleum extraction or mining activities can cause rapid

subsidence that affects human life and infrastructure. Detection, monitoring, and control of subsidence are always costly and challenging. SAR interferometry has the potential to provide a comprehensive monitoring plan with significantly less effort and cost, in particular, with less frequent ground surveys and on a global basis (Bürgmann et al., 2000). Here, some of InSAR applications will be reviewed in detecting subsidence related to extraction of fluids for energy production and groundwater extraction. InSAR application for monitoring mine subsidence will be later discussed in detail as an individual section (see section 3.1.5).

Extraction of petroleum, gas, or steam causes subsidence in many areas. Massonnet et al. (1997) used InSAR for monitoring subsidence over a geothermal field in southern California where extraction of hot fluid for electricity was causing 10-30mm/year of subsidence rate. In 1998, rapid subsidence caused by petroleum and gas withdrawal from the Lost Hills and Belridge oil fields were mapped by Fielding et al., (1998) using InSAR. Today, InSAR is used to map subsidence over several oil fields around the globe.

Groundwater consumption can be considered as the most widespread cause of land subsidence and occasionally uplift or rebound. Rapid extraction of groundwater to supply agriculture or urban areas has caused subsidence up to several meters (Bürgmann et al., 2000). Land subsidence in the Lancaster, California, area, were studied by Galloway et al., (1998) using InSAR. The area was undergoing a transition from agriculture to urban land. Groundwater withdrawal from deep wells has changed the water levels by 30-90m from 1970. InSAR detected up to 50mm of subsidence over a period of 26-months. Later hydrologic modelling of water level and hydraulic properties data from wells were used to produce a simulated subsidence pattern that confirmed the observed pattern by InSAR (Galloway et al., 1998).

3.1.4.5. Glacier and Ice Monitoring

InSAR is able to provide high-resolution, high-accuracy topographic maps of glaciers and ice sheets and also measure ice-flow velocity without any ground control. Using InSAR it is possible to identify the line separating floating ice from

grounded ice, and measure changes in surface-geophysical parameters (Goldstein et al. 1993, Hartl et al. 1994). Main limitations of InSAR for polar and glacier analysis is temporal decorrelation due to the change in snow or ice condition (Klees and Massonnet, 1999).

As an ending to this section, providing a glimpse of future of SAR and InSAR is necessary. Between 2000 and 2003, at the request of NASA, the Solid Earth Science Working Group (SESWG) developed a strategy for the highest priority objectives in solid earth science for the space agency over the next 25 years. In this report, the recommended observational strategy of NASA for surface deformation almost entirely based on InSAR techniques, which is as follow (Solomon, et al., 2003):

a. Immediate (1–5 Years):

Single dedicated InSAR satellite:

- L-band, left/right looking capability, and weekly access to anywhere on the globe.
- Precise orbit determination and ionospheric correction capabilities.
- 1 mm/yr surface displacement over 50km horizontal extents in selected areas.

b. Near term (5–10 Years):

Constellation of InSAR satellites:

- Improved temporal frequency of deformation maps to daily intervals
- Maps at several-hundred-km width with full vector surface displacements at accuracies of sub-millimetre per year over 10km spatial extents and 1-m spatial resolution
- Complementary ground and seafloor geodetic observations

c. Long term (10–25 Years):

Constellation of InSAR satellites in low-Earth or geosynchronous orbits:

- Hourly global access
 - Increased density of continuous ground and seafloor geodetic observations
-

3.1.5. InSAR and Mining

Studies that involved detecting and monitoring mining-induced subsidence were among earliest SAR interferometry studies. One of the earliest attempts was carried out on the Gardanne mine site in France using ERS-1 cycle images in 1992 (Carnec et al., 1996). Required data were selected from ERS-1 with respect to ideal season considering the vegetation and humidity change. Temporal baseline of data was 70 days (2 cycles of ERS-1) and perpendicular baseline was less than 150 m. DInSAR shows vertical movement up to 42 mm/70days. In the absence of any comparison with classical surveys, an elastic deformation model was used for data validation. The RMS errors were 3.7mm and 4.59 mm for two profiles. At the end of the studies, it was concluded by the authors that “DInSAR is not suitable for applications with high deformation gradients associated with short-time evolution on steeply sloping terrains.” Between 1992 and 1995, ERS-1 and 2 data were again used to study the same area. This time, three pairs with temporal baseline of 3, 12 and 15 days were processed to obtain 6, 17 and 23 mm subsidence respectively. The comparison showed that over a short period the amount of effective subsidence was similar with a maximum measured subsidence of less than 40 mm (Carnec and Delacourt, 2000).

The Vauvert salt mine in France with a depth of between 1900 and 2800 m and expected subsidence rate 5 ~ 10 mm/year, was studied by Raucoules, et al., (2003). During the studies InSAR pairs were selected from ERS-1 and 2 data, applying a restriction of perpendicular baseline less than 100m. The vegetation cover was problematic and using a small baseline was helpful to minimise geometric decorrelation and also topographic errors. Using the interferogram stacking method subsidence rate of about 20 ~ 22 mm/year were detected. Data validation between InSAR results data provided by ground truth showed mean and RMS error of 0.16 and 1.9 mm/year respectively (Chang, 2008).

ERS-1 and 2 data again were used in underground coal mining in Ruhrgebiet, Germany in 2000 (Wegmuller et al., 2000). Data were selected based on short temporal baseline of 35 or 70 days (1 or 2 cycles of ERSs) and also perpendicular baseline less than 200m. Respecting these restrictions during data selection process and also using winter acquisitions, made it possible to deliver higher coherence over

agricultural and rural area; however, strong phase noise caused phase-unwrapping problems. Nonetheless, DInSAR was able to precisely detect zones of affected ground by subsidence. Validation results between classical surveys and DInSAR represented good correlation in the area far from centre of the subsidence zone. It was then followed by underestimated magnitude of subsidence measured by DInSAR near the centre of the subsidence trough as a result of high rate of deformation and phase ambiguity problems. In order to solve the problem of high gradient changes, repeating the analysis using images with longer wavelength was recommended. Later, L-band JERS-1 data were tested on this site providing less sensitivity to movement and better results (Strozzi et al., 2003; Wegmuller et al., 2005).

Stow and Wright (1997) used ERS-1 and 2 data for subsidence analysis in Selby Coalfield in UK. Subsidence in this site is well-controlled and limited to 1m in total. Images were planned to be acquired only in winter seasons in order to optimise the coherence. Nonetheless, agricultural land at Selby was a source of problem. Pairs with temporal baseline longer than 6 months showed very poor coherence; Phase filtering was required and applied to improve phase statistics. InSAR detected subsidence of about 110mm over period of 35 days. No data validation was available.

Subsidence in Upper Silesia in Poland, one of the biggest coal mining fields in Europe, has been monitored using InSAR since 1998 (Perski and Jura, 1999). Around 50 ERS-1 and 2 SAR images were processed with variable baselines between 0 and 431m) adopting 2-pass, 3-pass and 4-pass approaches. Also, in order to reduce topographic effect, two sets of tandem data acquired in 1995 and 1999 were used. A single case study focusing on the town of Bytom showed that subsidence rates can reach more than 3.4 mm/day. It is also commented by Perski (2003) that the subsidence rate in this area is higher than the range detectable by C-band SAR data. Considering such high rate of subsidence, it was impossible to detect subsidence induced directly by mining; therefore only long term effect of subsidence was taken into the account. Long term interferograms from 1997-98 and 99 show the slow movement of 100-200 mm/year, which can be associated to post mining relaxation and reactivation of old cavities. The terrestrial levelling data collected in 1968 and 1989 show similar subsidence annual rates.

According to Perski et al., (2009), terrain deformation in Wieliczka salt mines in Poland can be categorised into three groups, based on their origin: salt mining, catastrophic suffusion caused by water inflows to the mine, and landslide. DInSAR and Persistence Scatterers Interferometry (PSI) were performed in this area in order to discriminate between these different types of deformation. ERS-1 and 2 data, acquired over 7.5 years between 1992 and 2000, were used for the processing. It was found that the deformation induced by water inflow into the mine cannot be detected by InSAR due to high gradient of change over a small area. Considering mine subsidence, the main trough shape could not be restored; however PSI was able to detect subsidence rate of about 6mm/year in some places. Assuming a very rough estimation of available levelling data, difference between PSI result and classical survey data was reported as very small. Similar results were produced by an independent study over the same area (Wasowski et al., 2007) confirming the results produced in previous studies.

Ge et al., (2003a) used a 4-pass approach involving ERS-1 and 2 tandem data and JERS-1 L-band images to map subsidence caused by coal mining in Southern Coalfield, NSW, Australia. As the first step, a high quality geocoded DEM was generated by a pair of ERS-1 and 2 tandem images. Then four interferograms were constructed using 5 L-band SAR images with perpendicular baselines between 94 and 577m and temporal baseline between 44 and 132 days. An external DEM was used to remove the topographic effect. The resulting interferograms were then used to generate differential results between JERS-1 data and the DEM leading to identify the possible or expected ground deformation. The expected ground deformation within the period of study was about 20~30 cm. Results generated by InSAR showed relative height change of about 29 cm. Table 3.3 shows a list of InSAR application for mine subsidence monitoring.

Table 3.3: InSAR application for mine subsidence monitoring (summary of presented case studies)

Mines	Sensor	Expected subsidence rate	DInSAR subsidence rate	Validation (RMS)	
				Model	Ground Truth
Vauvert (France)	ERS-1 and 2	0.5 ~ 1cm /year	2 ~ 2.2 cm/year	n/a	0.198cm/year
Ruhrgebiet (Germany)	ERS-1 and 2, JERS-1 (after 2003)	Max.34cm /70days	8cm/70days	n/a	Only correct up to 8 cm
Gardanne (France)	ERS-1 and 2	n/a	6mm/3days 17mm/12days 23mm/15days	3.7mm and 4.59 mm /35days	n/a
Selby (UK)	ERS-1 and 2	Up to 1m in total	11cm/35days	n/a	n/a
Wieliczka salt mine (Poland)	ERS-1 and 2	n/a	6 mm/year	n/a	Different very small
Upper Silesia (Poland)	ERS-1 and 2	n/a	100-200 mm/year	n/a	Similar with historic levelling data
Westcliff (Australia)	ERS-1 and 2, JERS-1	20 ~ 30cm /132days	29cm/132days	n/a	n/a

3.2. Principles of SAR Interferometry

3.2.1. What is SAR Imagery?

Klees and Massonnet (1999) defines a Synthetic Aperture Radar (SAR) as “an imaging radar device that images the radar backscatter of the Earth’s surface”. The SAR system is able to produce a radar backscatter map through scanning the surface of the Earth moving at uniform speed and altitude along the flight path of the satellite. The sensor moves along the satellite flight path and transmits microwave pulses and then receives the echoes of these pulses via the same antenna. The main parameter measured by SAR is the travel time of radar signals to propagate to the target and return to the sensor. Main components of SAR can be listed as follows (Jarosz and Wanke, 2004b):

- A transmitting antenna that emits a short electromagnetic (radar) signal in a specific direction,
- A receiving antenna for detecting the backscattered signal with directional precision,

- A clock that precisely measures the travel time of the signal (delay between emission and detection) and
- A scanning system that allows to scan the surface of the Earth with the directional beam and to determine position of the target.

Figure 3.2 provides a simplified sketch of a SAR imagery system. The direction along the Line of Sight (LOS) is usually called the slant-range direction. The SAR system precisely records movement of satellites. It then uses advanced signal processing techniques to simulate a larger sensor size and produces images with larger coverage and better quality. The spot on the Earth that is illuminated by a pulse is referred to as the antenna footprint while the imaged strip on the ground is called the swath. The antenna footprint moves at the satellite's speed along its orbit. The inclination of the antenna with respect to the nadir is called the off-nadir angle. The inclination angle is usually between 20° and 50° for available satellites. Due to the curvature of the Earth's surface, the incidence angle of the beam on a flat horizontal terrain is larger than the off-nadir, for instance 23° for ERS (Ferretti et al, 2007). As an example, for ERS-1 and 2, the satellite speed is set to be about 7430m/s; They cross the equator at an angle of 9° and an elevation of about 800 km (in a quasi-polar orbit). The footprint covers a swath of about 100 km wide in ground range on the Earth's surface, with the capability of imaging a strip of 445 km long each minute in strip map mode (Ferretti et al, 2007).

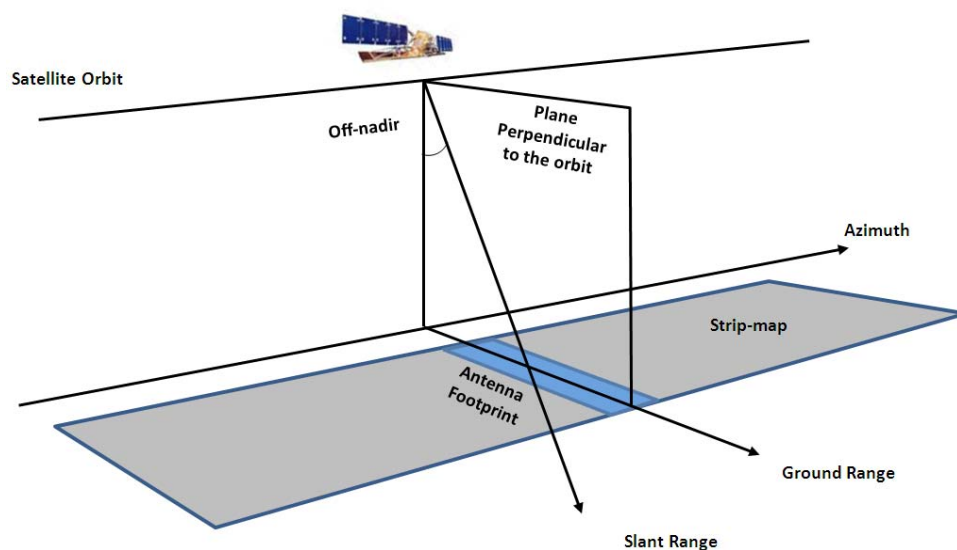


Figure 3.2: SAR Imagery System (After Ferretti et al., 2007)

The along-track location of the satellite is determined by the Doppler frequency shift. The Doppler Shift is a change in wave frequency as a function of the relative velocities of a transmitter and a reflector. In practise this means that the signal returned from the area ahead of the satellite sensor has higher (up shifted) frequency. Conversely, the signal from the area behind the sensor has lower (downshifted) frequency. Doppler frequency exists whenever the relative velocity between the radar and target is not zero (Rosen et al., 2000).

As illustrated in Figure 3.3, the position of the target can be geometrically represented by the intersection of a sphere centred at the antenna with radius equal to the radar range and a cone with a generating axis along the velocity vector and cone angle proportional to the Doppler frequency. A target in the radar image could be located anywhere on a circle formed by the line of sight of the radar and vector pointing from the satellite to nadir (Rosen et al., 2000).

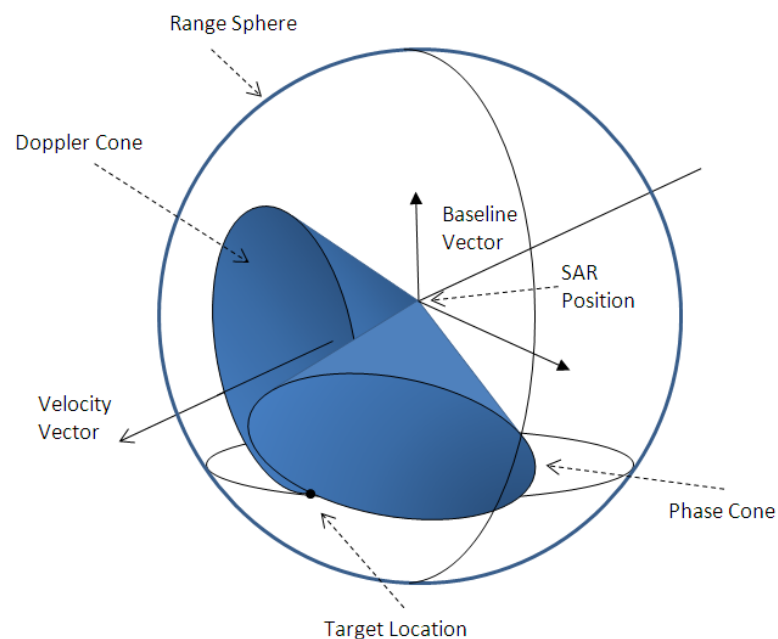


Figure 3.3: Target location in a SAR image, intersection of the range sphere, Doppler cone and phase cone (After Rosen et al., 2000)

The quality of the image depends on the sensor-scene geometry and accuracy of signal processing. There are two fundamental characteristics of a SAR system: First is the spatial resolution of the image in which the azimuth resolution is independent of the range, but the range resolution is linked to the position on the image (The

signal duration determines range resolution); Second is the point spread function (PSF) that determines the correlation and sampling properties of the image (Hovanessian, 1980).

A digital SAR image can be seen as a grid of pixels; each pixel in the image represents a small area of the Earth's surface (resolution cell). Dark areas in the image represent low backscatter while bright areas represent a high backscatter signal. Each pixel contains a complex number that carries amplitude and phase information processed from the backscatter signal from the corresponding resolution cell projected on the ground. The product is called Single Look Complex or SLC. In SLCs, rows are associated with different azimuth locations and columns are associated with different slant range location. The location and dimension of the resolution cell in azimuth and slant-range coordinates is defined by the SAR system characteristics. For instance, in the case of ERS-1 and 2, the SAR resolution cell dimension is approximately 5 metres in azimuth and 9.5 metres in slant-range; the distance between adjacent cells is about 4 metres in azimuth and about 8 metres in slant range (Ferretti et al, 2007).

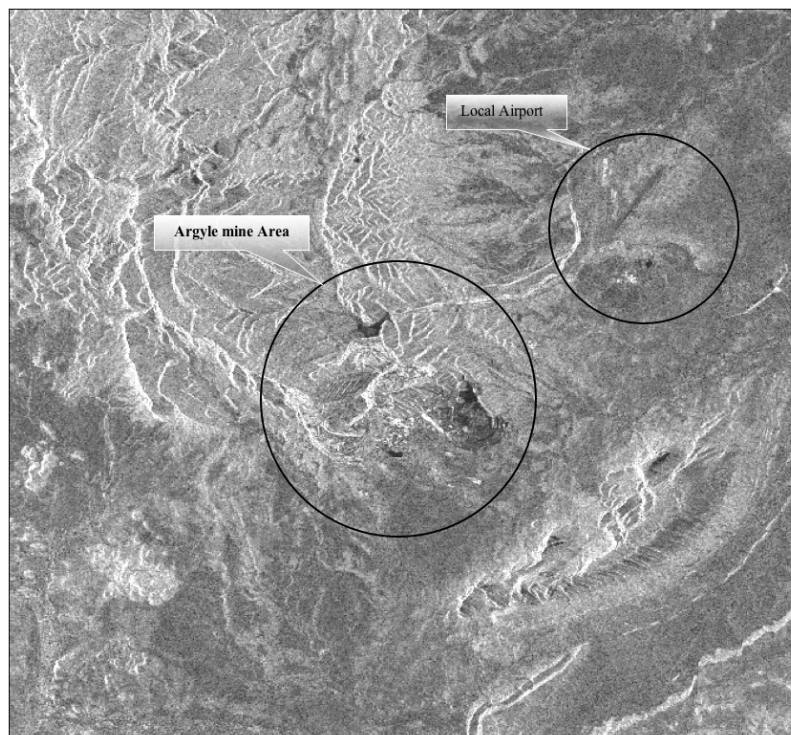


Figure 3.4: Sample of a SLC-SAR image acquired from Argyle Diamond Mine, WA, Australia (image source: ESA, Envisat ASAR data)

3.2.2. SAR Interferometry

In general, SAR interferometry makes use of SAR observations of the Earth's surface to acquire topographic information. By combining two SAR images taken from the same area, information about topography can be attained. This is achieved by subtracting the phase information of one image from the other, forming what is called the phase interferogram (see section 3.3.3)

With regards to the method employed to obtain SAR images, there are two approaches for SAR interferometry: Along-track or Across-track interferometry. In Along-track interferometry, two radar antennas are mounted on the same platform and in the same direction as the flight direction. One of the antennas transmits but both receive the backscatter signals; so both images are acquired by the same target at almost the same time. A slight time delay exists, which depends on the baseline and flying speed (Chang, 2008). The typical example of application of this method is the SRTM mission (see section 3.1.2). Across-track interferometry exploits repeated orbits of the same satellite to take images required for Interferometric processing (Figure 3.5). In this method SAR images are acquired by the same satellite or two satellites with same path and same imaging geometries (for example ERS-1 and 2) passing same the area but at different times. The distance between the two positions of satellite/s (or their orbits) in the plane perpendicular to the satellite/s path (or their orbits) is called the baseline and its projection perpendicular to the slant range is the perpendicular baseline (Ferretti et al, 2007).

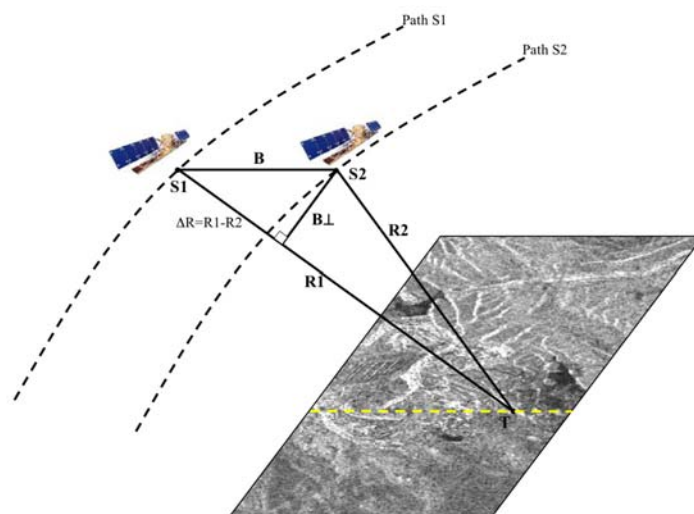


Figure 3.5: Geometry of acquisitions for InSAR processing. S1 and S2 are the 2 satellite positions, B the baseline, R1 and R2 the ranges to target T and B_{\perp} the perpendicular baseline.

Figure 3.5 represents that the relation between the phase and slant range R (The distance between antenna and target) can be defined as:

$$\varphi = 2\pi \frac{2R}{\lambda} + \varphi_0 \quad (3-1)$$

Where:

φ : Total phase

φ_0 : Scattering part due to interaction of the signal wave and the ground

λ : Radar wavelength

R : Slant range between satellite and target

Essentially, the total phase for each point is calculated as the sum of a propagation part, proportional to the round-trip distance ($2R$) and a scattering part due to interaction of the signal and the ground (Klees and Massonnet, 1999). Assuming two images acquired in two different times and with no difference in scatterer properties between the acquisition times, the phase difference can be written as a measure of the difference in slant-ranges:

$$\Delta\varphi = 2\pi \frac{2\Delta R}{\lambda} \quad (3-2)$$

Clarified by Equation 3-2 and Figure 3.6, given the phase difference, it is possible to estimate the displacement in range direction (ΔR) for each pixel of the image. It is highly important to understand that phase difference can be precisely measured but only as a fraction of the radar wavelength. A phase interferogram contains pixel by pixel fractional phase differences (Klees and Massonnet, 1999). In other words, $\Delta\varphi$ can be measured only modulo 2π :

$$\Delta\varphi = \Delta\varphi_{frac} + 2\pi N \quad (3-3)$$

Where, N is an integer representing the number of complete cycles that should be determined and added separately to fractional phase in order to reconstruct the real total phase difference.

For the purpose of detecting surface deformations, the ultimate goal is to keep the position of the satellite at the time of second acquisition identical to its position at the time of first acquisition ($B = B_{\perp} = 0$). In such situations there would be no sensitivity to topography and consequently any phase difference can be assumed to be the result of surface motion in the direction of the radar line of sight. However, in reality it is not possible and baseline between positions of satellite at the time of acquisition is not zero (Figure 3.6).

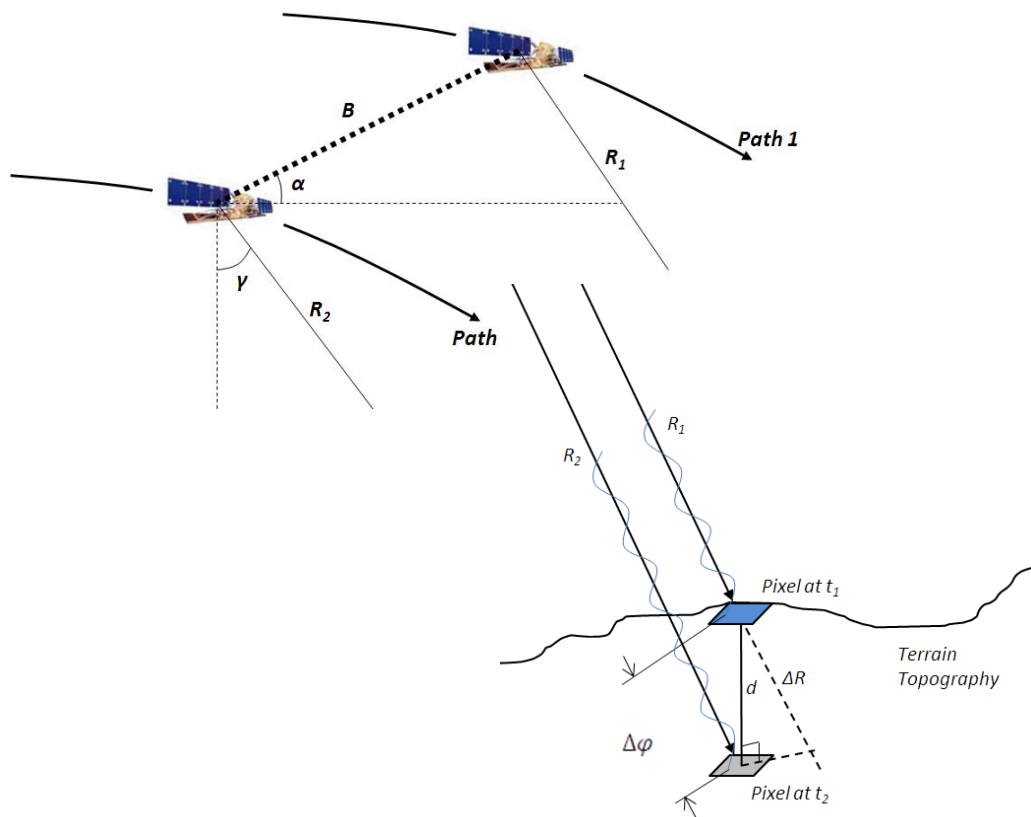


Figure 3.6: Geometry of InSAR with non-zero baseline (modified after Klees and Massonnet, (1999))

Taking non-zero baseline into consideration, Equation 3-2 should be rewritten as following:

$$\Delta\varphi = \frac{4\pi}{\lambda} \times \left(\Delta R + B \sin(\alpha - \gamma) + B \frac{\cos(\alpha - \gamma)}{R \sin \gamma} \right) \quad (3-4)$$

In order to have only the component associated with surface deformation, two new added terms should be removed. The first of added terms is related to the

baseline and satellite geometry, so it can be easily calculated. Second term is due to topography. Additional data is required to determine and remove this component. Availability of either a high resolution DEM or a third SAR image of the same scene is necessary for removing contribution of topography to the phase difference. In case of using a DEM the technique is called a two-pass InSAR. In case of using a third SAR image, it is a differential SAR interferometry or DInSAR.

Using a DEM, height information can be converted into phase and then be transferred to SAR coordinate. The result will then be subtracted from the phase interferogram that leaves a differential phase only related to surface deformation. If a third image is available, then two interferograms will be generated, one for images taken at the times t_0 and t_1 and one between images taken at the times t_1 and t_2 . Applying this situation in Equation 3-4 will lead to the following Equation:

$$\Delta R_{1,2} - \Delta R_{0,1} \frac{\bar{B}_{1,2}}{\bar{B}_{0,1}} = \frac{\lambda}{4\pi} \left(\Delta\varphi_{1,2} - \Delta\varphi_{0,1} \frac{\bar{B}_{1,2}}{\bar{B}_{0,1}} \right) \quad (3-5)$$

Where $\bar{B}_{1,2}$ and $\bar{B}_{0,1}$ are the components of the baseline parallel to the look direction in the images taken at t_1 and t_2 (Zebker et al., 1994). In the DInSAR technique, the first pair is only supposed to contain a topographic component. In order to achieve such a goal two images for constructing first pairs are usually selected with a smallest possible temporal baseline that keeps the surface deformation component as small as possible, near to zero. Assuming no surface deformation between the time t_0 and t_1 , surface deformation over the time interval t_1 and t_2 can be calculated using Equation 3-6:

$$\Delta R_{1,2} \approx \frac{\lambda}{4\pi} \left(\Delta\varphi_{1,2} - \Delta\varphi_{0,1} \frac{\bar{B}_{1,2}}{\bar{B}_{0,1}} \right) \quad (3-6)$$

This fundamental equation invokes critical considerations in surface deformation detection using InSAR summarised by Klees and Massonnet (1999) and also Dixon (1995). Some of these remarks are as follows:

- InSAR is only able to provide the line-of sight component of the three-dimensional surface displacement vector. For extracting two components of the deformation vector, processing of both ascending and descending images is required.

- As mentioned before, radar-scattering characteristics within each pixel must not change over the period between two acquisitions. Otherwise, the phase component caused by the interaction of the signal and the ground (φ_0) cannot be removed. If radar-scattering characteristics within each pixel strongly changes, it causes the temporal decorrelation which is one of the main limitations of InSAR. Vegetation, wind effects, soil moisture, snow fall and farming activities are the most common reasons for temporal decorrelation.
- The total phase difference can only be measured as modulo 2π ; Therefore, for each pixel of the interferogram, fractional phase difference must be converted to the total phase difference by adding complete cycles required for that pixel. This process is called phase unwrapping.
- Large, rapid displacements cannot be detected with InSAR. The displacement gradient between adjacent pixels must be less than half of the radar wavelength, otherwise the phase difference will be ambiguous.

To provide a better understanding, the total phase difference can be written as a sum of phase components due to topography, surface deformation and noise components including atmospheric effects. Different sources of phase noise will be discussed in the next section:

$$\Delta\varphi = \Delta\varphi_{Topography} + \Delta\varphi_{Surfacedeformation} + \Delta\varphi_{Noisesanderrors} \quad (3-7)$$

3.3. InSAR Limitations

3.3.1. Limitations due to Phase Noise and Errors

3.3.1.1. Atmospheric Effects

Considering different times for acquiring interferometric SAR images, the travel time for each acquisition can be affected differently by the atmosphere. Different atmospheric humidity, temperature and pressure between the two acquisitions may cause phase shift in total interferometric phase which can be detected in the

interferogram as additional fringes. Atmospheric effects impact on both altitude and terrain deformation measurements (Ferretti et al., 2007).

Carnec et al. (1996) showed that atmospheric effects have less impact on small scale deformations rather than large scale deformation and can be neglected during the data processing and interpretation process.

3.3.1.2. Temporal Decorrelation

As mentioned before, radar-scattering characteristics within each pixel must not change over the period between two acquisitions in order to be able to omit the phase component caused by the interaction of the signal and the ground (φ_0). Strong change in radar-scattering characteristic within each pixel will cause the temporal decorrelation which is mainly due to vegetation, soil moisture and snow fall or ice melting. This problem can be solved by using phase-stable targets, such as buildings, other anthropogenic infrastructure and rock or gravel outcroppings. If the natural targets are not available the artificial targets could be utilised as alternatives. Radar reflectors are the most widely used phase-stable targets which are installed specifically for this purpose. Also recently introduced SAR transponders can be utilised. Such approaches should also allow for accurate georeferencing of SAR scenes and consequently increase the accuracy of subsidence monitoring (Zebker and Chen, 2005).

3.3.1.3. Phase Noise due to Different Look Angle

Since the relative locations of the scattering cells depend on the satellite look angle, different observation geometries between acquisitions causes variation in the phase (Zebker and Goldstein, 1986). The different look angles are denoted by the satellite baseline or the difference in orbit position between two paths of the satellite (Power et al, 2006). Taking the above into consideration, there is a critical baseline above which the interferometric phase is totally noise. The critical baseline depends on the dimension of the ground range resolution cell (also the terrain slope), the radar wavelength and the slant range to the target. For ERS satellite, the critical baseline for a horizontal terrain is about 1150metres. The critical baseline decreases for

positive terrain slopes and increases for negative ones (Ferretti, 2007). This phase noise component can be removed from the interferogram using spectral shift or common band filtering.

3.3.1.4. Phase Noise due to Volume Scattering

Volume decorrelation usually occurs over vegetated regions. The dielectric properties and alignments of tree leaves and branches are sources for the variation of the backscattered radar signals and phase noise (Chang, 2008). In this case the noise changes depend on the depth of the volume occupied by the elementary scatterers (trees) and local weather conditions, such as rain and wind. It is possible to minimise the effect of volume decorrelation using SAR images with smaller resolution (Zebker and Chen, 2005).

3.3.2. Geometry Related Limitations

3.3.2.1. Geometric Distortions (Layover, Shadow and Foreshortening)

The Synthetic Aperture Radars are side-looking radars and they are affected by certain geometric distortions of the terrain. These distorted areas must be treated carefully during data processing and post-processing steps. The results obtained from these areas are usually useless for interferometry analysis. Main geometric distortion associated with SAR images are foreshortening, shadow and more important to mining applications, layover. Figure 3.7 provides a schematic view of these distortions describing their extent on the image (slant-range) and on maps.

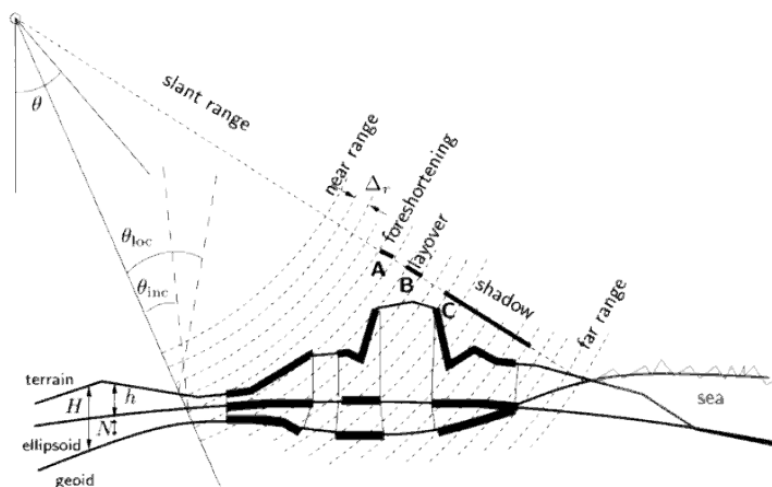


Figure 3.7: Geometric distortions, foreshortening (A), layover (B) and shadow (C) (Hanssen, 2001)

Foreshortening occurs when radar signal reaches the bottom part of a tall target, also tilted towards the radar, before it reaches its top. In this case, the slope will appear compressed and the length of the slope will be represented incorrectly on the image. The shadowing occurs when part of the terrain cannot be viewed by the sensor as angle increases with greater incident angle of the satellite.

Layover is commonly seen in SAR imagery containing severe terrain variations. It occurs when the top of a topographic feature is closer (of smaller slant-range) than features on the slopes; this results in the superposition of large areas into only small numbers of pixels in the slant range image which are useless for interferometric analyses. The altered terrain topography, involving steep slopes and deep pits are typical of any mining activity; this may lead to the layover of radar signal (Figure 3.8).

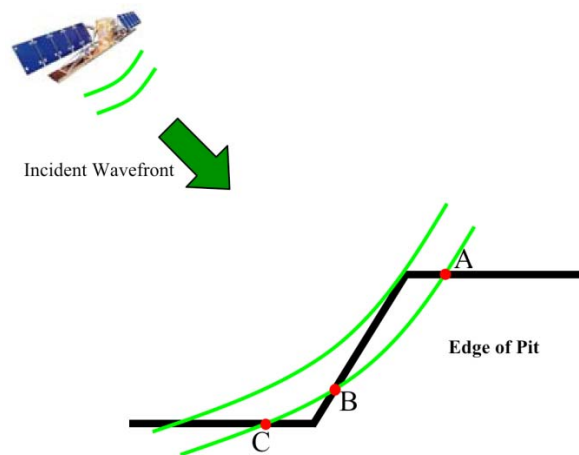


Figure 3.8: Layover points (A, B and C) will fall into the same cell of the SAR image

3.3.2.2. *Ambiguous Height*

This limitation can be described by considering the two aspects of Gradient and Ambiguity. As commented by Massonnet and Fiegl (1998) the maximum detectable deformation gradient in interferometry is one fringe per pixel. This means deformation rate cannot exceed the dimensionless ratio of the pixel size to the wavelength. This value depends on the satellite, for instance it is 0.003 for ERS. To avoid such problems, temporal baseline between images must be selected with respect to the gradient of deformation in order to remain below this threshold. However, deformations provoking large gradient limit, within a period of time less than the satellite's repeat cycle, are not datable by interferometry.

As mentioned in section 3.2.2, the total phase difference can only be measured as modulo 2π and therefore interferogram only contains fractional phase difference. At this stage, interferogram is termed “wrapped”. It is possible to “unwrap” an interferogram by adding complete cycles required for each pixel to the fractional phase difference obtaining the total phase difference. Phase unwrapping is very complicated and involves pure mathematics and also depends on different factors such as the imaging geometry, the terrain, and the phase noise level. The simplest method to find the true number of cycles is to simply count the fringes along a path, numbering each one in succession; however more sophisticated automatic algorithms were developed and used for phase unwrapping in today’s studies (Massonnet and Fiegl, 1998).

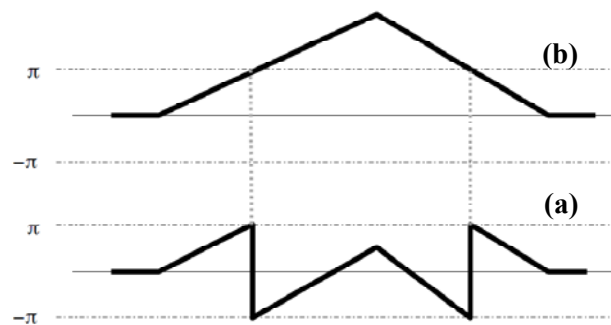


Figure 3.9: Wrapped phase (a) and unwrapped phase (b)

There is also another source of ambiguity. Interferograms only record relative changes in phase and not absolute changes and so it is allowed to add a constant value to all the pixels. Selection of a proper constant would be problematic. This ambiguity exists even after the unwrapping step. Usually, this constant is set by assuming no deformation at one point or using independent measurement by GPS or classical surveys (Massonnet and Fiegl, 1998).

3.4. General InSAR Processing Steps

General procedure for InSAR implementation is shown in Figure 3.10. It starts with selection and acquiring required data usually in SLC (Single Look Complex) format and ends with DEM or deformation map.

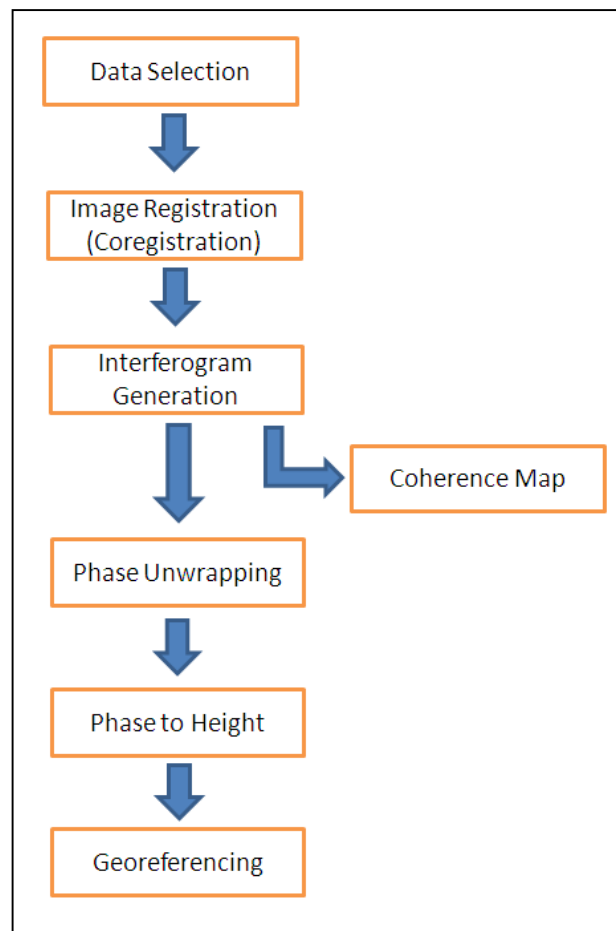


Figure 3.10: General procedure for InSAR implementation

3.4.1. Data Selection

Adopting a well-defined data selection strategy and taking all aspects of the application into the account is crucial for any interferometry analysis. Using a suitable set of images, it would be possible to optimise reliability and accuracy of the results, as well as minimising adverse effects of noise and errors. General parameters necessary to be considered in the process of data selection can be listed as following:

- Purpose of the study (DEM generation or surface deformation analysis)
- Adopted interferometry technique (2-pass, 3-pass, 4-pass)
- Which Look angle is available and required (Ascending or Descending passes)?
- Geometrical baseline
- Temporal baseline
- Time of the acquisition

- Expected phase noise
- Meteorological conditions

3.4.2. Coregistration

The basic concept of SAR interferometry is to calculate the phase difference, pixel by pixel between two different images, so it is critical to precisely relate two images together ensuring that each ground target contributes to the same pixel (range, azimuth) in both images. This process is called coregistration.

According to Massonnet and Fiegl (1998), coregistration involves three steps:

1. Evaluation of the geometric differences between the two radar images: From different approaches adopted by different studies of conventional correlation of amplitude image patches, it is more suitable considering its accuracy (up to 0.03 pixels) (Li and Goldstein, 1990; Massonnet, 1994).
2. Modelling the geometric differences; usually least squares method is used.
3. Resampling one of the images (usually referred as slave image) in order to be superposable to the other (usually referred as master image) with respect to the phase content. Conventional resampling process usually includes one of nearest neighbour, bilinear or cubic methods.

3.4.3. Interferogram Generation

After precisely overlying the two SAR images, interferogram containing the pixel by pixel phase difference can be calculated. Interferogram is mathematically defined as the Hermitian product of two coregistered images. It requires the pixel to pixel computation of following Equation (Graham, 1974):

$$v_i = u_M \times u_S^* \quad (3-8)$$

Where:

u_M : Master images and u_S : Slave image

An illustration of SAR interferometry concept is shown in Figure 3.11.

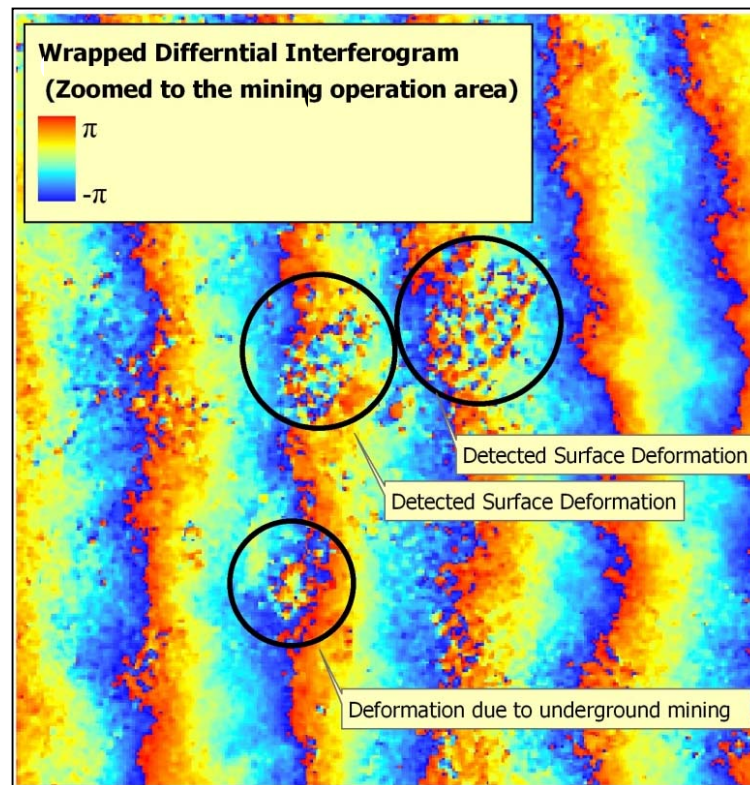


Figure 3.11: Sample of a phase interferogram resulted from differential SAR interferometry for Perseverance Mine, WA, Australia (Jarosz and Zahiri, 2007)

3.4.4. Complex Multilooking

The interferogram is usually noisy, and in particular in case of repeat-pass acquisitions in which strong effects of temporal decorrelation may introduce more noise to the interferogram. Reducing the noise can be done by averaging over neighbouring pixels that improves the signal-to-noise ratio (Ferretti et al., 2007). This process is called complex multilooking. The result would be a less noisy interferogram and with square shape pixels. It should be mentioned that before interferogram generation and during the step for reading images, the multilooking process is usually performed in order to decrease the amount of calculations and also improve image visualising.

3.4.5. Generating Coherence Map

Coherence provides a useful measure that determines quality of the interferogram. It is the complex correlation coefficient of the two SAR images and is calculated from Equation 3-9:

$$\hat{\gamma} = \frac{\sum_{n,m} u_1(n,m).u_2^*(n,m).e^{-j\varphi(n,m)}}{\sqrt{\sum_{n,m}|u_1(n,m)|^2 \sum_{n,m}|u_2(n,m)|^2}} \quad (3-9)$$

Where: $\varphi(n,m)$ is the phase contribution due to topography, with the linear approximation (Ferretti et al., 2007)

Coherence ranges from 0 to 1. In fact, it is a complex quantity; however usually it is the absolute value which is commonly used. Coherence measures the reliability of the measurement. A value close to zero means a meaningless phase measurement (Massonnet and Fiegl, 1998).

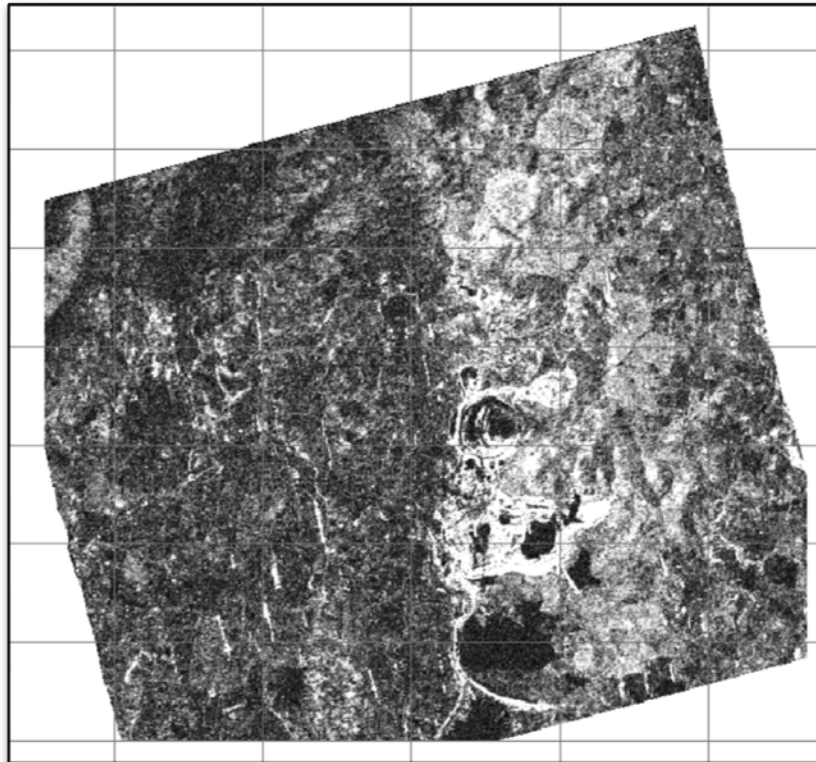


Figure 3.12: Coherence map over Ridgeway gold mine, NSW, Australia, generated from two ALOS images with temporal baseline of 44 days

3.4.6. Phase Unwrapping

As mentioned in section 3.3.2.2, phase unwrapping is a necessary step in which the total phase difference is calculated by adding complete cycles required for the given pixel to the fractional phase difference in that pixel. Having the total phase difference of the interferogram, it would be possible to calculate the height or deformation of the terrain. The most commonly used phase unwrapping techniques are path-following methods (Branch-Cut algorithm by Goldstein et al., 1988), and Minimum-Norm methods.

3.4.7. Phase to Height

The calculated total phase difference will be converted to height using Equation 3-4. It is again necessary to be noted that interferometry only measures the relative height differences between the pixels and one or more reference points are required to obtain the absolute height information.

3.4.8. Georeferencing

So far all processing steps are done in SAR coordinate and in slant-range; However in order to properly use the resulted map it is necessary to transfer the image from slant-range projection into a standard geographic coordinate system. This process is referred as Georeferencing or Geocoding.

3.5. Chapter Summary

This chapter aimed to provide an overview of SAR interferometry development, stages of its evolution and applications. It discussed principles of SAR imagery, SAR interferometry and limitations of the technique including limitations due to phase noises (e.g. atmospheric effect, temporal decorrelation...) and geometry related limitations (geometric distortion and height ambiguity). General InSAR processing steps were also discussed in details.

Chapter 4

Geographical Information Systems

Background

Chapter 4

Geographical Information Systems Background

4.1. What is GIS?

The Geographical Information Systems (GIS) is an environment consisting of tools that deals with spatial realities. It combines data and information with computer technology and its supporting infrastructure (Davis, 2001). There are numerous definitions of GIS that reflect its different applications. Considering its application as a toolbox, Burrough (1986) defines GIS as a powerful set of tools for collecting, storing, retrieving at will, transforming and displaying spatial data from the real world. Smith et al. (1987) defined GIS as a “database system in which most of the data are spatially indexed, and upon which a set of procedures operate in order to answer queries about spatial entities in the database”. With respect to databases, Aronoff (1982) defined GIS as “any manual or computer based set of procedures used to store and manipulate geographically referenced data”. Furthermore, Ozemoy et al. (1981) defined that GIS is “an automated set of functions that provides professionals with advanced capabilities for storage, retrieval, manipulation and display of geographically located data” which can be considered as an organisation based definition. According to Fischer et al. (1996) GIS is a set of tools for analysing spatial data involving four main functions: data input, data storage, management data analysis and retrieval, and output.

As a comprehensive definition, GIS software developer ESRI (Environmental Systems Research Institute) defines GIS as “An integrated collection of computer software and data used to view and manage information about geographic places, analyse spatial relationships, and model spatial processes. A GIS provides a framework for gathering and organizing spatial data and related information so that it can be displayed and analysed” (ESRI, 2009).

As commented by Davis (2001), GIS functionalities can be categorised into following categories:

- **Collection:** Gathering data from many sources including remote sensing, digitising paper maps, internet and other digital products, fieldwork, tabulated data, reports and human input.
- **Storage and Management:** Providing digital storage, administering and keeping track of data including integration of different datasets into common database and database management.
- **Retrieval:** Possibility to select and view data in a variety of ways
- **Conversion:** Changing the data form or map format to match another, this task includes converting map projections or reclassifying them.
- **Analysis:** Analysing data to provide a new set of information using various techniques including data investigation, spatial analysis and other supported methodologies in the GIS environment.
- **Modelling:** Simplifying and generalising data into a form which is easy to understand and to explain the relationships between objects and observed phenomena.
- **Display:** This function generates flexible visual and interactive maps, photos, graphs and reports.

GIS allows a large amount of data to be easily handled within the environment provided by a spatial framework. It provides easy access to information regarding the relative location of objects and events. GIS also has the ability to link different types of objects and events. Hence, GIS has the capability to utilise integrated methods to combine different spatial datasets and to uncover and estimate the relationships between them, and then provide a range of diverse spatial models (Zahiri and Baafi, 2008; Fischer et al. 1996).

4.2. What is Spatial Data?

Two types of information are provided by spatial datasets; positional and thematic data (Fischer et al., 1996). Positional data specifies the locations of objects in space, topology and spatial relationships that may be projected in point, line or

polygon formats. Thematic data are non-spatial attributes of objects that describe the various characteristics of the geographic features. In other words, spatial data shows the spatial characteristics of the object and thematic data describe various characteristics of the object (Zahiri and Baafi, 2008).

Spatial data in GIS are commonly displayed in two formats, raster or vector (Figure 4.1). The raster format represents an area by dividing the area into a grid containing a number of uniform grid cells (Martensson, 2000). A cell is the smallest size in which any feature can be projected and each cell is given a specific value or single feature identity. Satellite images including SAR-SLC images and also Digital Elevation Model (DEM) are examples of data in raster format. The digital datasets produced by digitising or the remote sensing process are commonly in the raster format. Most of the spatial analysis functions provided in GIS extensions require data in the raster format.

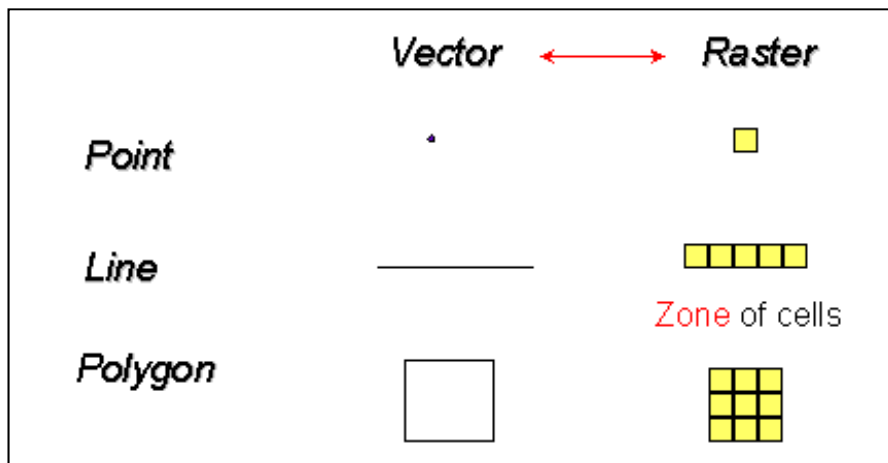


Figure 4.1: Positional data in raster and vector format (Zahiri and Baafi, 2008)

Vector data represents an object's position and direction. GIS based maps produced using vector data are similar to a drawn map of the area. Each of the points, lines or polygons in vector format are analogue and they are not broken into cells (Davis, 2001). In general, the vector format data provides images more similar to the real world than the raster datasets (Davis, 2001). Vector format data is more suitable for projecting individual features such as sampling locations, watercourse, infrastructures or a mine working area.

Figure 4.2, vector-based representation results in images similar to reality, though providing less flexibility for analysis of the data. Nevertheless, a raster-based representation produces different classes for different landscape features. The problem with the raster data is the limitation caused by definition of cell size. The problem is that the borders between the different classes may not coincide with the cell borders that cause many cells to be a mixture of several classes. However the classified grid structure provides more suitable data for spatial data analysis allowing greater ease for storing and computation of data.

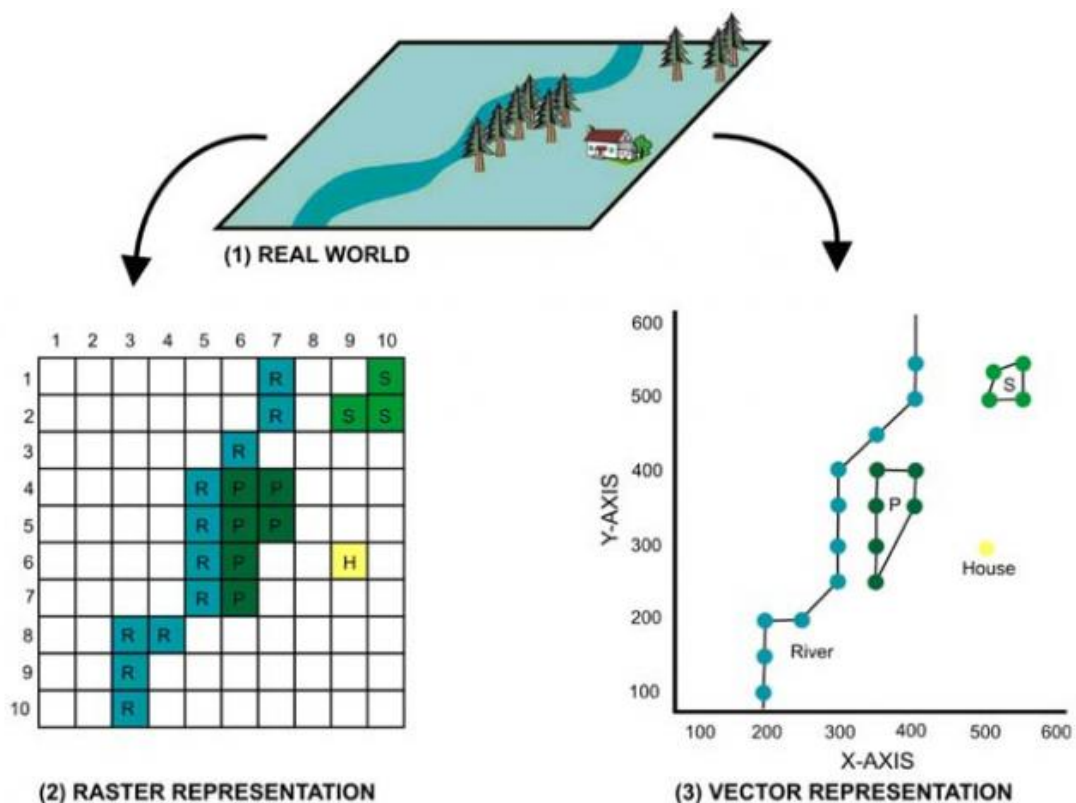


Figure 4.2: Raster and vector format (HLURB, 2007)

4.3. GIS and Spatial Analysis

In general, spatial analyses are quantitative techniques and procedures to analyse the pattern of spatial data. Spatial analysis includes two main aspects of statistical data analysis and spatial modelling. Statistical analysis allows calculating of descriptive and inferential statistics. Spatial modelling aims to generate different

types of models describing spatial datasets. These models can be deterministic and stochastic process models, location-allocation models, spatial interaction models, spatial choice models or predictive models (Zahiri and Baafi, 2008).

Today, spatial analyses are part of almost any GIS projects and are used in a wide range of applications including spatial planning, developing models, methodologies and decision-making tools. The spatial analyst tool in common GIS software provide sets of tools to perform different sorts of analyses including create, query, map, and analyse cell based raster data, create surfaces using interpolation tools, perform statistical analysis, zonal analysis, calculate complex terrain attributes, find suitable locations based on multiple attributes and prepare data for further analysis or display.

4.4. GIS, InSAR and Geoprocessing

Numerous tools are usually available in any GIS software; however there is a lot of demand to develop new tools and add further capabilities into GIS environment. The geoprocessing provides a framework for users to design and develop their own small new software which can be managed by the system and be a part of that. ERSI (2009) defines geoprocessing as “A GIS operation used to manipulate GIS data. A typical geoprocessing operation takes an input dataset, performs an operation on that dataset, and returns the result of the operation as an output dataset. Geoprocessing allows for definition, management, and analysis of information used to form decisions.” In ArcGIS Desktop, geoprocessing can be carried out using two main approaches or their combination:

1. Models and ModelBuilder that allow users creating new tools by chaining existing tools into a sequence.
2. Scripting, that allows users using a scripting language to write their own tool from scratch. There are two types of programming languages: system languages such as C++ and Java and Scripting languages, such as Python and Perl. System languages use low-level primitives and the raw resources of the computer to develop an application from scratch. Scripting languages use built-in higher level functions or modules to

glue applications together. They are obviously easier to learn rather than system languages. The most commonly used programming language between ArcGIS Desktop users is Python. It is well supported by ESRI and also there are a lot of Python modules (set of functions dedicated to the specific application) which are available to ease the scripting task and working with spatial data.

There is not much to mention regarding integration between GIS and InSAR. Though integrating GIS capabilities into interferometry data processing can be very advantageous; however none of the previous InSAR studies highly involved GIS or directly performed using a GIS-based approach. GIS functionalities usually have been used only for post-processing of the result or InSAR result visualising (Ge et al., 2003b; Change et al., 2004; Jarosz and Zahiri, 2007).

Many valuable tools can be generated using geoprocessing to ease the interferometry process. GIS can be involved in feasibility and data selection studies allowing detecting levels of ambiguity or areas affected by geometrical distortion. GIS can also be used as a value-adding tool and its functionalities will be employed to post-process, interpret and assimilate disparate InSAR results. GIS provides a powerful environment for comparing and integrating InSAR results with other available data at the mine, including: classical surveying, geology and mining progress data. GIS can be integrated into the interferometry process in two ways: It is possible to use GIS and geoprocessing to a develop set of tools to be used in different stages of the process or even whole process can be written in GIS environment.

4.5. Chapter Summary

The chapter provided a brief background of Geographical Information Systems (GIS), its definitions and key functionalities. It also discussed possible applications of GIS and geoprocessing to ease the InSAR process.

Chapter 5

InSAR Toolbox

for Mine Subsidence Monitoring

Chapter 5

InSAR Toolbox for Mine Subsidence Monitoring

5.1. What is InSAR Toolbox?

The main objective of the current research was to use GIS-based methodologies and integrate them with conventional InSAR techniques to improve and facilitate the general InSAR process and also with respect to its applications in mining domain, particularly subsidence monitoring. Using GIS functionalities, InSAR process can be facilitated; result validation can be improved; integration with other method can be eased and more practical results can be generated. On other hand, new GIS-based tools can be developed in order to detect InSAR limitations and to determine their level of influence on the produced results. These research follows two main approaches, one is to modify the technique taking specifications of mining-induced deformations into the account; and second is to focus on dealing with InSAR limitations.

The SAR interferometry by itself is complicated and consequently InSAR processing software has a high level of complexity that requires a relatively long time to be understood and mastered. Several open-source and commercial software are available which are dedicated to the SAR interferometry data processing and offer different levels of complexity. Despite the variety of such software, only a few of them include options or provide tools to conveniently integrate InSAR process and results with GIS environment and one of the objectives of the thesis was to provide GIS-based software capable of performing SAR interferometry with a reasonable level of complexity suitable for ordinary users. This provides the possibility to perform whole process inside the GIS environment and employing GIS functionalities before, during and after processing.

The thesis introduced a set of new GIS-based developed tools and methodologies in the shape of a toolbox, covering three main stages of pre-processing, data processing and post-processing. The objectives of producing such tools are:

- Providing a mining-oriented methodology for InSAR,
- Providing a simple and user-friendly environment to run InSAR processing steps,
- Integrating InSAR and GIS in order to propose an optimum data processing methodology.

The InSAR module was developed as a toolbox inside ArcToolbox of ArcGIS desktop as one of the most popular GIS software used by mining industry. Toolbox is an object in ArcGIS that contains toolsets and geoprocessing tools performing similar task or covering different aspects of a processing chain. ArcToolbox is where all these toolboxes can be accessed: a user interface in ArcGIS that provides several tools and toolboxes for accessing, organizing, and managing a collection of geoprocessing tools, models, and scripts (ESRI, 2009).

Raspberry is a set of scripts originally developed for Matlab 7.4.0 (R2007a) for ALOS PALSAR data processing which is later modified to be able to also process ERSs, Envisat and TerraSAR-X data. Raspberry upgrading is still continued by its developer to add new capabilities including a PSI algorithm implementation (Sowter, 2009). Only phase unwrapping from the SAR interferometry data processing chain is not included in Raspberry which is due to its high level of complexity. To perform phase unwrapping, the free Snaphu programme designed by Stanford Radar Interferometry Research Group (Chen and Zebker, 2000a) was used.

Figure 5.1, shows the structure of the InSAR toolbox that includes three levels of processing and one toolbox containing miscellaneous tools.

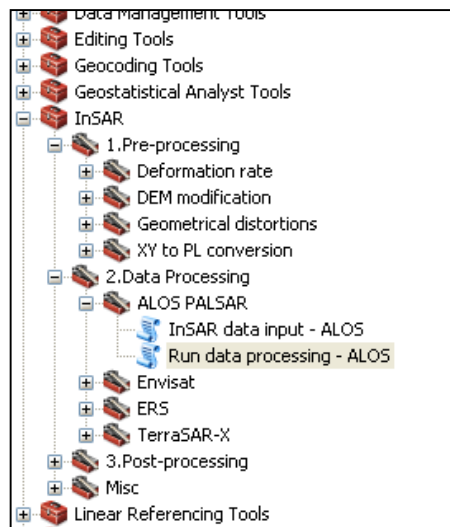


Figure 5.1: Snapshot of InSAR Toolbox in ArcGIS Desktop

Geoprocessing framework provided by ArcGIS Desktop supports three of the most popular languages: VBScript, JScript, and Python. Between them Python is most recommended as the best choice for writing scripts in ArcGIS by developer (ESRI, 2009). Considering advantages offered and its easy integration into ArcGIS Desktop, Python was selected for developing designed tools and body of the InSAR data processing toolbox.

The main advantage of using Python is the ease of use of a scripting language as well as the programming capabilities of a complete developer language. Furthermore, it is a platform-independent programming language and can operate on a variety of operating systems, therefore by applying very small modifications, the developed scripts can be used as stand-alone programs outside of the ArcGIS environment and also in different platforms including UNIX, Linux, and Windows. Python 2.5 and PythonWin 2.5.1 (Python IDE¹ and GUI² Framework for Windows) were used to write scripts.

Some of the Python advantages are as following:

- Python is simple to learn because of its clean syntax and simple, clear concepts.

¹ IDE: Integrated Development Environment

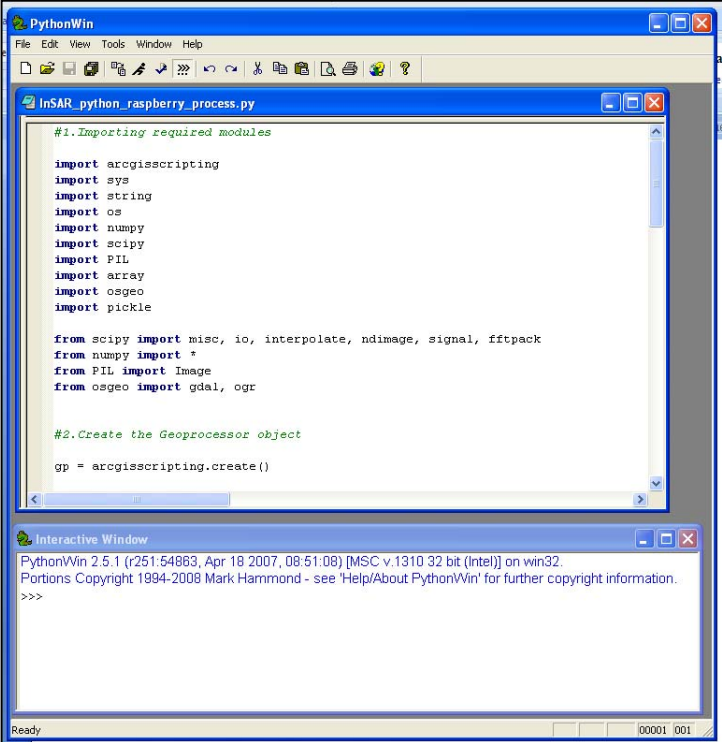
² GUI: Graphical User Interface

- Python supports object-oriented programming in an easy-to-understand manner.
- Documenting Python is easy because it has readable code.
- Complicated data structures are straightforward to work with in Python.
- There are numerous python binding methods (libraries containing tools and functions) that are available to be imported to Python IDE and used for performing specific tasks.
- Python is free.

As mentioned above, lots of Python binding are available which can be imported to Python IDE to run different sorts of analyses. One of these libraries is ‘arcgisscripting’ that includes all the geoprocessing functions available within ArcGIS. It creates an object that provides a single access point and environment for the execution of any geoprocessing tool available in ArcGIS, including extensions (ESRI, 2009). Along with arcgisscripting library, GDAL (Geospatial Data Abstraction Library) is also used for reading and writing raster geospatial data formats. GDAL is an open-source library with a Python compatible binding that support almost the entire available raster formats, even several types of SAR images. It also includes several functions for data translation and processing.

Two other important bindings used for scripting are Scipy and Numpy. Scipy is an open-source library of algorithms and mathematical tools specifically designed for Python. It provides several modules covering tasks such as optimization, linear algebra, integration, interpolation, special functions, FFT, signal and image processing (Scipy, 2009). Numpy is a Python binding for working with large, multi-dimensional arrays and matrices; it provides a large library of high-level mathematical functions to operate on these arrays (Numpy, 2009). Scipy and Numpy together offer similar capabilities as Matlab. During the development of the InSAR toolbox, these libraries were used in many occasions to translate Matlab scripts to Python easing the process. It might be interesting to mention that as the next step of this research, all data processing steps can be directly written in Python to avoid using Matlab in the background; however the now process uses a combination of

Matlab and Python scripts which requires invoking and running Matlab in the background.



```
PythonWin
File Edit View Tools Window Help
InSAR_python_raspberry_process.py
#1.Importing required modules
import arcgisscripting
import sys
import string
import os
import numpy
import scipy
import PIL
import array
import osgeo
import pickle

from scipy import misc, io, interpolate, ndimage, signal, fftpack
from numpy import *
from PIL import Image
from osgeo import gdal, ogr

#2.Create the Geoprocessor object
gp = arcgisscripting.create()

Interactive Window
PythonWin 2.5.1 (r251:54863, Apr 18 2007, 08:51:08) [MSC v.1310 32 bit (Intel)] on win32.
Portions Copyright 1994-2008 Mark Hammond - see 'Help/About PythonWin' for further copyright information.
>>>
```

Figure 5.2: Snapshot of PythonWin IDE and necessary imported bindings

This chapter introduces new developed tools and methodologies for InSAR application in mining. In the pre-processing stage various tools and procedures will be discussed to deal with different aspects of the techniques including: data selection, data preparation, data review, level of ambiguity and geometric distortions. For the first time, it was possible to implement all InSAR data processing steps inside the ArcGIS Desktop environment. The data processing section describes an InSAR toolbox to run data processing. Furthermore, result interpolation and result preparation steps will be discussed in post-processing section.

It is necessary to mention that the research was carried out under close collaboration with the Institute of Engineering Surveying and Space Geodesy (IESSG) based at the University of Nottingham. The source code for Raspberry, a Matlab script for SAR interferometry developed by Dr Andrew Sowter from IESSG, was used as the main reference for developing tools introduced in this thesis (Sowter, 2009).

5.2. Pre-processing stage, considerations and tools

A typical InSAR study is started with determining suitability of the technique for the given application and data selection or data planning processes. Pre-processing stage also involves processes to detect and determine possible adverse issues due to InSAR limitations. In this section, problematic layover and deformation rate issues will be discussed and some GIS-based tools will be introduced to help to provide better determination of level of their influence on the final result. Also, data selection process and some practical considerations will be discussed in detail.

5.2.1. Layover Analysis

As described in Chapter 3.3.2.1, layover is the most commonly seen distortion in SAR imagery containing severe terrain variations. It occurs when the top of a topographic feature is actually closer (of smaller slant-range) than other features on the slopes. This results in the superposition of large areas into only small numbers of pixels in the slant range image; this situation means layover pixels are useless for interferometric analyses.

Figure 5.3 illustrates the geometry of the descending ERS orbit geometry for a typical open pit. ERS is viewing the pit from the East at an incidence angle of approximately 23° . The satellite sends out short, high energy, pulses and listens for the response; ideally, the oblique incidence angle of the satellite means that only one response from each target on the ground will be received and that, therefore, responses from adjacent targets will not be confused. As can be seen from the figure, this is not the case on the Western side of the pit where the radar wavefronts are striking three or more points simultaneously: on the floor of the pit; on the Western wall; and on the original topographic surface. This means that, in the SAR image, all points will be superimposed, forming a very thin but bright area on the image. This is a region of Layover and the superposition of targets means that an interferometric signal cannot be discriminated, making it a useless area for the analysis.

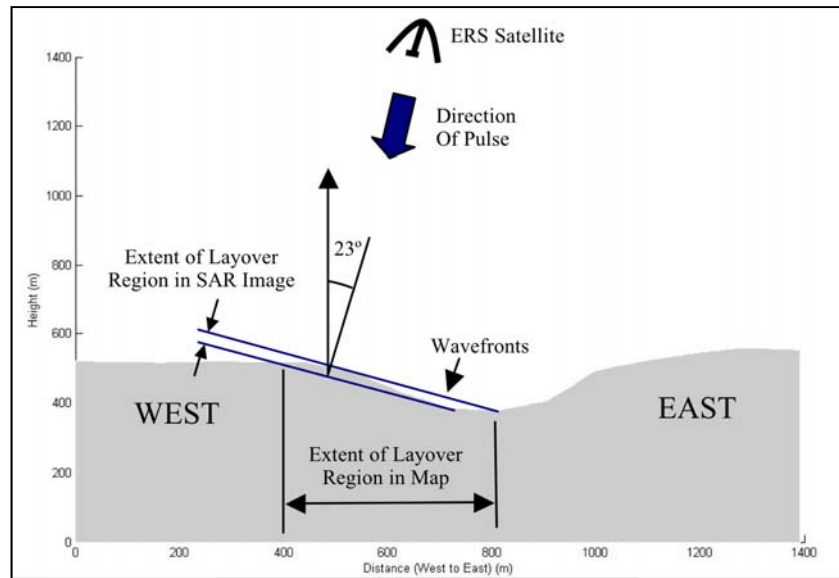


Figure 5.3: Height profile across the pit indicating the layover scenario

It also illustrates that, although a layover region appears small in a SAR image, its extent on the ground can be very large indeed. In the presented example, the layover effect covers an area extending some 400 m across the ground, eliminating the Western half of the pit and a large part of its edge from the interferometric analysis.

In theory, identifying layover pixels in an image should be simple. Assuming a model of the terrain is available, the layover criterion can be expressed as follows: if more than one position on the ground is mapped to the same pixel on the image, then that pixel is in layover. In practice, this is very difficult to implement as the relative size of pixels in relation to the sampling of DEM postings could result in mapping more than one posting to the same pixel without being in layover. A better algorithm is to work along the path of a range line, along the ground, and calculate the change in slant range from posting to posting. If the slant range increases, the pixel is not in layover; if it decreases then the pixel is in layover and every subsequent pixel is too, until the first slant range value is restored. An example of this type of algorithm is shown in Figure 5.4.

The satellite-ground geometry of each DEM posting along a range line is calculated starting at the near-range position and working along each point in turn towards the far range direction. The change in slant range from point-to-point is

calculated. If slant range increases, as for points 1 and 2 in the figure, this is consistent with there being no layover present; when it decreases between adjacent points, as for points 9 and 10, there is layover. In fact, for the latter case, point 9 represents the start of a layover region: all points after that will be labelled as layover until the original slant range value at 9 is restored. In this instance, point 14 is the first point to emerge from the layover region. Once a layover region has been identified using this algorithm, there is some tidying up to do to make sure that some points do not slip through the net.

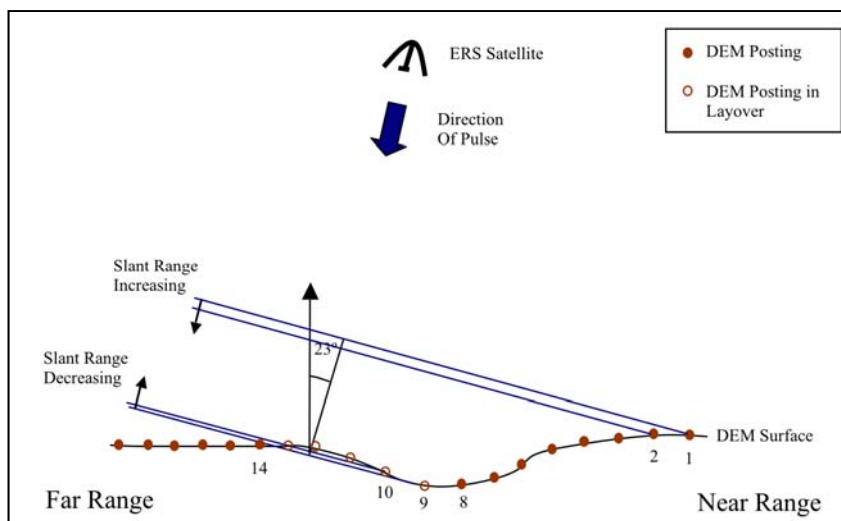


Figure 5.4: Estimating the layover from the DEM postings

The most difficult part of this task, though, is to identify where each image range line falls on the terrain model. A backward georeferencing algorithm, using range and Doppler equations along with a satellite model (Schreier, 1993), was implemented to determine the range line number of every DEM posting. Then, each range line was traced in turn, calculating the slant range along the path from near to far range. Every layover pixel could then be identified in the slant range image and also on the map frame.

When undertaking the InSAR analysis, it was important to identify the precise extent of the layover area as part of the analysis. Distortion tool was developed with such aim. This tool can be used to determine the areas affected by layover and shadow and produce layover-shadow masks for SAR images. The main advantage of having such a tool is the possibility of accessing effect of distortions even before

running whole InSAR processes that can be very helpful in terms of processing time, data selection and quality of results. Such a tool was not available before as a stand-alone tool. SAR values obtained for layover and shadow areas will be rejected during result interpretation process. Figure 5.5, shows input data window of the tool for ERS data.

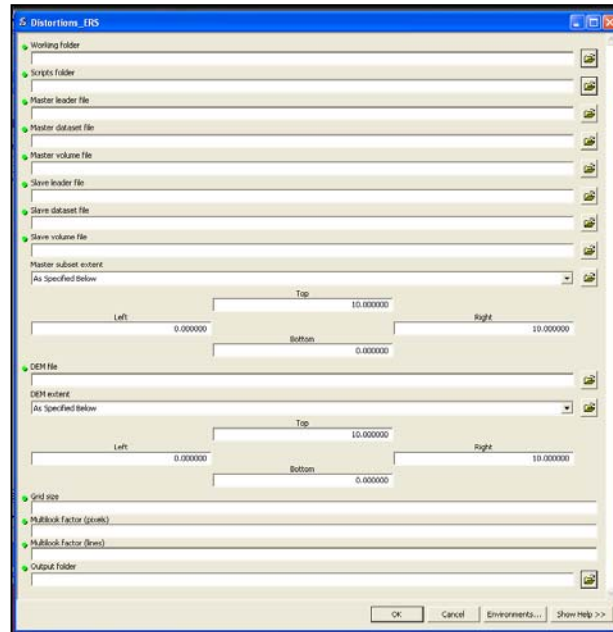


Figure 5.5: Input data window for distortion tool

Figure 5.6 depicts the result of a distortion tool generated for Perseverance pit in Western Australia. The original SAR image for the case study is shown alongside the image with the layover mask superimposed. At the figure presented, the ERS satellite is viewing the terrain from the right hand side of the image.

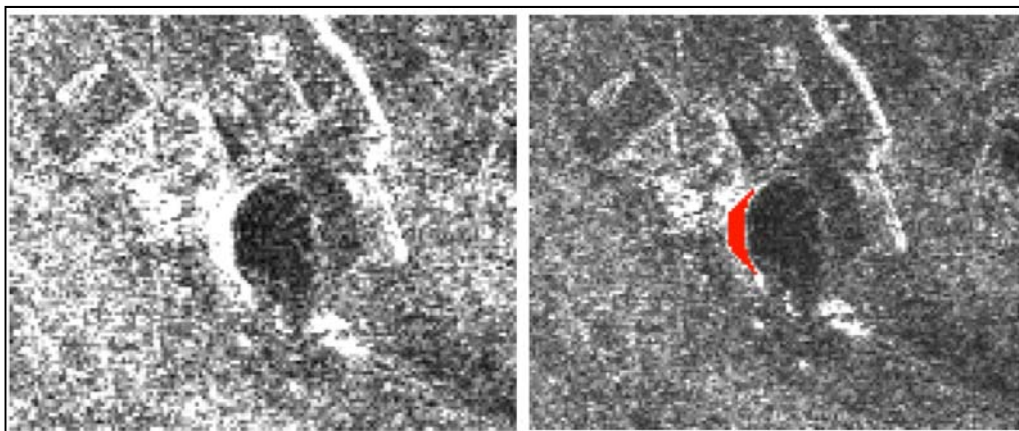


Figure 5.6: A slant range SAR image of Perseverance mine (left) and with layover area highlighted in red (right)

5.2.2. Effects of Using Current and Accurate DEM

The distortion tool made it clear that using an accurate and up to date topographical model is critical for distortion analysis and later data processing. During data processing steps, existence of an accurate DEM improved quality of the result as the topography contribution to phase difference could have been precisely removed. However, the real need of a current DEM is in layover-shadow analysis.

Today, the most common DEM source used in SAR interferometry analysis is the SRTM DEM. The SRTM DEM was generated from data acquired during 2000 (Farr et al., 2000). Therefore, those sites that have experienced significant changes in topography between 2000 and the dates of the SAR acquisitions may find that the SRTM DEM is not accurate enough. In such cases, utilising a current DEM must be considered to include more recent topographical changes into the analysis.

Topographical data are among the most basic data used in any mining application and due to their importance are regularly updated; however this data usually covers small areas directly affected by mining, such as pit, and sometimes not even all mine surface infrastructure, which is subject to mine subsidence. As a solution to this problem SRTM DEM can be used as the main source of the elevation data and then subset of elevation values can be replaced with new values obtained from topographical data provided by mine where they are available. To integrate the new, smaller DEM with the much larger SRTM DEM, the larger DEM should be resampled, as the new data has usually much higher resolution and covers more details. The DEM modification tool accepts topographic data in DXF format (Drawing Exchange Format). DXF format were selected as almost any mine design software can import and export data such as DTMs to DXF format. The final product is a high resolution DEM with up-to-date elevation values. The tool offers different types of resampling methods; the use of an appropriate resampling method that avoids creation of a terrace effect at the boundaries of insertion area, is crucial. Figure 5.7 shows data input windows for the DEM modification tool.

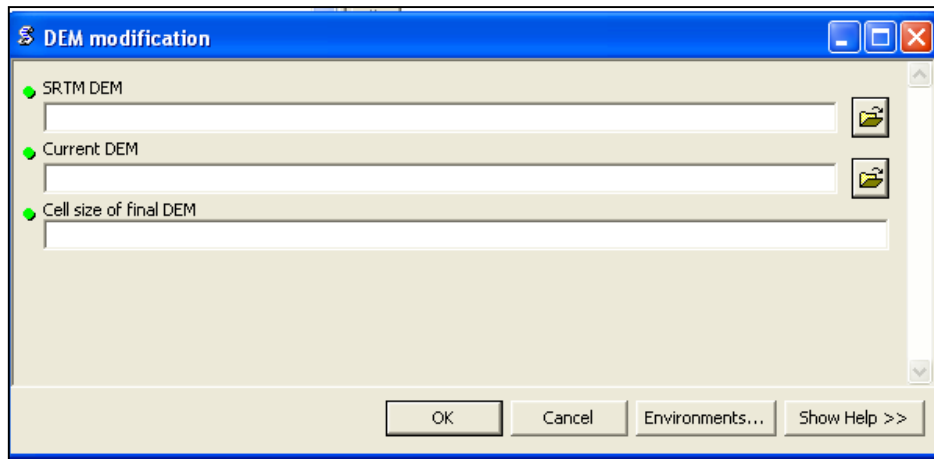


Figure 5.7: DEM modification tool

In order to illustrate the effect of employing current DEM against SRTM DEM for layover analysis, another case study will be briefly discussed, that of Argyle Diamond Mines located in North of Western Australia. The analysis for this site carried out utilised Envisat SAR images with a 7-year gap between the SRTM observations and the acquisitions of the Envisat images. During this time, due to extensive mining activities, noticeable changes of the topography occurred around and inside the pit.

The results of georeferenced SAR image and layover masking using the SRTM DEM and the most current DEM are shown in Figure 5.8. In this image, Envisat is viewing the geometry from the left so the Western wall of the pit is very clear on the left of the image. Inspection of the figure indicates that the SRTM DEM has only partly been able to rectify the image and that the areas we would expect to be smoothly rectified are instead strangely shaped and with inconsistencies in them. For example, the layover area on the Eastern side of the wall still retains some of the sigmoid shape in the original SAR image and there is a dark “hole” in its centre, consistent with there being a mismatch between the simulated distortion and the distortion in the image. The layover mask, although roughly in the correct position, is also strangely shaped and does not match the shape of the bright pixels, which is further evidence that the SRTM DEM is not describing the mine topography properly.

It is evident that there have been significant changes in topography over the study area due to substantial mining activities between 2000 and 2007. To this end a new DEM representing these changes was created using a DTM generated from up-to-date classical and photogrammetric surveys. The new regenerated DEM has been used for creation of a new layover mask. This is shown in Figure 5.8. It is clear from the comparison of Figure 5.8 and 5.9 that a detailed DEM leads toward much more accurate layover mask and therefore better confidence in the InSAR results.

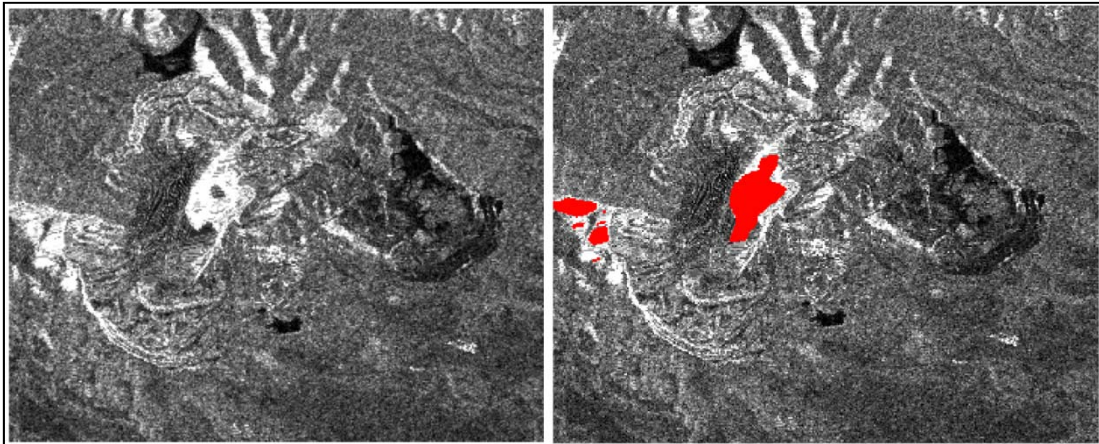


Figure 5.8: The results of Terrain Correction (left) and Layover Masking (right) using the SRTM DEM for the Argyle Diamond Mines

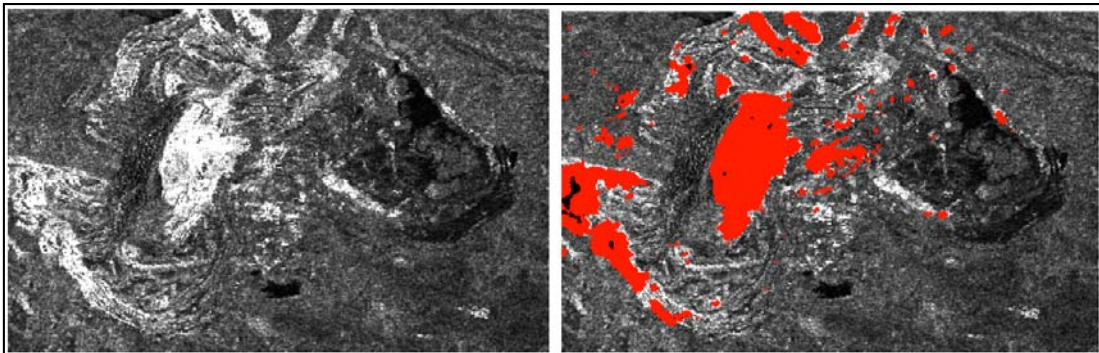


Figure 5.9: A georeferenced SAR image of Argyle Diamond Mines (left) and with layover area highlighted in red (right) using current DEM

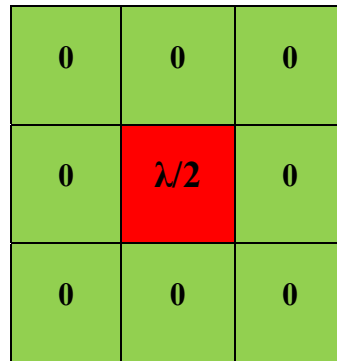
5.2.3. Deformation Rate Analysis

As stated before in Section 3.3.2.2, the maximum detectable deformation gradient by interferometry, is one fringe per pixel which means deformation rates cannot exceed the dimensionless ratio of the pixel size to the half of the wavelength (Massonnet and Fiegl, 1998). A basic solution to avoid such a problem is to select

SAR images with proper temporal baseline; however it is not always possible to find such images, in particular, in areas where satellite coverage is limited and only small numbers of images are available. In other hand, it must be taken into account that small scale, highly dynamic deformations induced by mining activities are prone to produce high gradient changes, impossible to detect by interferometry. So, conducting a deformation rate analysis before starting any data processing would be very advantageous. Through such analysis, it is possible to understand how much InSAR results are affected by ambiguity and more importantly, in which parts of the area InSAR results are acceptable. In order to provide such estimation, GIS-based methodologies can be used. One approach, adopted by this research, would be to use available elevation data such as digital elevation models (DTM) to calculate deformation rate between neighbouring pixels for the period between SAR acquisitions and then compare it with acceptable limit defined by satellite wavelength. As a result it would be possible to map which portions of the area of interest can be studied by InSAR without possibility of error due to height ambiguity issue.

A Python scripts was developed based on adopted methodology and then later was implemented into an ArcGIS Desktop tool. Deformation rate analysis tool, receives two raster grid files representing elevation models for times t_0 and t_1 . Dates in which these models were generated (e.g. flights date for DTMs generated by photogrammetry) should be also provided. To have better estimation this period must include periods between two SAR acquisitions. This information along with acquisition dates of SAR images will be later used to provide a rough estimation of deformation associated with the period between two SAR acquisitions. The result is a raster grid file containing deformation values from which calculating slope of the value will provide deformation rate over the area of study. However, according to Massonnet and Fiegl (1998) detectable deformation rate is defined by the dimensionless ratio of the pixel size to half of the wavelength of the selected satellite; Therefore, a reference raster grid file, as presented in Figure 5.10, is generated using provided satellite wavelength and used SAR pixel size. Maximum value of slope calculated in this reference grid will be considered as threshold for deformation rate. As a final step, raster grid file containing deformation rates will be resampled using provided pixel size and reclassified to map area with deformation

rate lower or higher calculated threshold. Figure 5.11 shows the input data window for this tool.



0	0	0
0	$\lambda/2$	0
0	0	0

Figure 5.10: Reference grid used in deformation rate analysis tool

As an example, Figure 5.12 depicts a final raster grid file generated by the deformation rate tool considering ERS as data provider for Perseverance mine in Western Australia. The result represents deformation occurred in almost 35% of the area mostly outside of the pit, and large deformation boundaries are detectable by InSAR. More details will be presented in next Chapter.

In the case of using elevation models generated by photogrammetry, it should be considered that there is a large difference between levels of InSAR sensitivity and accuracy of elevation data collected from the mine site. This means that even noises existing in collected data are larger than limit of elevation change detectable by InSAR. In such cases, elevation models must be modified to remove noise or more accurate datasets should be used.

It is very important to understand that deformation rate tool provides very rough estimation as it used simple interpolation to calculate deformation occurred in the period between two SAR acquisitions. Therefore, results must be considered as a general guide. Results must only be used when no accurate analysis is possible. Furthermore, it should be taken into consideration that a high rate of deformation is not only source of height ambiguity issues and that errors due to phase unwrapping techniques can still exist and affect the results.

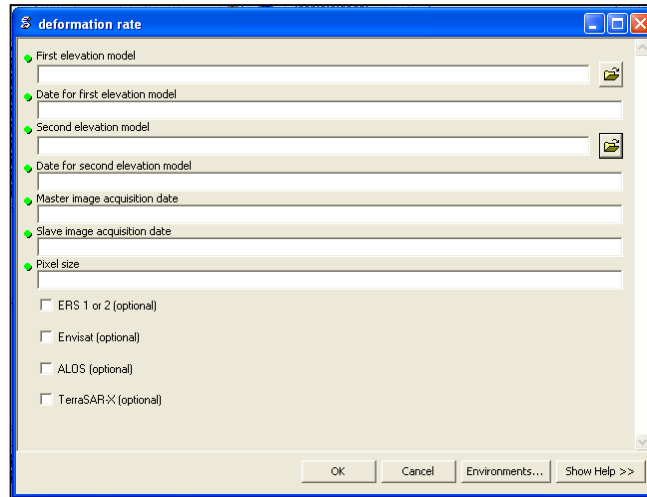


Figure 5.11: Input window for deformation rate tool

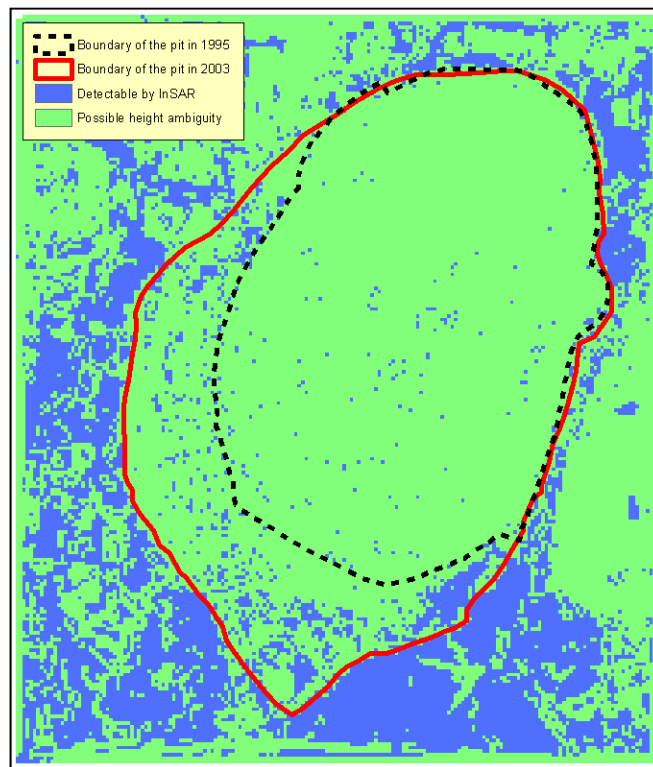


Figure 5.12: Deformation rate analysis result for Perseverance mine generated by deformation rate tool

5.2.4. Optimum Acquisitions Selection and Planning

Quality of InSAR final results is highly dependent on the availability and quality of the processed data; therefore adopting a robust data selection policy is very crucial for any SAR interferometry study. There are several criteria which must be carefully taken into consideration in order to select data from archives or planning future

acquisitions. Basically, data selection process means finding an optimum set of images balancing data availability and data suitability; therefore there is no definite answer, in particular, in case of regions with less satellites coverage such as Australia. Here, the ultimate goal is to use optimum data acquisition policy to produce the best possible results. Using a practical approach, we will discuss data selection process through discussing main questions which should be answered specifically for any given case studies:

What rate and extent of deformation is expected for within the area?

The first step in a data selection process is to obtain a rough estimation of deformation rate and its extent within the area of study. This information can be collected from different sources including classical survey data and previous studies over the area. This information can be very helpful to select suitable radar wavelength, reasonable image extent and resolution in order to avoid or minimise ambiguity issues.

What is the vegetation coverage over the area?

As stated in chapter 3, highly vegetated areas may lead to producing less coherent images and consequently poor results. Information describing types of vegetation over the area, vegetation density and period of dry seasons provide clues to decide about suitable wavelength (to be able to penetrate vegetation cover) and selection of a favourable time for data acquisitions. L-band radar signals are able to penetrate into vegetation cover due to longer wavelength and so are recommended for such areas. On the other hand, X-band data provides much more detailed phase information and very fine resolution (down to 1m for TerraSAR-X mission) however they are very sensitive to the vegetation resulting in image incoherency.

What level of distortion is expected based on geometry of the target and topography of the area?

As described in the sections explaining distortions, for a target to be detected by a SAR sensor, first radar signal must reach to the target (as it is the case for optical sensors) and moreover each backscatter signal should correspond with only one target. Otherwise, distortions such as layover and shadow will exist. Having information regarding topography of the area of study and geometry of the target

during data selection period can be advantageous in order to choose optimum look angle and acquisition path (ascending or descending passes). Taking pit or subsidence crater geometry into consideration and also small-scale deformation calls for paying even more attention to target geometry in case of mining-related application.

Since pit walls and waste dumps are usually designed with slopes larger than satellite look angle, in most cases one side of the pit will be in layover area or one side of the waste dump will be affected by shadow. In this case and if satellite coverage allows, using either both ascending and descending paths or different look angles is recommended.

Based on the deformation rate what range of geometrical baselines is suitable?

Geometrical baseline between two images should be selected depending on the objective of the study. In case of DEM generation baseline should be long enough to be sensitive only to the topography component. As opposite to DEM generation, baseline and in particular perpendicular baseline between images selected for deformation analysis must be as small as possible to minimise contribution of topography component into the phase difference (see section 3.2.2). Geometrical baseline is not a selective parameter and even in the case of planned acquisitions it is not possible to control satellite travelling path to deliver a designed baseline. Baseline decorrelation is more an issue with rather older missions such ERS-1 and 2. Critical baseline for ERS-1 and 2 is equal to 1150m in comparison with critical baseline of 13km for ALOS (for pairs of FBS mode); therefore baseline decorrelation is not an issue with ALOS (Sandwell et al., 2007).

Which wavelength range is more suitable for the application?

Selection of reasonable wavelength is a very critical step. As seen so far, ambiguity problems can be minimised utilising a proper wavelength; this is similar for incoherency due to effects of vegetation cover. However, since wavelength is one of the parameters predefined for each satellite, there are not many options to consider, in particular, for areas covered by a few or in some cases only one satellite.

Based on the deformation rate what range of temporal baselines is suitable?

With this question, the rate of the deformation date on which mining commenced, date on which mining deformation reached or will reach the surface for the first time, future plan for mining, mass movement data and any other data indicating deformation rate and extent should be collected and analysed. This data in addition to satellite repeat cycle will be used to define a comprehensive scenario for the data acquisitions either available as historical data or planned acquisitions.

How do satellites cover the area? How many images are available in the archive and with what specifications?

Satellite coverage delivering selected specification and data availability are main challenges for case studies located in areas with less satellite paths. For instance, though Western Australia is very rich in terms of mining activity, the vast mostly uninhabited areas in WA are not a primary targets of satellite missions, hence the archived data is scarce and without any continuity. Unfortunately, as shown by Table 5.1, the number of acquired images in other parts of land of Australia does not show better coverage. Hopefully this problem will be solved by launching more satellites in the future.

Table 5.1: Number of SAR images acquired by ERS 1-2 and Envisat missions over Western Australia, New South Wales and Western Europe, until end of Oct. 2008

Satellite	No. of Scenes in WA	No. of Scenes in NSW	No. of Scenes in W-Europe
ERS-1 and 2	817	690	more than 42000
Envisat	491	486	more than 8500

Is it possible to plan acquisitions to obtain required data? and what data acquisition policy can be applied?

If data is not available in satellite data archived, the only option is to plan data acquisitions to deliver required data. Almost all satellite missions offer the option of data acquisition planning. Using this option is more expensive and obviously time-consuming which depends on the satellite repeat cycle. Considering this, data acquisition planning is recommended for case studies with a need to perform long-term analysis; for instance where InSAR would be used as a monitoring technique. In

such cases, temporal baseline between images must be carefully selected with respect to the expected deformation rate.

Which interferometry technique (2-pass, 3-pass, 4-pass, PS) would be possible to perform?

Based on the number of available images, nature of the study and also availability of additional data (DTMs, DEMs), it can be indicated which interferometry technique is possible and will be performed (see section 3.1.5 and 3.2.2).

What are the meteorological conditions of the area at the time of data acquisitions and is atmospheric effect considerable or not?

Different atmospheric conditions (precipitation, temperature) between the two acquisitions may introduce noises to total interferometric phase. It is highly recommended to check atmospheric condition ordering or planning data. This data can be collected from metrological stations located at mine site or nearest station. Such data are usually publicly available. However, as commented by Carnec et al. (1996), atmospheric effect has less impact on small scale deformations such as mine subsidence and can be neglected during the data processing and interpretation process.

Does Doppler Centroid issue exist between pairs (specific to ERS-2 data)?

This problem is specific to ERS-2 data. In 2000 ERS-2 suffered from gyro malfunctions and by the end of 2002 there were no operating gyros on the satellite. This causes problems in the processing of SAR data acquired after 2000 due to the difficulty in stabilising the geometry (Doppler values). This is a major limiting factor for interferometric processing since it is required that the geometry be similar in the two SAR images. Selected data should be checked to identify level of Doppler Centroid dissimilarity between them. Pairs with large differences should be rejected in order to avoid problems with image decorrelation. In current research, Doppler Centroid frequency greater than 750 Hz is used as a threshold.

Searching all missions data catalogue looking for favourable set of data can be time-consuming and frustrating, however it is highly recommended as unfortunately

there is not a universal catalogue that contains all acquired data around the world. Today, the most comprehensive data archive is EOLi (Earth Observation Link) developed by the European Space Agency for Earth observation catalogue and ordering Services. Using EOLi, user would be able to browse, preview images and order data acquired by the satellites Envisat, ERS, Landsat, IKONOS, DMC, ALOS, SPOT, Kompsat, Proba, JERS, IRS, Nimbus, NOAA, SCISAT, SeaStar, Terra/Aqua. Radarsat and TerraSAR-X data are not included in this catalogue and to obtain data acquired by these missions their own catalogue should be searched. Moreover, it is very important to consider that there are several ground stations all over the globe that acquire data from the satellite; in theory, all of these stations must share their data archive and their records should be found in EOLi catalogue, however it is always true that on one hand the process of updating catalogue is not very sufficient and that on the other hand some of these stations do not intend to share their data. It means that some of the data acquired by ground stations located in China or even Australia cannot be found in EOLi catalogue and in order to check their availability catalogues developed by organisation in charge of the station should be searched. The data acquired by Alice Spring, Hobart, HEOC and TKSC ground stations are available in an online catalogue developed by National Earth Observation Group (previously known as ACRES).

5.2.5. Cartesian (XY) Coordinate to Pixel and Line Tool

One of the basic parts of any InSAR application is to define a proper extent for the study. SAR images usually cover large areas on earth (100 km×100 km), therefore it is recommended to use small areas, focusing on designed extent for analysis. It may significantly decrease the complexity and time of the interferometric process. This task is even more important in case of small-scale studies such as in mining-related applications. SAR interferometry is performed in pixel and line coordinates and so it is required to accurately convert Cartesian coordinates to pixel and line. This simple task can be sometimes hard to perform and is usually done using trial and error; therefore having a tool to do this conversion can be advantageous.

XYtoPL tool uses a Newton-Raphson method to iteratively solve the Doppler equation and converts Cartesian coordinates defined by user onto the master image pixel and line coordinates. This tool was created in three different versions, working with ERS, Envisat and ALOS data. Figure 5.13 and 14 show snapshots of the XYtoPL-ALOS data input and result windows.

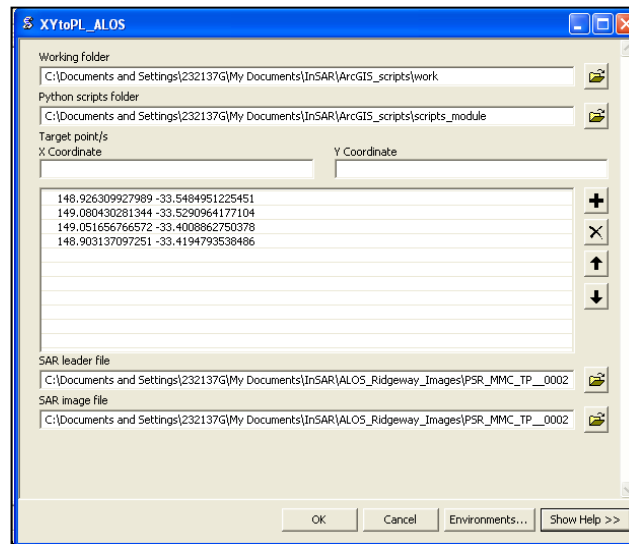


Figure 5.13: Data input window for XYtoPL tool

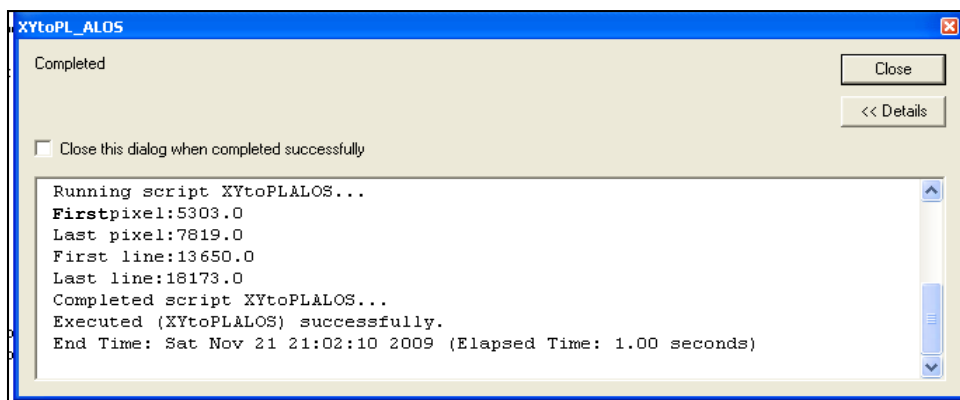


Figure 5.14: Snapshot of result window of XYtoPL_ALOS tool

5.3. Data Processing Stage

After the data selection step and also collection of additional required data such as topographical data, the data processing stage can be commenced. Data processing stage involves several processes and sub-process. Main processes of SAR interferometry studies were already discussed in Chapter 3 and summarised in Figure

3.10. Basically any given InSAR analysis and data processing software follow the same path including these steps. The difference is in techniques adopted by each software (e.g. different techniques for images coregistration or phase unwrapping) and also more additional sub-processes to improve level of accuracy and reliability of the results. Figure 5.15 shows details of the methodology adopted by the author for interferometry data processing. The methodology was designed based on Raspberry data processing software and then was introduced to the GIS environment.

The process is started with reading master and slave header information and also reading and processing additional information such as precise orbit data, if it is necessary (e.g. for ERS1 and 2 data). Then it is followed with extracting complex SAR data and dumps it into binary files. In case of using a 2-pass technique, available DEM should also be processed; this processing involves transformation of DEM into master image coordinates and adjustment of DEM resolution and then simulation of an interferogram containing phase references obtained from the DEM. In case of 3-pass or 4-pass analysis, phase component representing topography is acquired from the other pair of SAR images.

The next step would be image coregistration. This is usually performed in two steps; coarse coregistration providing parameters for image overlying with pixel accuracy and fine coregistration providing parameters for image overlying with sub-pixel accuracy. Using calculated parameters by coregistration step, slave image is resampled to be matched with the master image. The next step is subtracting master and slave phase components generating a complex interferogram. Having interferogram and DEM or another interferogram representing topography phase component, differential interferogram can be created that leads into removing topography component and retrieving only deformation. Nonetheless, values of calculated deformation are in modulo 2π , so in the next step deformation values will be unwrapped. The final step is to convert phase values to height, georeference and prepare data for presentation or data post-processing.

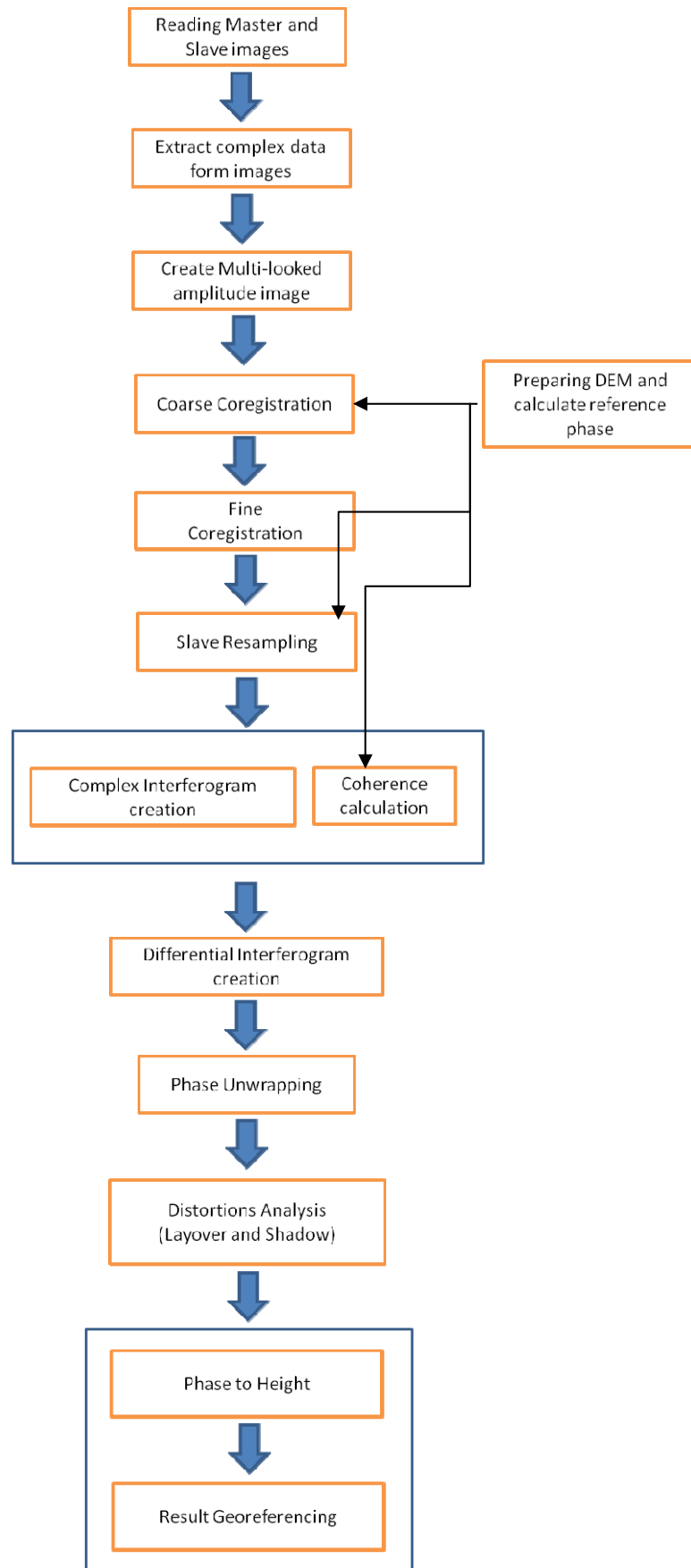


Figure 5.15: Interferometry processing chain

5.3.1. Data Input and Processing Steps Windows

One of the main problems of almost all open-source InSAR processing software is the difficulty of defining input data and also the definition and editing processing parameters. It is one of the main reasons why working with these software could be very difficult for ordinary users. It makes the processing time usually very long and also causes many unnecessary repetitions. For example the definition of input data or editing processing parameters in software such as DORIS requires a high level of knowledge of programming, as well as InSAR processing insights. Working with DORIS requires working with several input files in order to define selected parameters and run each step which is sometimes very confusing. In other cases, other type of InSAR processing software such as RIO-Pack have been consisted of a set predefined scripts and related commands to run them from the command-line and consequently provides a very small level of flexibility in terms of applying different processing parameters. InSAR toolbox tries to overcome these problems by providing a much faster, more stable, more sophisticated and more user-friendly environment compared to all open-source InSAR processing software.

The process is commenced with organising parameters defined by user via InSAR data input window (Figure 5.16). This information is read by Python and stored in several files to be used later in Python and Matlab. This window is almost similar for all supported satellites and asks for following inputs:

- Workspace to store intermediate and result files,
 - Folder containing raspberry and Python scripts,
 - Location for master and slave images,
 - Location for additional required files (e.g. precise orbit files (ODR) for ERS)
 - Extent for subset in which analysis should be performed in Pixel and Line coordinates,
 - Location of the DEM file (Only GeoTiff format is accepted),
 - DEM extent in latitude and longitude coordinates,
 - Output cell size, and
 - Multilook ratios for Pixels and Lines
-

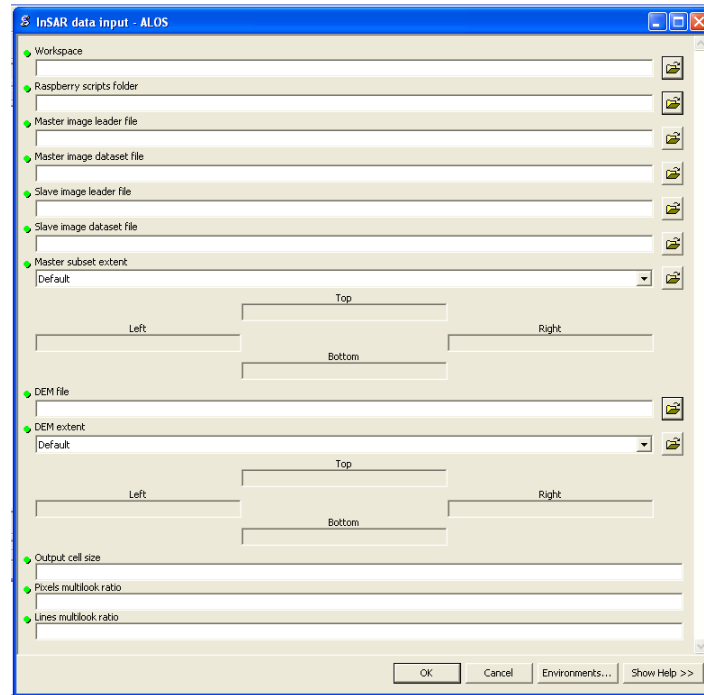


Figure 5.16: InSAR data input windows for ALOS data

The next step is to run the process. Figure 5.17 shows the processing step selection window. One or more steps can be selected and run together or individually. In order to run each step, it is also important to run its pre-mandatory step first. Selected steps can also be rerun with no problem, however it must be noted that results will be overwritten.

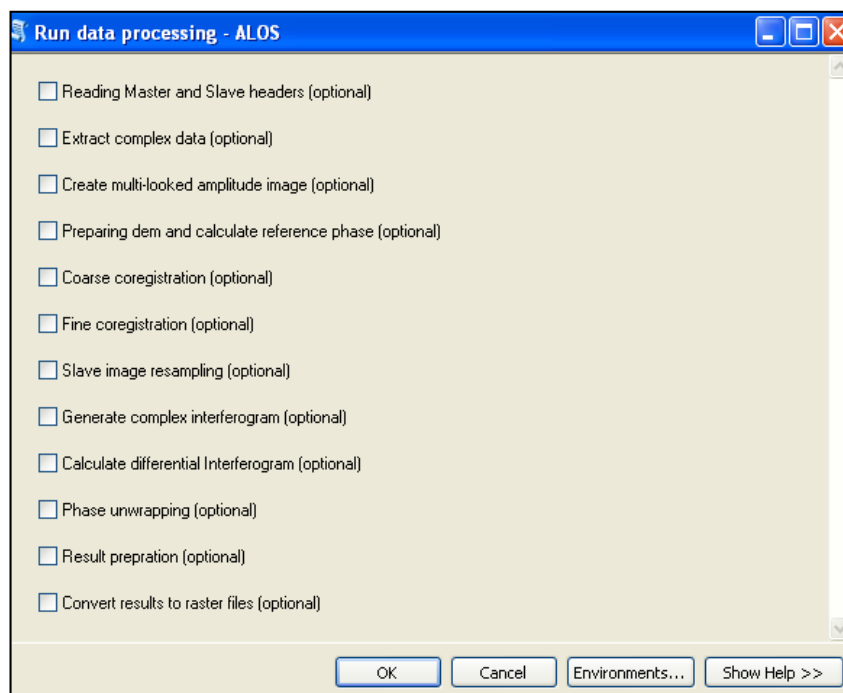


Figure 5.17: Processing steps selection window

5.3.2. Reading Master and Slave images

This step involves four sub-processes:

1. Reading in necessary processing parameters to be extracted from master and slave images and orbit interpolation. In case of ERS and Envisat data processing, precise orbit analysis is also included in this sub-process
2. Reading in DEM file and related information,
3. Estimation of centre lat/longs and
4. Geoid height identification for the area of interest.

SAR products usually consist of several binary files. For SAR products distributed in CEOS (Committee on Earth Observation Satellites) revised standardised formats, basic parameters are stored in Leader and Data files of the product. Leader file stores annotation data, ancillary data and other types of data related to the image which stored in Data file. These parameters include information such as length of facility related data records necessary to find each parameter inside the binary file, number of pixels, number of lines, pixel and line spacing, satellite information and orbital parameters to be used in orbit interpolation. All these parameters are stored in different Python or Matlab files to be loaded again during the process.

For now, scripts only accept DEM in GeoTiff format and any other formats such as DXF or Grid should be converted to GeoTiff. In this step DEM data is read and converted into an object to be used during the process. DEM modification tool along with predesigned ArcGIS tools can be used prior to this step to prepare available elevation data to be used in the process.

The scripts include several loops and iterative calculations. Most of these iterations need an initial value to run; Latitude and longitude at master image centre is calculated here and will be used as this initial value. After this, approximate height of Geoid above reference ellipsoid (at master image centre) is calculated based on WGS84 Geoid height provided in 'ww15mgh' grid file. This file is included in distribution and also can be downloaded from: <http://earth-info.nga.mil/GandG/wgs84/gravitymod/egm96/egm96.html>

5.3.3. Extract Complex Data from Images

This process extracts complex SAR data from master and slave Data files and dumps in two binary files. Figure 5.18 provides a simple illustration of how SAR data are stored inside the Data file. As shown Data file starts with a header part containing data file summary (e.g. 720 bytes for ALOS) which must be skipped. Each line also starts with a header part (e.g. 412 bytes for ALOS data) which must be skipped too. Then, start at line 1, pixel 1 (azimuth, near range) data is written line by line with major row order. Each complex pixel is written as 4 bytes real part, 4 bytes imaginary part. At this stage, there is no separation between real and imaginary parts of the complex image; for each line and pixel, first real part and immediately after that imaginary part are stored to a binary file.

<i>Data File Summary</i>				
<i>Header</i>	Real, Imag	Real, Imag	Real, Imag	...
<i>Header</i>	Real, Imag	Real, Imag	Real, Imag	...
<i>Header</i>	Real, Imag	Real, Imag	Real, Imag	...
<i>Header</i>	Real, Imag	Real, Imag	Real, Imag	...
<i>Header</i>

Figure 5.18: Simple illustration of a SAR image data file

5.3.4. Create Multilooked Amplitude Image

The binary file created by previous steps for master image and multilook pixel and line ratio defined by user will be used to generate an array containing multilook amplitude values. This array is saved and will be used later during the process. As the result of this step, an ArcGIS grid raster file is generated representing area of study (Figure 5.19). This image can be reviewed to confirm suitability of the selected subset and multilook ratios.

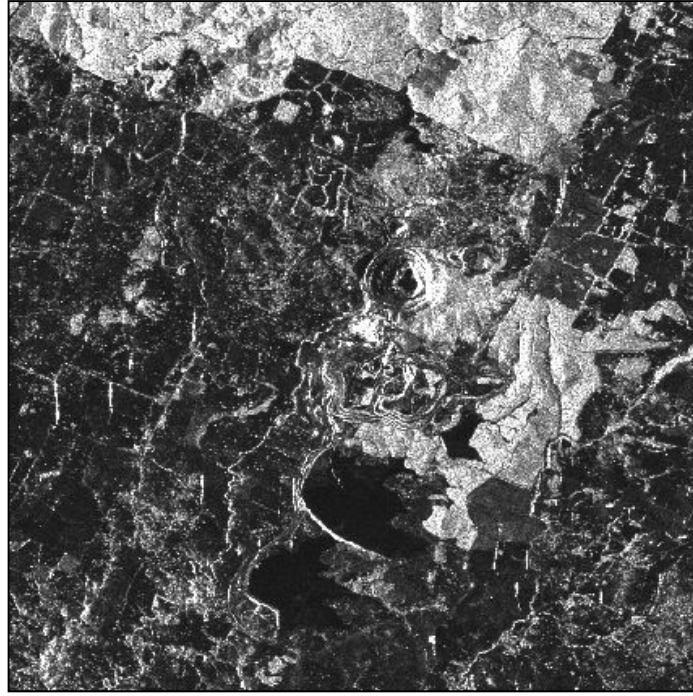


Figure 5.19: Multilooked amplitude image created for Ridgeway Gold Mine, NSW, Australia

5.3.5. Preparing DEM and Calculate Reference Phase

Available DEM or results of the DEM modification tool should be first subset and resampled or oversampled (depending on its original resolution) to follow defined resolution for SAR processing. In order to perform this step, a bilinear resampling technique is used. All parameters defining the new generated DEM are stored in a separated file. These include information such as DEM extent on SAR image (in pixel and line), its Cartesian coordinates and number of pixel and lines.

After reading DEM parameters and its preparation, the next sub-process is to calculate reference phase based on elevation values. This calculated phase represents the topographic component in Equation 3-7. At this step, script generates a simulated interferogram in multi-looked SAR image coordinates which will be later subtracted from the total phase difference to retrieve the phase difference representing only deformation. The algorithm also calculates the orbital baseline and its components and the terrain height of each image coordinate. A sufficient DEM oversampling is essential as at least a 1-to-1 mapping of the DEM onto the image should be available.

5.3.6. Coarse Co-registration

Master and slave images (for same scene) are produced from two different acquisitions with different parameters for satellite geometry and consequently do not overly accurately. The difference in starting time of image acquisition and geometrical baselines between two images are main reasons for this issue (Baran, 2004). On the other hand, sub-pixel accuracy between master and slave images is essential in order to obtain a coherent interferogram. Therefore, an accurate coregistration process must be undertaken between master and slave images. Franceschetti and Lanari (1999) define coregistration as a geometric image transformation function of lining up master and slave images. Same as almost any coregistration process, InSAR toolbox coregistration steps includes two main processes: coarse coregistration that performs images overlying with pixel accuracy and fine coregistration that provides precise image overlying with one-eighth pixel accuracy.

Coarse coregistration process is carried out in three steps:

1. Generating grid of reference point (tiepoint) positions in SAR image coordinates
2. Lining up master and slave images and generating a transformation polynomial
3. Coarse coregistration of images at tiepoint positions

The first set of tiepoints is created covering whole area of master images and then each of these points are mapped onto the ellipsoid using a range-doppler algorithm and then mapped onto the slave using the inverse. Now images are ready to run main process of coarse coregistration; In simple words, two intensity chips or kernels are extracted from master and slave image, then script tries to match them to pixel accuracy and also calculate the offset between them. This process is repeated over the whole scene. Script also detects possible outliers and filters them out. Last step then is to fit a polynomial to the result. The extracted kernels are produced in such manner that kernel extracted from slave image is larger than one for master image. Then the smaller image moves over the larger until the maximum value of the correlation coefficient is found.

5.3.7. Fine Coregistration

Fine coregistration process is almost the same as coarse coregistration. Differences are in using smaller kernels and one additional process of kernels oversampling; Kernels are oversampled by a factor of 8 to provide more precise kernel matching. Same as coarse coregistration, script detects possible outliers, filters them out and then fits a polynomial to the result. The final result is a transformation polynomial which accurately matches master and slave images together.

5.3.8. Slave Image Resampling

According to the estimated transformation model calculated by coregistration processes, slave image must be resampled over the master image. Two following steps are performed:

1. Calculating slave image coordinates for every position in master image.
2. Finds slave pixel values at master image positions

Based on Raspberry descriptions, windows of slave images are read in one at a time and then algorithm interpolates each window eight times. The master image position is mapped onto the interpolated window and the slave value will be extracted. As a result of this process an ArcGIS grid raster file is generated that represents multilooked resampled slave image.

5.3.9. Complex Interferogram Creation

According to Equation 3-8, a complex interferogram is a point-wise multiplication of corresponding pixels in the master image and the complex conjugate of slave image. In simple words, phase values for each pixel in master image is subtracted from phase values for corresponding pixel from slave image, so the result would be slave minus master in terms of phase values. Assuming no atmospheric effect, this phase difference is due to deformation component and topography. Next step is to create a multilook interferogram and also calculate coherence image based on the complex correlation coefficient. To reduce level of noise and increase the quality of the result a filtering process is also performed on the

multilooked interferogram using a Modified Goldstein filter introduced by Baran et al. (2003).

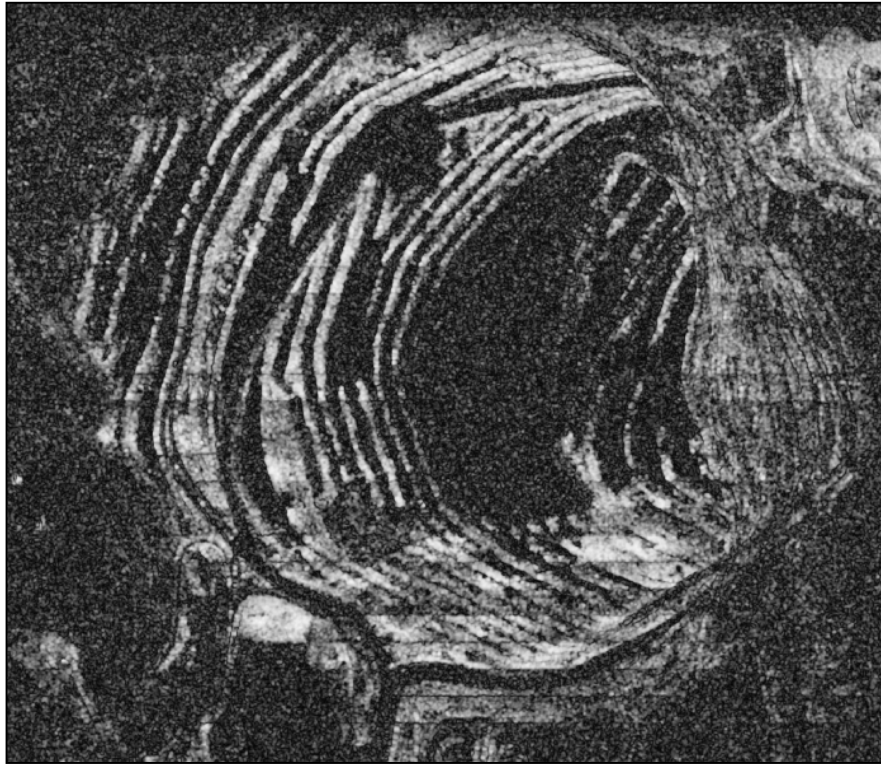


Figure 5.20: Multilooked coherence images generated from two TerraSAR-X spotlights images with 11 days temporal baseline, over the Cadia hill pit, NSW, Australia

5.3.10. Differential Interferogram Creation

This step is similar to the previous step, however this time; the result is a complex differential interferogram. Phase values represented by differential interferogram are resulted by subtracting actual interferogram minus simulated interferogram containing reference phase (generated by DEM preparation process). Assuming high chance of availability of topographical data for any mining-related case studies, the presented toolbox and procedure mainly focus on 2-pass interferometry technique; however the simulated interferogram can be also generated using another pair of SAR images providing possibility to perform 3-pass or 4-pass analysis.

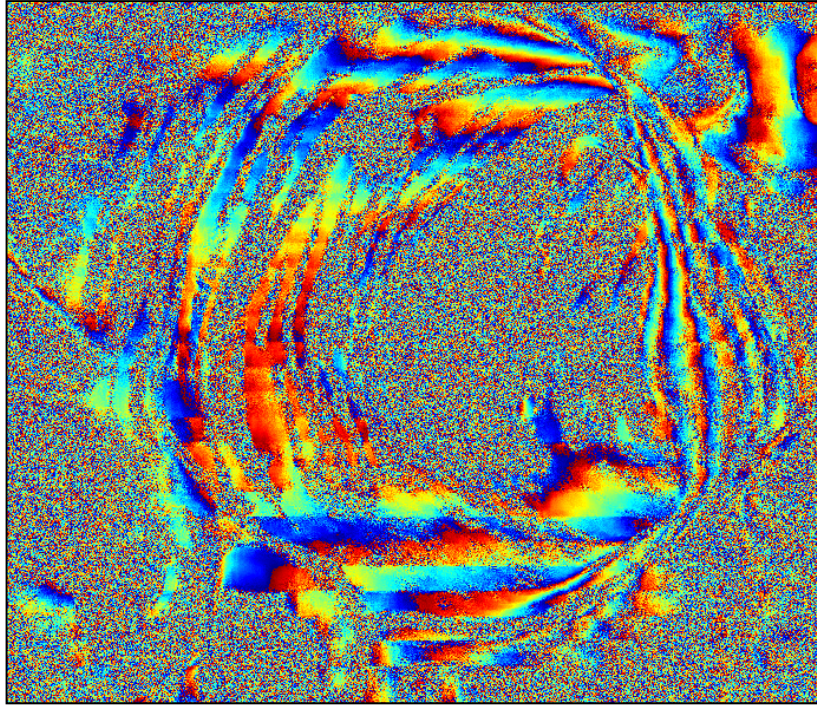


Figure 5.21: Multilooked differential interferogram generated from two TerraSAR-X spotlights images with 11 days temporal baseline, over the Cadia hill pit, NSW, Australia

5.3.11. Phase Unwrapping

As stated before, phase values presented by interferograms are module 2π and must be converted to real phase difference; Two-dimensional phase unwrapping is the process of recovering unambiguous phase data from a 2-D array of phase values provided by interferogram. To perform unwrapping process Snaphu 1.4.2 software, developed by Stanford Radar Interferometry Research Group, was used (Chen and Zebker, 2000a). Snaphu applies a statistical-cost, network-flow algorithm for phase unwrapping proposed by Chen and Zebker (2000a, 2000b, 2002). As introduced by Sanphu manual, this algorithm considers phase unwrapping as a maximum a posterior probability (MAP) estimation problem and sets an objective to compute the most likely unwrapped solution given the observable input data. Considering that statistics relating the input data to the solution depend on the measured quantity, there are three built-in statistical models are offered by Sanphu, one for topography data, one deformation data, and one for smooth generic data. Since Snaphu performs an iterative optimization procedure, processing time depends on the difficulty of the interferogram.

Snaphu was designed to be run under Unix/Linux. To run Snaphu from Windows platform, scripts use Cygwin, a Linux-like environment for Windows. As the first step, the unwrapping process generates four binary files containing complex interferogram, coherence, master and slave amplitude data for input to Snaphu. Then it calls Cygwin and runs Snaphu inside Linux environment in the background and then reads back Snaphu output and continues the process. Obviously Snaphu should be previously installed on Cygwin. To avoid using cross-platforms process, an unwrap module available in Scipy module in Python can also be used however it is yet not well-documented and tested for interferometry analysis. Therefore, it was decided to use well-recognised Snaphu to be included in the toolbox.

5.3.12. Results Preparation

The last step is to prepare the final results; this includes three main sub-processes of:

- detecting and masking out areas affected by layovers and shadows,
- orthorectifying and georeferencing, and
- phase to height conversion.

As a final data processing step, several raster grids will be created to be used in data post-processing.

The algorithm for detecting area affected by layover and shadows is already explained in previous sections; the same algorithm is applied to the unwrapped layer and affected area will be masked out. These areas will be later treated as ‘NoData’.

After masking out distorted areas, the following equation can be used to convert values of unwrapped phase (uw) to height (H) where λ is the signal wavelength:

(5-1)

$$H = \frac{uw\phi \times \lambda}{4\pi}$$

It is necessary to be reminded that height values produced by interferometry analysis are relative, line of sight deformations. Positive values in final deformation layer represents movement toward the satellite line of sight or uplifts and negative values

show movement against the satellite or subsidence (+ve = up, -ve =down). All results are orthorectified based on provided DEM and then georeferenced into UTM coordinate system.

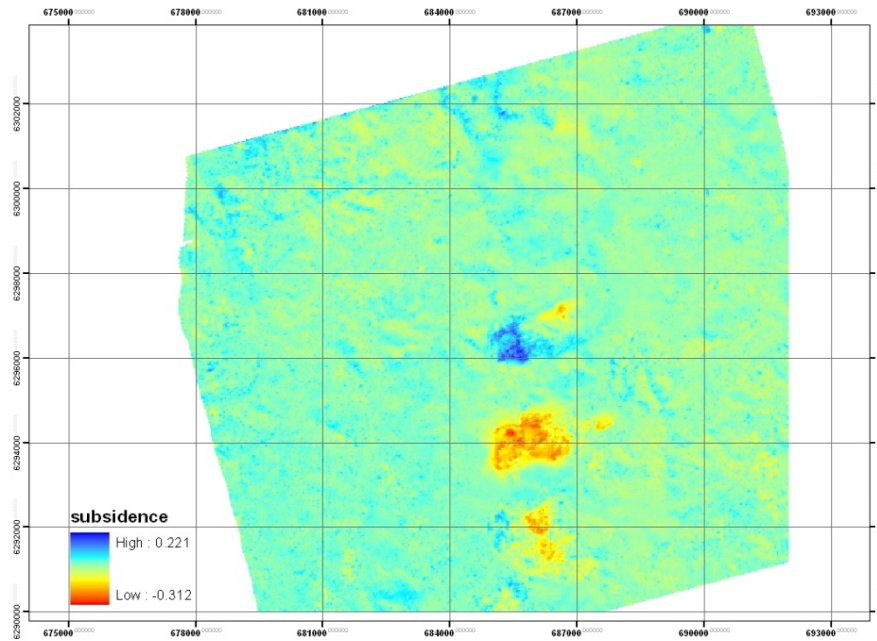


Figure 5.22: Subsidence detected by InSAR for two ALOS PALSAR images with almost one year (368 days) temporal baseline, Ridgeway Gold Mine, NSW, Australia

It is obvious that data processing is a chain of process and sub-processes which should be called and performed in their respective order. However, it is possible to repeat each step for an unlimited number of times if the process before that has already been performed and its results are stored in a working folder. It is also important to consider that with each time repeating one step generated results from previous iteration will be overwritten.

5.4. Post-processing Stage

The main advantages of running data processing stage inside a GIS environment is the possibility to use GIS functionalities to store, organise, modify and visualise InSAR data. GIS can be used for interpreting and assimilating disparate InSAR results. It can also be used for validating InSAR results and integrating them with other available collected data from the mine, such as classical surveying, geology

and mining progress data. In this section some GIS tools and procedures will be introduced that can be very helpful to add value to the data produced by InSAR technique.

5.4.1. Phase Trend Removal

With respect to principles of interferometry, accurate calculation of interferometric baseline is critical since without an accurate transformation to the reference datum all produced data are meaningless. Therefore any orbital errors will directly contribute as error in detected deformation. Orbital error shows itself as an obvious residual phase trend extended over interferogram which should be carefully removed from the result. Nonetheless, it is necessary to understand that orbital error is not the only reason causing this issue; atmospheric effect and DEM error can also produce such trends in InSAR results. It would be helpful to identify sources of phase trend before adopting any method to remove the trend (For further information see Hanssen (2001) and Massonnet and Feigl (1998)). To ensure if atmospheric effect is the source, a review of meteorological data for acquisition dates is necessary. As proposed by Baran (2003) processing steps can be repeated with each time shifting DEM slightly from its original position to find if DEM error is the source for phase trend. In the case of DEM errors or atmospheric effects, discussion about reliability of the results will arise and well-defined methods are required to remove the phase trend. However, the most possible source for phase trends is orbital error. Such a trend can be easily detected by ArcGIS trend tool and later subtracted from original data.

Trend tool is able to interpolate a surface from points using a trend technique. Linear or Logistic trend techniques can be used. The linear method uses a polynomial regression to fit a least-squares surface to the input layer. The logistic option generates a trend surface appropriate for prediction of the presence or absence of certain probability phenomena for a given set of locations in space and is not useful for phase trend removal (ESRI, 2009). The tool allows selecting the order of the polynomial used to fit the surface; however phase trend due to orbital errors can be represented by a first order polynomial.

As experienced by current research, phase trend is more an issue in case of ERS1-2 data (Figure 5.23) and newer satellites with updated navigation systems show no or small phase trend. Nonetheless, checking results produced by other satellites for presence of any phase trends and trying to remove it, is recommended.

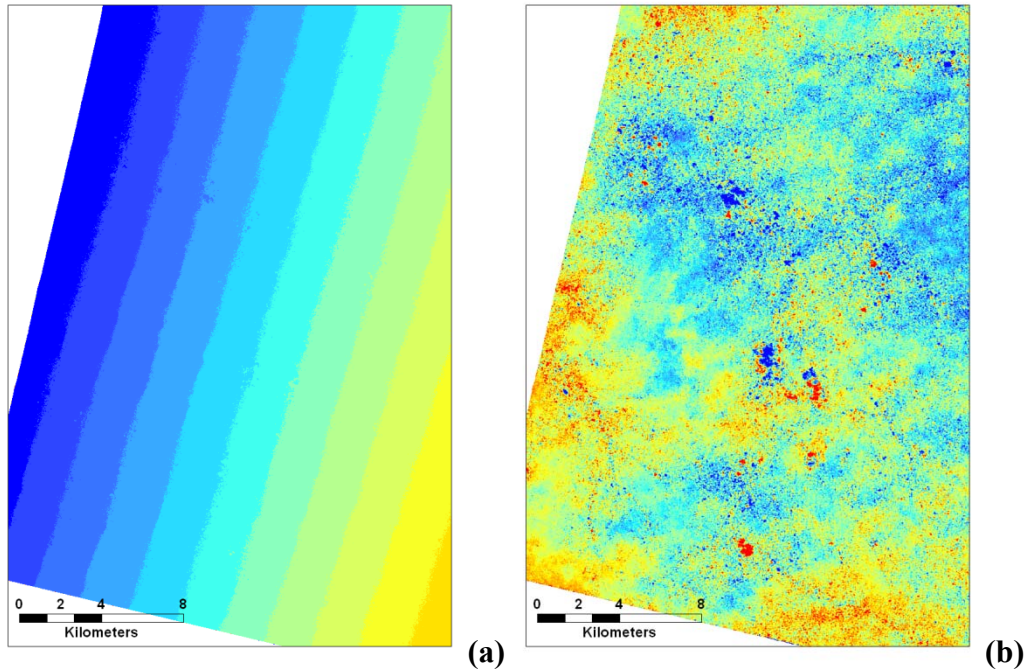


Figure 5.23: Unwrapped phase image generated using two ERS2 SAR images over the Leinster area, WA, Australia, a) before trend removal b) after trend removal

5.4.2. Result Interpolation

InSAR usually produces very disparate results due to its high sensitivity to elevation changes and noises. Therefore, in most cases result interpolation can be very helpful in order to provide a better view of the extent of deformation fields and their magnitudes. Result interpolation must be performed very carefully as result smoothing might remove small deformations. Sophisticated interpolation tools, available in almost any GIS package, can be used for InSAR result interpolation. Geostatistical analyst extension in ArcGIS desktop is one of the most comprehensive interpolation and surface generation tools which can be used to interpolate and smooth InSAR results. This extension offers several types of interpolators including inverse distance, global and local polynomial interpolation and kriging. Using this tool it is possible to interactively control interpolation by iteratively setting new

parameters and observe their effects on the final result. At the end and depending on the selected interpolator, interpolation validity factors including errors are reported.

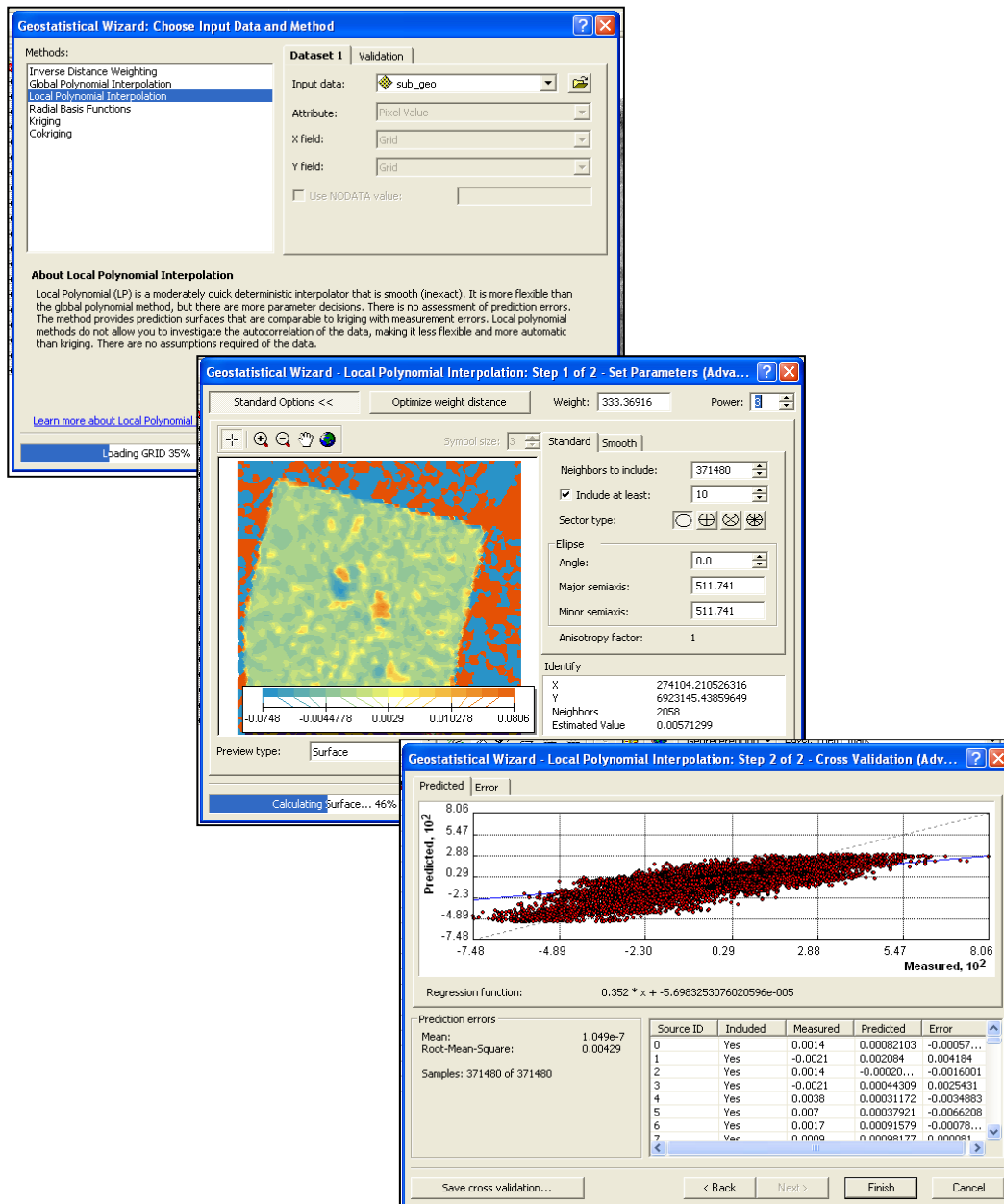


Figure 5.24: Snapshots of Geostatistical analyst performing local polynomial interpolation of sample InSAR results

5.4.3. Precise Georeferencing and Coordination Transformation

As mentioned before, results of InSAR toolbox are orthorectified and georeferenced using provided DEM and in UTM coordinate system. However, considering the fact that mining sites usually use their own local coordinate system, it is necessary to have a tool to convert InSAR results to new projection systems.

Moreover, sometimes accuracy of the provided georeferencing is not enough and more precise overlying between mine data and InSAR results is required. There are two tools available in the ArcGIS desktop package (and also InSAR Post-processing toolbox) which can be used to perform reprojecting task or precise georeferencing: Project raster tool and Georeferencing toolbar.

If spatial reference of local mine site coordinate system (*.prj file is required by ArcGIS desktop) is available or the mine site uses one of the known coordinates systems, project raster tool can be used to convert InSAR result projection to the one used by mine site. In this case there is no need for any reference points.

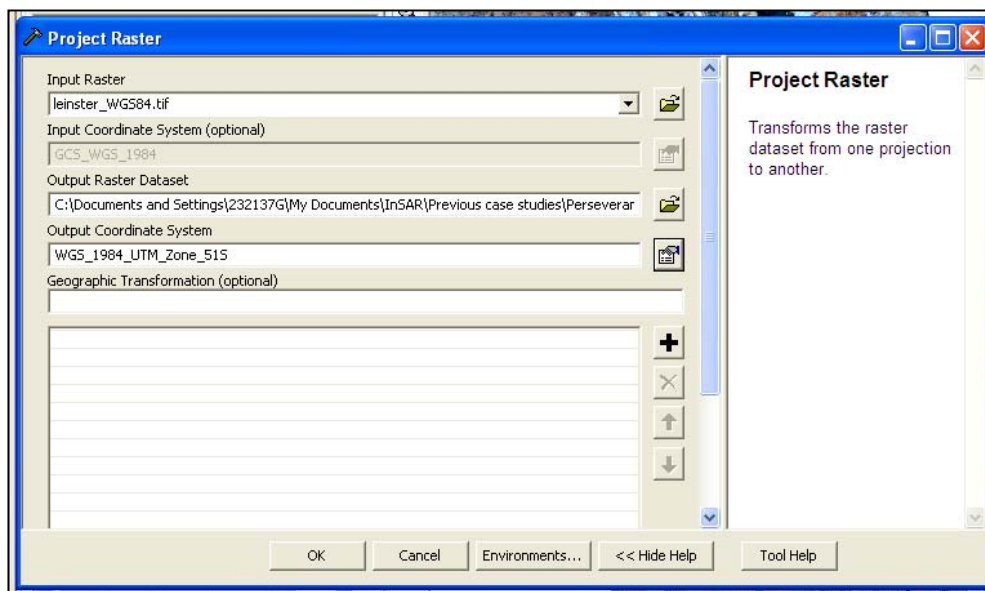


Figure 5.25: Project raster tool

In case the mine site uses its own local coordinates system or if any further precise georeferencing is required, georeferencing toolbar of ArcGIS Desktop must be used. Using this extension, control points selected over InSAR result are linked to known positions in map coordinates provided by mine site. Old and new coordinates for each control point are reported and can be saved to be used later for other layers of data. Three transformation methods can be used using spline or first-order polynomial, second-order polynomial, third-order polynomial. The residual error for each link and the RMS error are also reported. When best fit was obtained, raster file produced by InSAR toolbox will be resampled and will be saved with new spatial references.

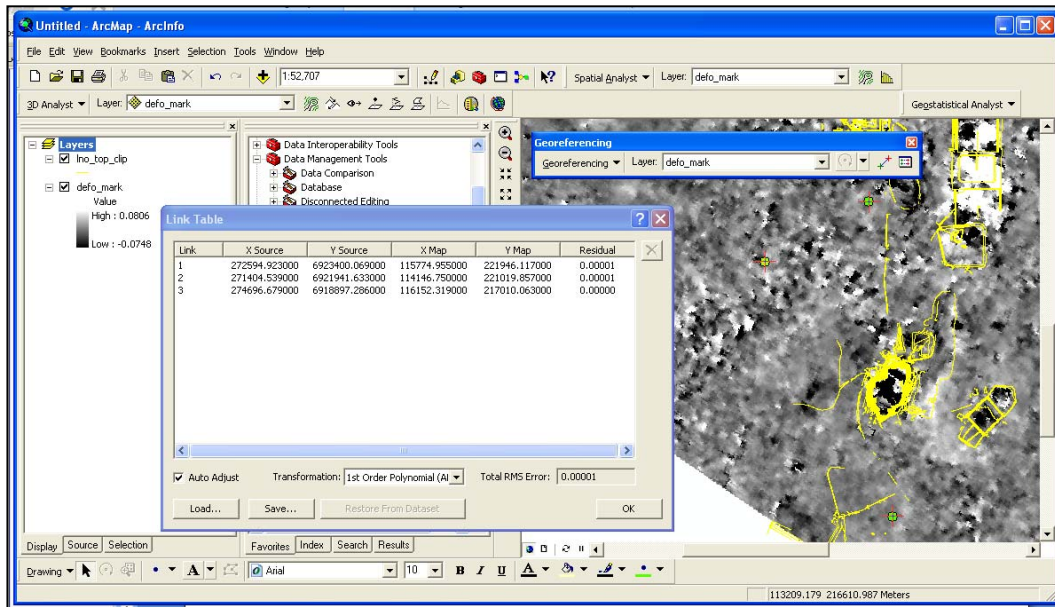


Figure 5.26: Sample InSAR result georeferencing process performed using georeferencing toolbar

5.5. Chapter Summary

This chapter introduced new developed tools and methodologies for InSAR application in mining. In the pre-processing stage various tools and procedures discussed to deal with different aspects of the techniques including: data selection, data preparation, data review, level of ambiguity and geometric distortions. For the first time, it was possible to implement all InSAR data processing steps inside the ArcGIS Desktop environment. The data processing section described an InSAR toolbox to run data processing. Furthermore, result interpolation and result preparation steps discussed in post-processing section.

Chapter 6

Case Studies

Chapter 6

Case Studies

Following the detailed presentation of the adopted methodology and also new developed tools, this chapter will discuss results generated using the InSAR toolbox. The methodology and tools were used for small-scale deformation detection in three different case studies in Australia: Perseverance (Leinster nickel mining operation), Argyle (diamond mine) located in Western Australia and Ridgeway (gold mine) in NSW. Studies planned to use data acquired by four different satellites (ERS-2, Envisat, ALOS and TerraSAR-X); it was due to the different nature of projects and also in order to test the methodology and tools using different sets of SAR data. Several issues arose during the period of studies including unavailability or poor topographical data for generating required elevation models and lack of classical survey data that limited result validation process. Nevertheless, the problem of lacking satellite coverage and the consequent issue of unavailability of suitable SAR acquisitions was found to be the main problem.

6.1. Perseverance- Leinster Nickel Mining Operation

6.1.1. Case Study Overview

The Leinster nickel mining operation is located approximately 375 Km north of Kalgoorlie and almost 600 Km northeast of Perth in the Eastern Goldfields region of Western Australia (Figure 6.1). The history of the operation backs to 1971 when a nickel sulphide deposit was discovered in the area. The operation was commenced in 1989 by starting an open pit (Rocky's Reward) which was later followed by other open pits, a concentration plant and underground mining operations. Production in the Perseverance open pit commenced in 1995 and the first ore from the Harmony open pit was extracted in 2000.

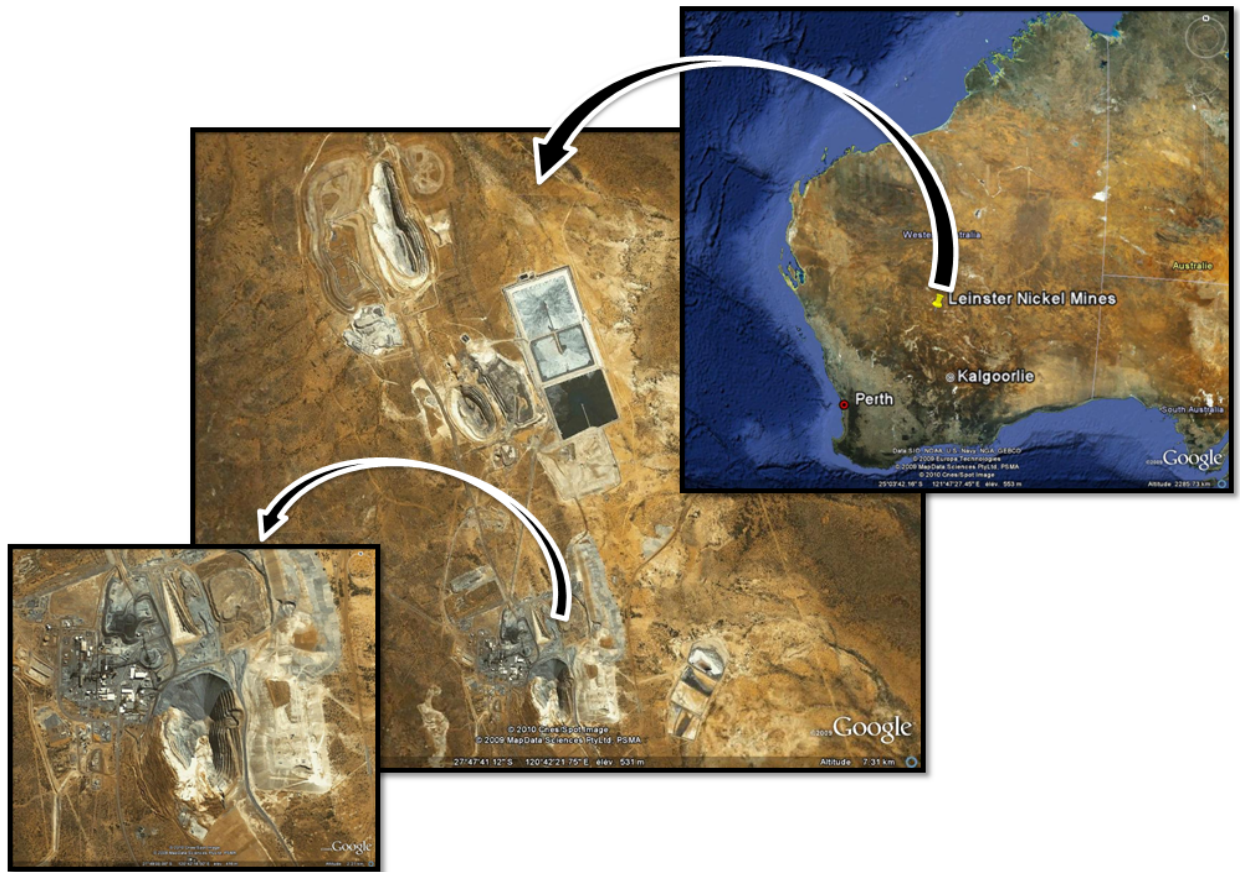


Figure 6.1: Location of Leinster Mining Operation and Perseverance open pit and underground operations (Google Inc., 2009)

Leinster operation now is operated by Nickel West Company which is owned by BHPBilliton. The Leinster Nickel Operation concentration plant has an operating capacity of three million tonnes of ore per year. This concentrate will be later shipped by rail to Nickel West's Kalgoorlie Nickel Smelter for further processing.

Following the commencement of underground mining in 1996, surface deformation was detected in 1997 inside and in the vicinity of the Perseverance open pit. Figure 6.2 describes extent of induced deformation for the period between 2001 until 2006. As shown in the figure, the extent of deformation has increased as underground mining progresses below the pit. This trend still continues.

The long-term objective of the project (not considered here) was to provide help with tuning of a finite element model representing deformation of rock mass and with the analysis required for planning and design of the next mining phase.

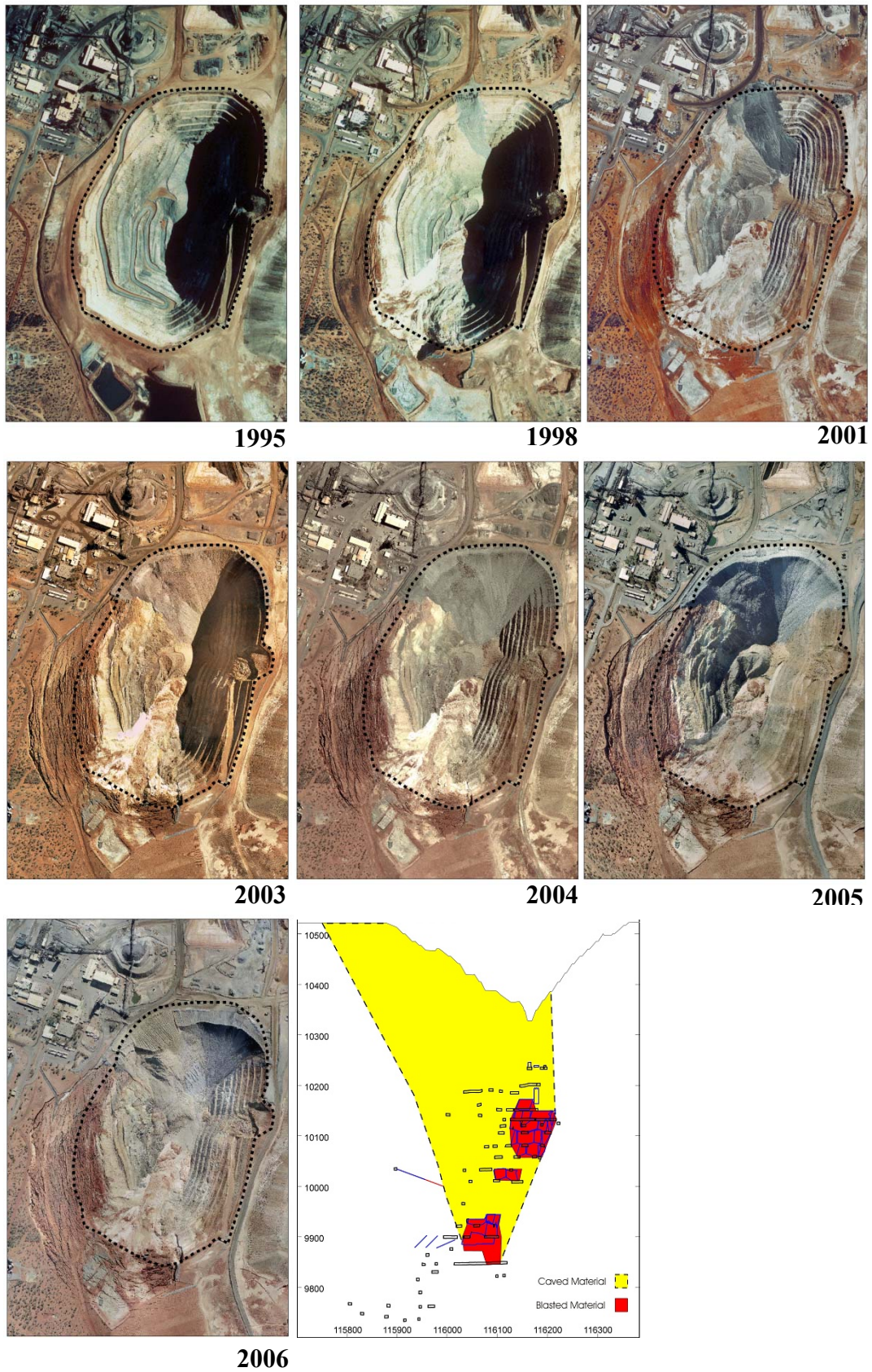


Figure 6.2: Surface deformation over Perseverance open pit between 1995 and 2006 (Black dash line: boundary of the pit in 1995) and caving profile in 2000

The research work included assessment of ground surface subsidence (including inaccessible areas) using InSAR technique, verification of InSAR results against deformations (subsidence) determined using other surveying and mapping techniques and also preparation of subsidence data for the Perseverance Deeps Project (PDP) for use with the numerical modelling code ABAQUS (as a means of model calibration). The InSAR processing and analysis incorporated:

- Development of comprehensive planning procedures for SAR data acquisitions that involve:
 - ✓ Determination of the best sensor to be used,
 - ✓ Determination of the best orbital and geometric parameters,
- Development of an accurate algorithm allowing determination of layover masks.
- Optimisation of the data processing procedures.
- Further validation of InSAR results through comparison with data gathered using the classical surveying techniques.
- Development of methodology allowing for resolution of ambiguity that may be present in InSAR results.
- Selection of suitable SAR image pairs from the available data to perform interferometric analysis,
- Generation of deformation maps representing distribution of terrain subsidence with possibility to import the results into other software packages.
- Comparative analysis of subsidence results.

The comparative subsidence analyses included:

- Collection and analysis of data collected by the mine's surface subsidence monitoring system,
 - Collection and analysis of scheduled topographic surveys (utilising aerial photogrammetry),
 - Determination of long-term subsidence including yearly changes and deformation rates.
-

6.1.1.1. Previous WASM Research Experience in Mining Application of InSAR

In 2001 the Mine Surveying Program at WASM initiated a research project on Leinster Nickel Operations that investigated if the method of Synthetic Aperture Radar Interferometry (InSAR) can be applied to monitoring of surface deformations in the vicinity of large open pit mining operations. The study was planned to apply a 3-pass technique using images acquired by ERS missions over the period 1995 and 2003. The processing of available data for the selected period of time resulted in only one pair of SAR images, acquired on January and March 2003, with 378m baseline. The research results suggest that the InSAR method is capable of detecting vertical ground movement over relatively small areas. However, it also noticed that the quality of results is highly dependent on a geometric configuration of satellite data availability. The result confirmed the applicability of the InSAR technology as the initial method for determination of subsidence in mining active areas and for forward planning of other monitoring techniques. Implementation of differential interferometry for monitoring of mining deformations could increase safety margins of such operations and decrease the costs of monitoring process (Jarosz and Wanke, 2004a).

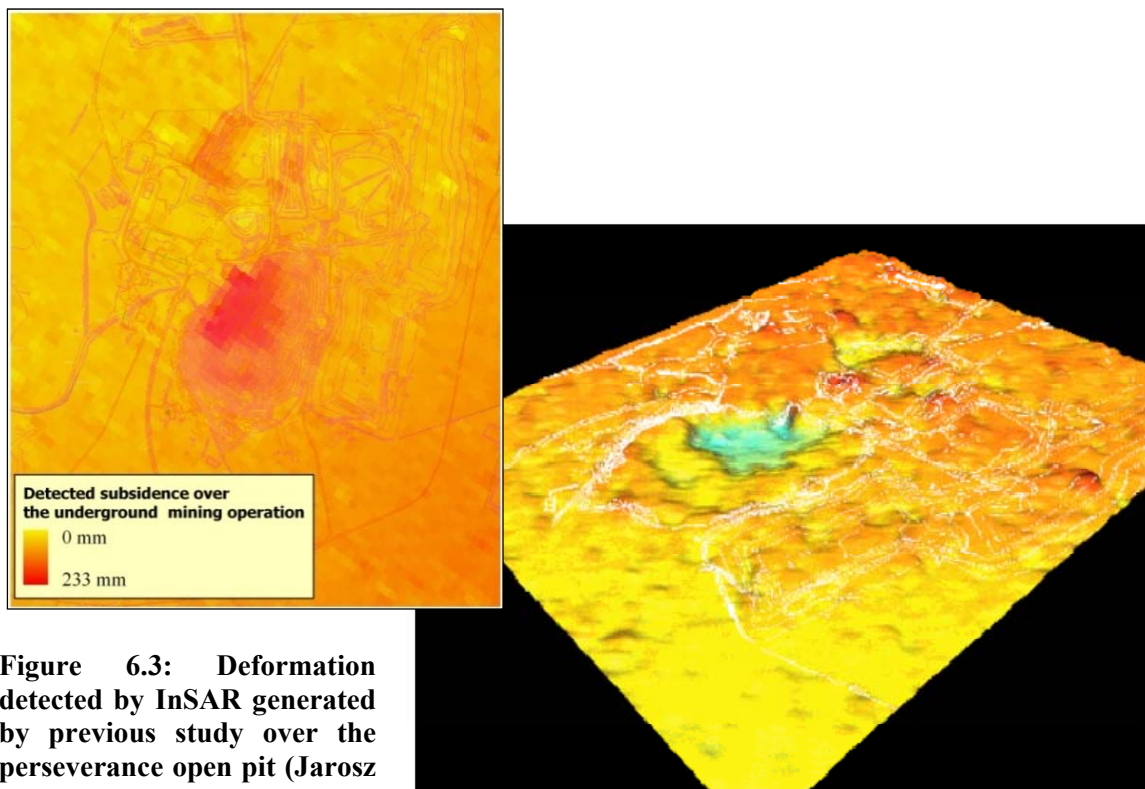


Figure 6.3: Deformation detected by InSAR generated by previous study over the perseverance open pit (Jarosz and Wanke, 2004)

6.1.2. Deformation Rate

The deformation rate tool described in Chapter 5 was used in order to estimate the level of possible ambiguity issue over the area of study. Two DTM layers, generated by photogrammetry with 323 days temporal baseline (30/04/2003 and 18/03/2004), were used as required elevation models. Considering ERS data, almost 35% of the area, mostly outside of the boundaries of the pit and large deformation area, can be accurately detected by InSAR (Figure 6.4).

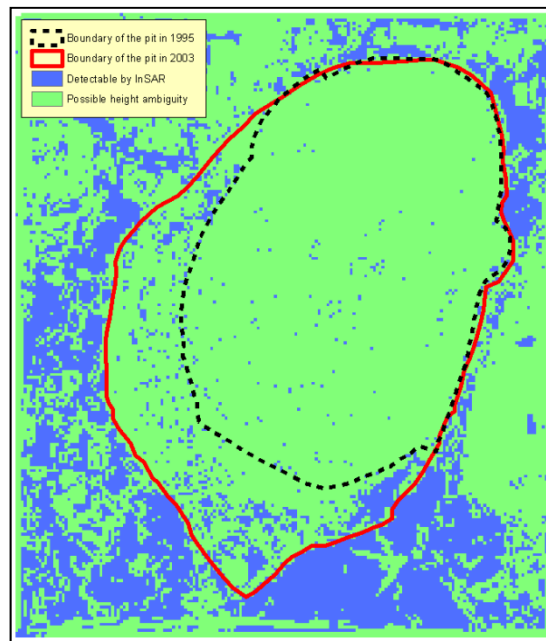


Figure 6.4: Deformation rate analysis results for Perseverance mine generated by deformation rate tool in case using ERS (C-band)

In order to evaluate how using data acquired using different wavelengths can help to avoid ambiguity problems, the test was run again assuming ALOS satellite as the data provider. As shown by Figure 6.5, it is obvious that using longer wavelength extents of the areas affected by ambiguity is dramatically decreased. Using ALOS data 57% of the area is detectable by InSAR and therefore regardless of any other considerations (e.g. required accuracy, vegetation or satellite coverage), it is recommended to use longer wavelengths to avoid ambiguity issue. However, in the case of the Perseverance operation, it was impossible to use ALOS data; considering the objective of the project, analysis was necessary to use historical data and the time period selected for images acquisition was even before launching ALOS.

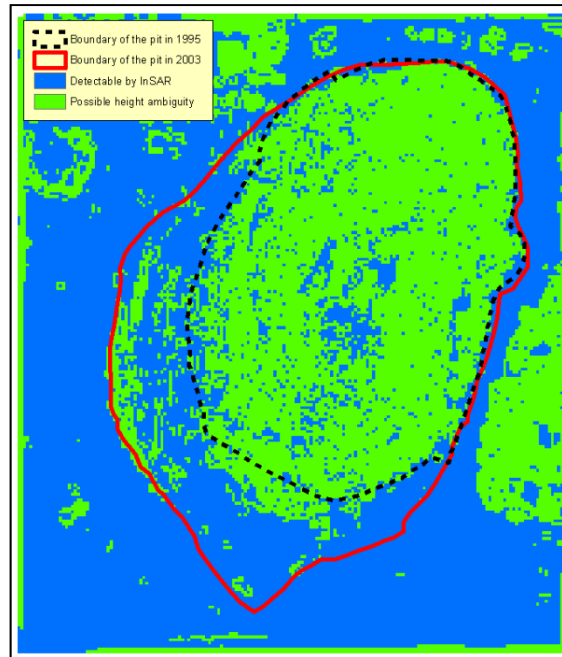


Figure 6.5: Deformation rate analysis results for Perseverance mine generated by deformation rate tool in case using ALOS-PALSAR data (L-band)

To have an idea of using images produced using a smaller wavelength, Figure 6.6 shows the deformation rate tool result for TerraSAR-X data (X-band). As described by the figure, the extent of ambiguous area will increase.

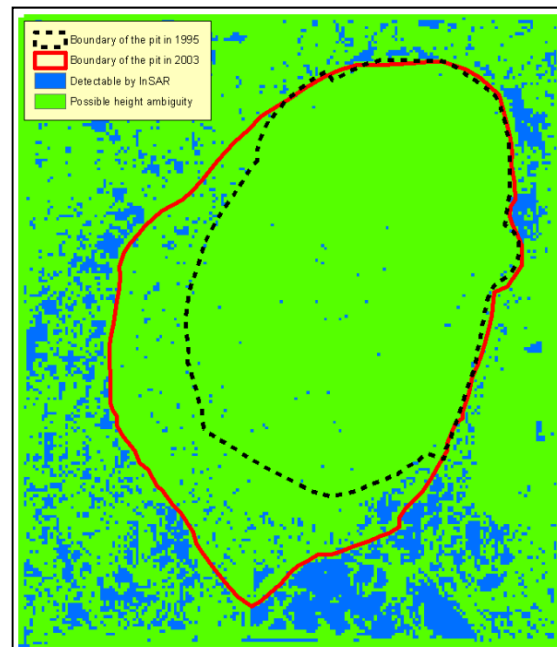


Figure 6.6: Deformation rate analysis results for Perseverance mine generated by deformation rate tool in case using TerraSAR-X data (X-band)

Using TerraSAR-X data only 14% of the area is detectable by InSAR without unwrapping; however it should be noted that TerraSAR-X spotlight sensor is able to

produce images with $1\text{m}\times 1\text{m}$ resolution that provides much more smooth and detailed description of deformation and consequently less ambiguity. Nonetheless, such small wavelength makes TerraSAR-X data highly sensitive to vegetation leading to incoherency of the images.

6.1.3. Data Selection

The main objective of the project was to test if InSAR could be used to provide required data for calibrating rock strata deformation models ; therefore the focus for this site was placed on the utilisation of available historical SAR data. The ESA archives listed only 10 ERS-2 SAR images for the particular mine site acquired after 2000. There was no SAR data covering the mine area available from other satellites, such as Envisat or ALOS. All of the ERS-2 data was acquired from the same path of a descending orbit, meaning that the radar was viewing the (near) east to west direction. The available data is shown in Table 6.1.

Table 6.1: Available SAR scenes

Date	Orbit
2 Jan 2002	35041
18 Dec 2002	40051
22 Jan 2003	40552
26 Feb 2003	41053
2 Apr 2003	41554
7 May 2003	42055
11 June 2003	42556
17 March 2004	46564
21 April 2004	47065
13 Oct 2004	49570

From 10 SAR images it was possible to create 45 pairs for InSAR processing without considering the number of linear independent combinations. However, not every pair is likely to result in an interferogram, and there are many reasons for this, mainly:

- Images did not correlate due to temporal/surface changes,
- Orbital separation (baseline) was too large,
- Inconsistent instrument pointing causing decorrelation (dissimilar Doppler Centroid) was present.

The last reason above is a problem specific to the ERS-2 data. As mentioned before, in 2000 ERS-2 suffered from gyro malfunctions and by the end of 2002 there were no operating gyros on the satellite. Taking into account these limitations, the possible pairs were shortlisted to those that might result in an interferogram. Two main parameters were used in the selection process:

- **Orbital Baselines:** The pairs that result in an orbital baseline greater than 400m were rejected as those with a larger baseline are not optimal for 2- and 3-pass InSAR methods.
- **Doppler Frequencies:** Following recommendations from the European Space Agency, the pairs that have a difference in Doppler Centroid frequency greater than 750Hz were also rejected.

Table 6.2, 6.3 and 6.4 show the orbital baselines, Doppler Centroid separations and temporal baselines for all possible pairs. The pairs that match the specific criteria are highlighted. Only six pairs matched both criteria and these are highlighted within Table 6.4.

Table 6.2: Orbital baselines of all pairs (m)

ORBIT	40051	35041	40552	41053	41554	42055	42556	46564	47065	49570
40051	0									
35041	447.3	0								
40552	1277.9	830.74	0							
41053	846.75	402.01	437.28	0						
41554	1342.1	895.3	79.505	507.96	0					
42055	769.96	322.77	508.38	102.67	573.03	0				
42556	788.84	342.01	489.89	68.386	557.23	36.388	0			
46564	844.38	401.75	444.79	22.039	517.26	115.95	79.912	0		
47065	633.5	186.49	644.8	216.99	710.75	138.08	155.54	218.97	0	
49570	446.09	80.045	842.63	406.08	911.57	342.66	354.33	401.47	206.04	0

Table 6.3: Doppler Centroid separations for all pairs (Hz)

ORBIT	40051	35041	40552	41053	41554	42055	42556	46564	47065	49570
40051	0									
35041	918.8	0								
40552	912.6	-6.2	0							
41053	2588.5	1669.7	1675.9	0						
41554	1164.6	245.8	252	-1423.9	0					
42055	1579.3	660.5	666.7	-1009.2	414.7	0				
42556	2435.2	1516.4	1522.6	-153.3	1270.6	855.9	0			
46564	1731.1	812.3	818.5	-857.4	566.5	151.8	-704.1	0		
47065	527.4	-391.4	-385.2	-2061.1	-637.2	-1051.9	-1907.8	-1203.7	0	
49570	-3407.9	-4326.7	-4320.5	-5996.4	-4572.5	-4987.2	-5843.1	-5139	-3935.3	0

Table 6.4: Temporal baselines of all pairs (days)

ORBIT	40051	35041	40552	41053	41554	42055	42556	46564	47065	49570
40051	0									
35041	350	0								
40552	35	385	0							
41053	70	420	35	0						
41554	105	455	70	35	0					
42055	140	490	105	70	35	0				
42556	175	525	140	105	70	35	0			
46564	455	805	420	385	350	315	280	0		
47065	490	840	455	420	385	350	315	35	0	
49570	665	1015	630	595	560	525	490	210	175	0

Of the six possible pairs, only two of them coregistered sufficiently well enough to create acceptable interferograms. This is most likely due to temporal ground changes between the two images. These pairs are summarised in Table 6.5:

Table 6.5: Description of the three acceptable pairs

Pair	Time Separation	Baseline
41554-40552	70 Days	79m
46564-42055	315 Days	115m

Since there are no common images between these three pairs, a DEM is required to derive the differential phase (i.e. 3-pass cannot be used here). These three pairs of images have been processed to identify possible ground deformation.

6.1.4. Layover Mask

To generate the layover mask, SRTM mission data (USGS, 2007) was used. Although the difference in date between the SAR images and the SRTM DEM was some three years, the results of the layover analysis seemed to agree very well with the image analysis. The original SAR image for the case study is shown in Figure 6.7, alongside the same image with the layover mask superimposed. This figure is presented such that the ERS satellite is viewing the terrain from the right hand side of the page. In the slant-range image, the layover region is small and clearly in a crescent-shaped area on the left of the pit. The shape and position of the layover mask confirms that the SRTM DEM is sufficient to describe it.

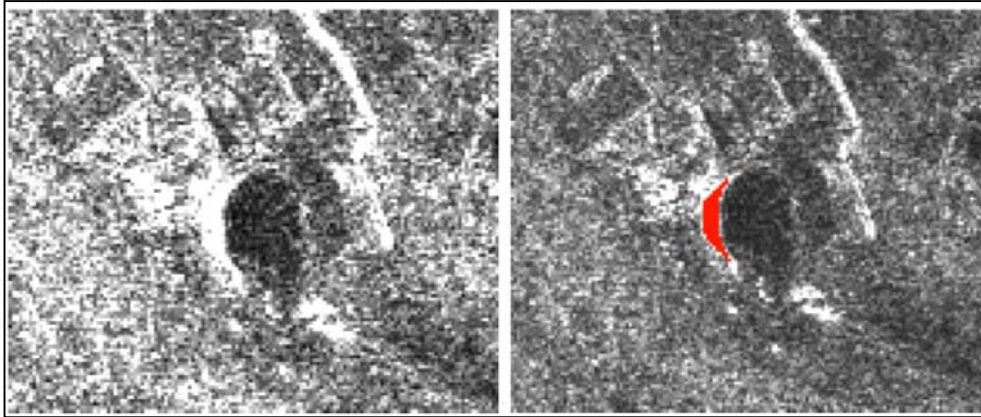


Figure 6.7: A slant range SAR image of Perseverance mine (left) and with layover area highlighted in red (right)

The terrain-corrected images are shown in Figure 6.8, where the input SAR image and the layover mask have been rectified to their proper shape and relative positions as would be seen on a map. It is clear that the rectification process has had a huge effect, considerably increasing the size of the layover area and decreasing the size of the Eastern wall of the pit. Much of the pit is obscured from view and the drastic effect of layover will clearly limit the available interferometric signal on the Western side of the feature.

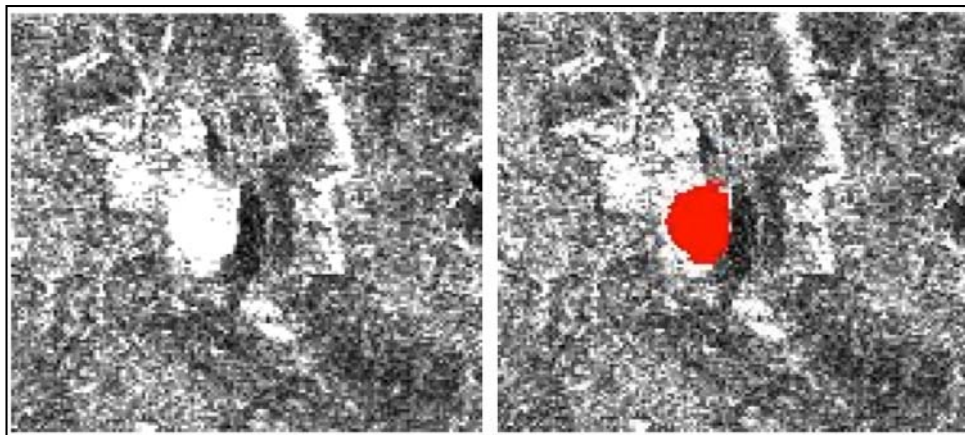


Figure 6.8: A geocoded SAR image of Perseverance mine (left) and with layover area highlighted in red (right)

6.1.5. Data Processing and Results

The interferometric processing has been performed using the InSAR toolbox together with precise orbits (Scharroo et al., 1998) from the Delft Technical University. Phase unwrapping has been performed using the Snaphu software from

Stanford University (Chen and Zebker, 2001). As described in the previous section, the high accuracy up-to-date DEM was used as the terrain model for the differential interferometry processing and for generation of the layover mask. The mask was applied to the data prior to phase unwrapping. Due to zero-weighting the phase data that corresponds to the mask, these regions should therefore have no effect on the neighbouring pixels. The mask is also applied to the final products so that erroneous measurements are not considered. However, the comparison of results generated with and without masking suggested that the applied mask made no significant difference to the InSAR results.

The masked line-of-sight deformation maps based on two selected pairs were generated. The temporal baselines of the interferograms were 315 and 70 days respectively, which means that any deformation shown took place in this time period. All of the available data was acquired from the satellite descending orbits, meaning that the radar was viewing in the (near) east to west direction. This caused the west wall of the pit to be in an area of layover. However the east wall of the pit was in good view of the radar.

Despite generating interferogram for two pairs, results of only one pair were acceptable. Little or no deformation identified from the 315-day interferogram was in contrast with deformation seen for the 70-day interferogram. This appears contradictory but may be due to a signal ambiguity. The analysis of topographic changes, based on the historical topographical data, suggests a high amount of subsidence in 2003 equivalent to a linear rate of 6.0 m/yr or 16.4 mm/day in the southwest area of the pit. Over 70 days, between the SAR acquisitions, the vertical component of movement reached 1144 mm. Such change happened over a horizontal distance of 22.3 m, meaning that the change between neighbouring SAR pixels reached a similar value. Such a high rate of subsidence leads to ambiguity issues that cannot be resolved by InSAR processing. However, the InSAR processing provided highly valuable information regarding the deformation in the large area surrounding the footprint of underground extraction. The 70-day subsidence detected by InSAR, north of the pit is shown in Figure 6.9-a. In order to eliminate the impact of local distortions on the far-reaching subsidence trough, a global polynomial was best fitted to the masked layer containing subsidence detected by InSAR. The applied mask

eliminated the layover areas and the areas of known man-made terrain disturbance. The best fit of a polynomial was characterised by: power = 3, mean error = $3.98e^{-5}$ m and RMS = 0.002451 (Figure 6.9-b).

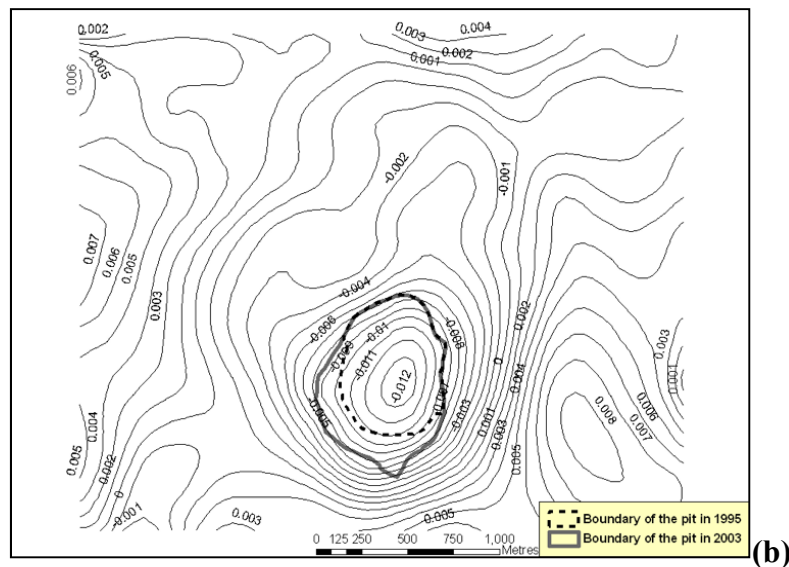
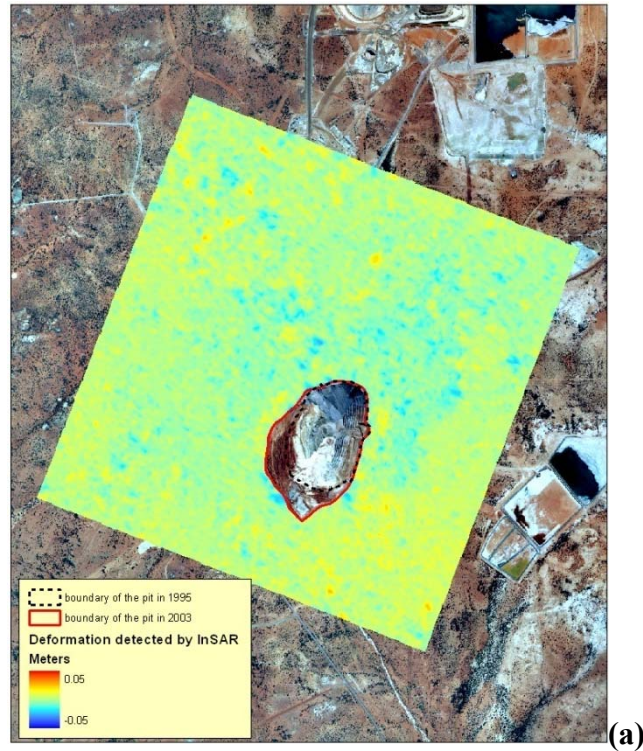


Figure 6.9: Subsidence detected by InSAR over Perseverance mine for pair 41554-40552 with 70 days temporal baseline

The Snapu unwrapping algorithm used in this project is based on a minimum cost flow solution and therefore any localised subsidence effects that cause ambiguities may be lost if there is an obvious discontinuity within the neighbourhood

of the subsiding area. This is the case for most of the available unwrapping techniques. It was not possible to validate the unwrapping algorithm using ground truth since the area covered by ground control stations was relatively small and did not cover any significant deformation. Other surveying techniques such as laser altimetry can be considered as a resolution of InSAR ambiguity issue. However, considering the fact that monitoring deformation is not seen as a crucial component of mine production process, the cost of utilising such techniques practically precludes their application.

6.1.6. Comparison with Subsidence Analysis Using Classical Surveys

The slope stability monitoring system initially included 71 points that were observed from the permanent theodolite station located on the top of waste dump and east of the open pit. Unfortunately, over time, a significant number of the reflectors were lost, reducing the value of the collected data in the subsidence active area. This area covered the southwest slope of the pit and the adjacent region southwest of the pit's crest. Replacement of the lost reflectors was not possible due to safety reasons (the area was classified as inaccessible). However, the network of monitoring points was expanded further towards the west, through the establishment of 38 new monitoring stations. The locations of the monitoring stations are presented in Figure 6.10. The RTK GPS technology was used to monitor the movement at these new stations, providing relatively high positioning accuracy.

A review of existing data suggests that the achieved positional accuracy was in the range of: ± 1 mm (horizontal) and ± 1 mm (vertical). A quality analysis of the GPS results and particularly a stability assessment of the GPS base station used for the surveys was not available. Using the deformation database, created by the 'Quick Slope' software, the three components of movement (dx, dy, dz), for each monitoring point, were extracted for the period between the acquisition dates of the SAR data. The extracted components were then used to approximate a continuous field of movement in the regions west and southwest of the pit. Very small vertical movements, reaching the value of -3 mm, were detected at the monitoring points during the period between the SAR acquisitions (Figure 6.11).

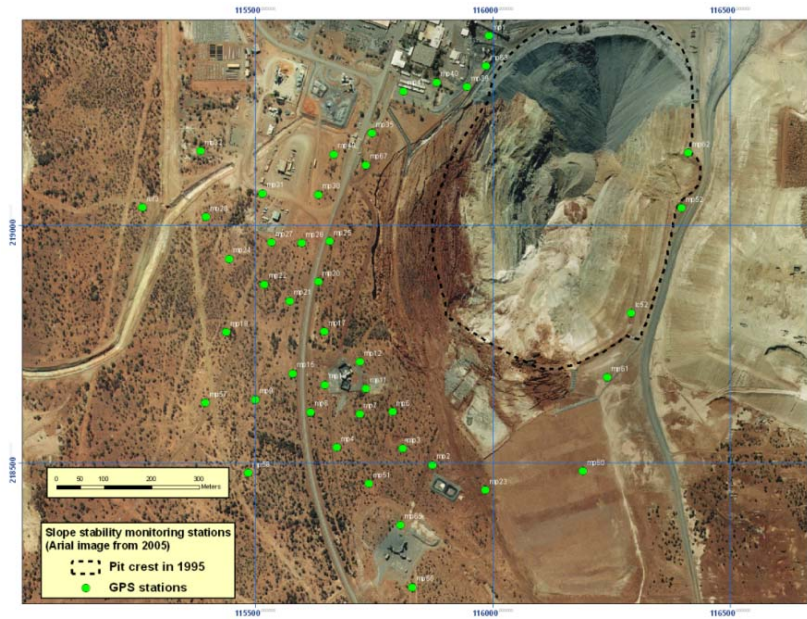


Figure 6.10: Slope stability monitoring stations over the area of study

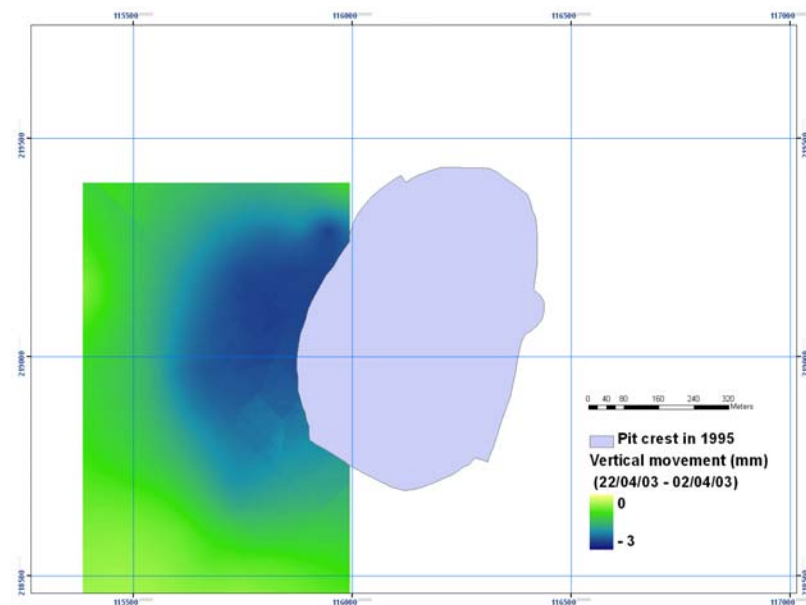


Figure 6.11: Vertical movement detected by classical surveys between the dates of processed SAR acquisitions (41554-40552)

A comparison between Figure 6.9 and Figure 6.11 shows that, unfortunately, the GPS survey did not cover the area of greatest deformation from the InSAR results. Also, the level of deformation detected is within a noise level of InSAR and only limited agreement was anticipated. According to Table 6.6, the obtained results suggest small agreements between GPS and InSAR results in their common area of coverage. The average difference is 2 mm and the standard deviation of differences is ± 3 mm.

The InSAR results suggest existence of subsidence in this area, to the value between 0 and 10 mm, as a natural extension of the gentle subsidence trough detected to the north of the open pit. Considering the density of observations over a specific area, InSAR results can be better justified. However, it has to be noted that this comparison was performed over a limited area and a better agreement between both methods may exist elsewhere.

Table 6.6: Monitored deformation by InSAR vs GPS (over 70 days)

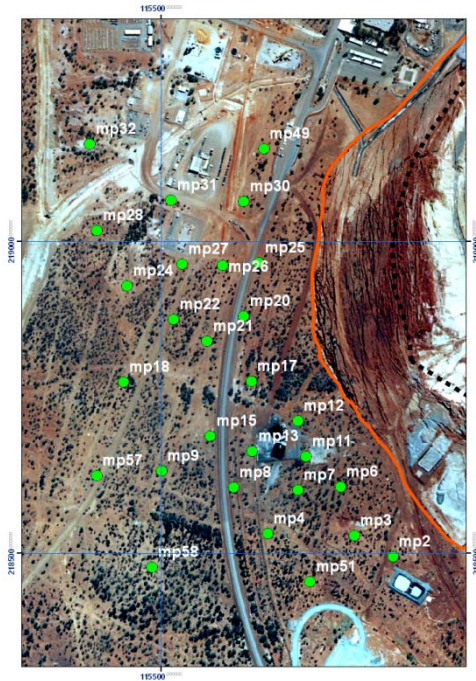


Figure 6.12: Set of GPS monitoring stations used for comparative analysis

Target	InSAR (m)	GPS (m)	Diff (m)
mp2	0.003	-0.001	0.004
mp3	0.000	-0.001	0.001
mp4	0.001	-0.001	0.002
mp6	-0.003	-0.001	-0.002
mp7	0.000	-0.001	0.001
mp8	0.002	-0.001	0.003
mp9	0.001	-0.001	0.002
mp11	-0.004	-0.002	-0.002
mp12	0.001	-0.002	0.003
mp13	0.001	-0.001	0.002
mp15	0.004	-0.001	0.005
mp17	-0.004	-0.002	-0.002
mp18	0.001	-0.001	0.002
mp20	0.001	-0.002	0.003
mp21	0.000	-0.002	0.002
mp22	0.001	-0.001	0.002
mp24	-0.002	-0.001	-0.001
mp25	0.003	-0.002	0.005
mp26	-0.003	-0.002	-0.001
mp27	-0.001	-0.001	0.000
mp28	0.000	-0.001	0.001
mp30	0.006	-0.002	0.008
mp31	-0.007	-0.001	-0.006
mp32	-0.002	-0.001	-0.001
mp49	-0.002	-0.002	0.000
mp51	0.001	-0.001	0.002
mp57	0.000	-0.001	0.001
mp58	0.010	0.000	0.010

6.1.7. Mine Specific Deformation Analysis

6.1.7.1 Apparent Heave

The subsidence results obtained from the analysis of topographical surveys and from InSAR processing, suggested that some portions of the open pit slopes had

experienced uplift (heave) not subsidence. Detailed analysis of the slope movement explained this phenomenon as not real but apparent uplift. It became clear that a change of elevation at any location is the result of two components: vertical movement (subsidence) and horizontal shift of the ground. If these two movement components have an effect on a slope or a mining bench, and the horizontal movement acts toward the centre of a pit, it can result in an apparent heave of the ground (as shown in Figure 6.13).

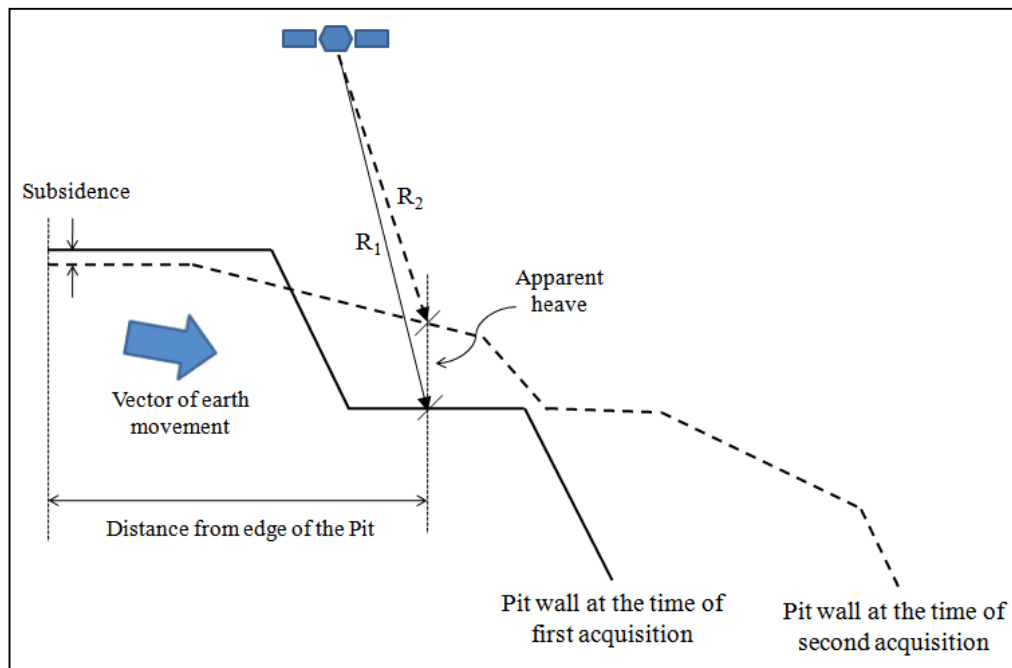


Figure 6.13: Apparent heave of the ground

6.1.7.2 Deformation Rates and the Issue of Ambiguity

The irregular rate and highly dynamic character of deformation induced by mining may lead to an ambiguity issue. The ambiguity problem arises when high rate deformation occurs over a small area and happens when the vertical movement between the neighbouring cells (pixels) of the SAR image is greater than quarter of the wavelength of a radar signal. InSAR can only measure phase change as a fraction of a single wavelength and any motion that causes greater phase changes will still be given modulo one wavelength. This ambiguity cannot be resolved by the InSAR processing procedures and techniques. Any further studies should take ambiguity issues into account since its appearance is very likely the case of high rate, dynamic deformation fields such as mining induced deformation.

In order to clarify the importance of the deformation rate and the ambiguity issue in mining related applications of InSAR, six DTMs, based on topographical surveys (aerial photogrammetry), between 2001 and 2006 were used to determine the vertical components of movement (subsidence) occurring between dates of topographical surveys (Table 6.7).

Table 6.7: Digital terrain models

Year	Date	DTM Format
1995	24/09/1995	DXF
1998	17/10/1998	DXF
2001	15/03/2001	DXF
2002	12/03/2002	DXF
2003	30/04/2003	DXF
2004	18/03/2004	DXF
2005	15/04/2005	DXF
2006	21/06/2006	DXF

To determine the vertical component of movement (subsidence) that occurred between dates of topographical surveys, the collected DTMs were converted into digital elevation models (DEM) and then differences were created using GIS analytical software (ArcGIS). To remove systematic errors from individual DEMs, the common stable reference areas (Figure 6.14) were selected and average elevations for each area were calculated (Table 6.8).

Table 6.8: Average elevations and elevation differences for reference areas (m)

Year	Area 1	Area 2	Area 3	Area 4
1995	10523.20831	10523.002	10520.77073	10526.88293
1998	10523.00245	10522.991	10520.01586	10526.6729
2001	10523.23096	10523.144	10520.40752	10526.85752
2002	10522.9192	10523.023	10519.97869	10526.94959
2003	10523.0308	10523.033	10519.87825	10527.05478
2004	10523.32016	10523.443	10520.33245	10527.2093
2005	10523.30592	10523.077	10520.17952	10527.29713
2006	10523.42825	10522.902	10519.92229	10527.49736

By comparing these average elevations, calculated for individual DTMs, the systematic component of elevation errors was determined and later removed from the calculated subsidence. The subsidence utilised the DTM from 2001 as the base. The examples of subsidence, spanning years 2001-2003 and 2001-2006, are presented in Figure 6.15 and 6.16.

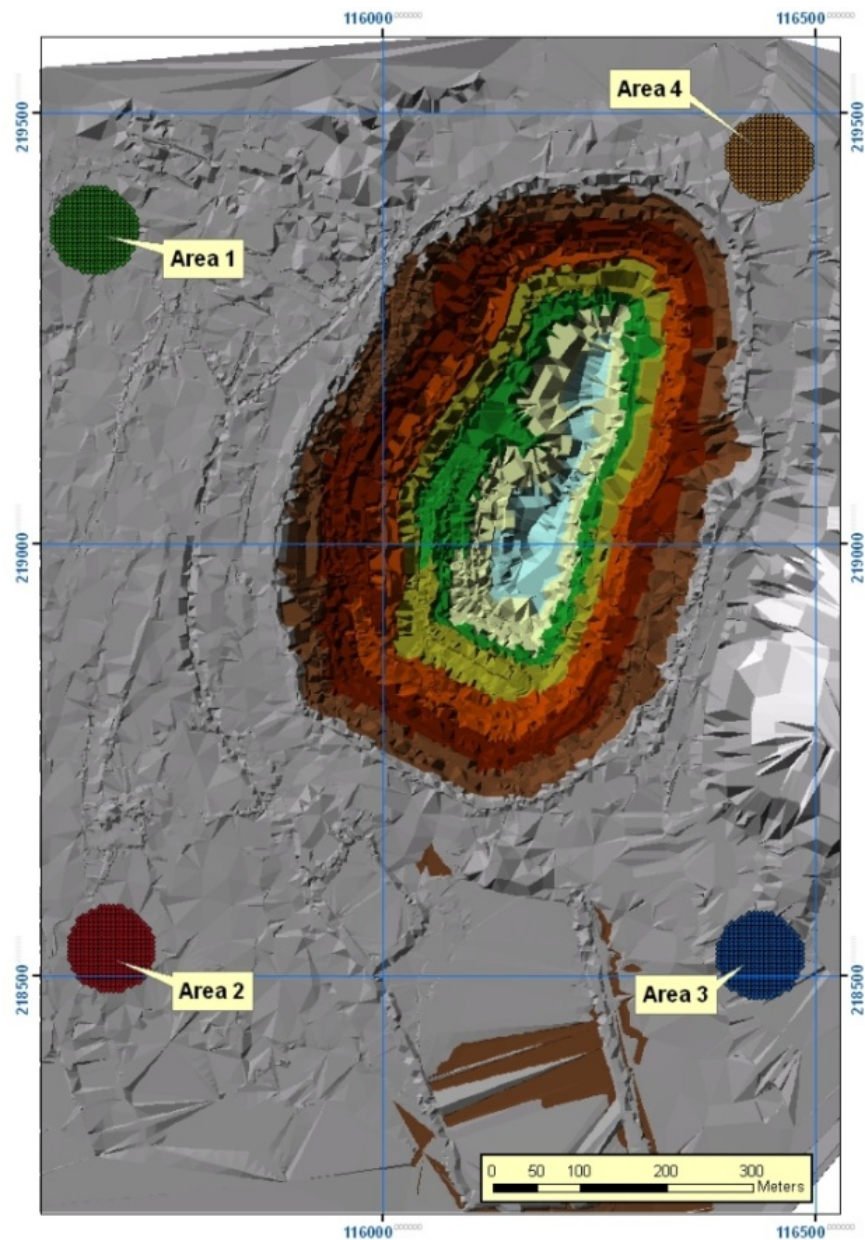


Figure 6.14: Location of reference areas over 1995 DTM.

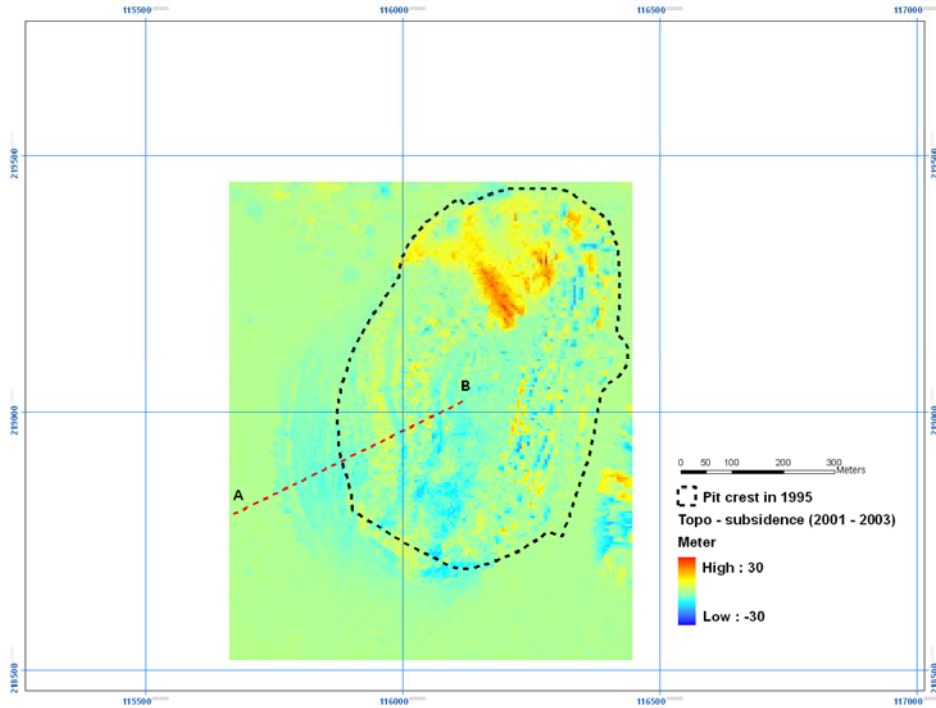


Figure 6.15: Subsidence between 2001-2003 derived from topo surveys for Perseverance mine

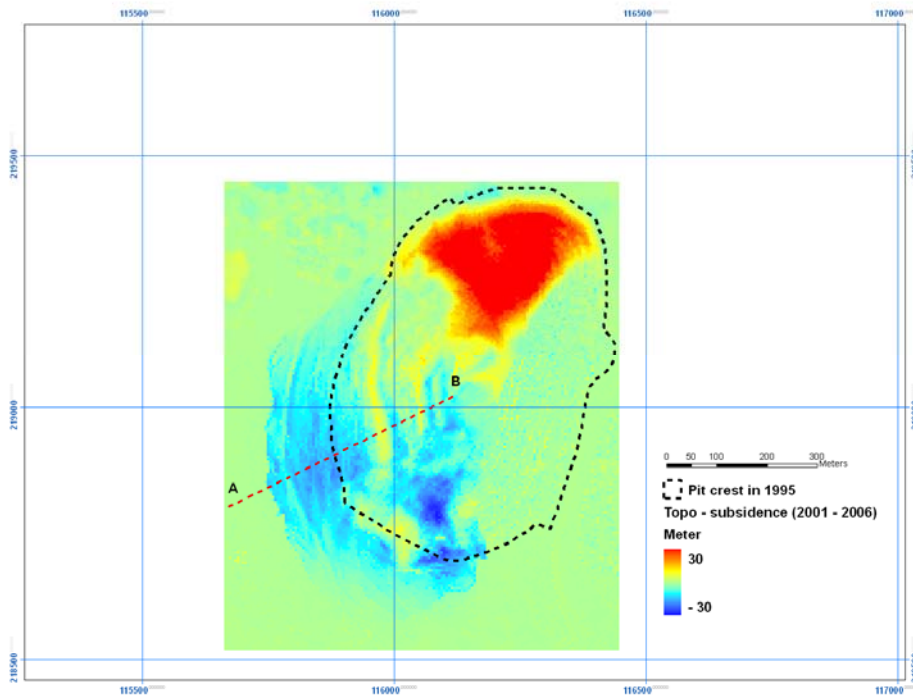


Figure 6.16: Subsidence between 2001-2006 derived from topo surveys for Perseverance mine

Figure 6.17 shows the series of cross-sections, representing the dynamics of ground movement along the profile A-B. It is clear that the area with greatest

subsidence (south-west of the pit) experienced a total of -17m of vertical movement between years 2001 and 2006, with the average yearly equivalent subsidence rate reaching -3.8m/yr (in 2005).

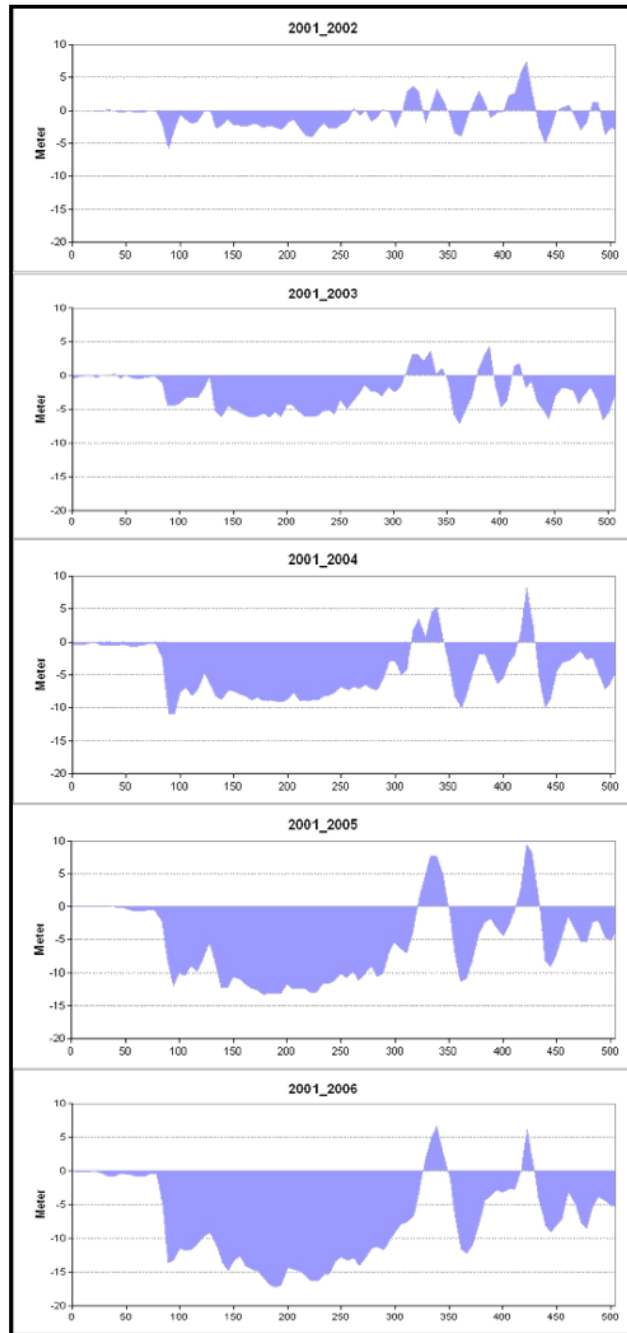


Figure 6.17: Subsidence along A-B cross-section referenced to 2001 DTM

Figure 6.18 shows the development of subsidence between 2001 and 2006. To eliminate inconsistency of detected local subsidence values represented by the individual pixels, the maximum rate was determined by averaging subsidence over an area of sixteen pixels ($20\text{m} \times 20\text{m} = 4 \times 5\text{m}$ by $4 \times 5\text{m}$). The analysis suggests a high

amount of subsidence during the period of SAR acquisitions that were used for processing (e.g. between 22/01/2003 and 02/04/2003). According to the values presented in Figure 6.19 the equivalent subsidence rate has reached the level of 6.0 m/yr or 16.4 mm/day over the distance of 22.3 m, which definitely should lead to ambiguity issues in InSAR processing.

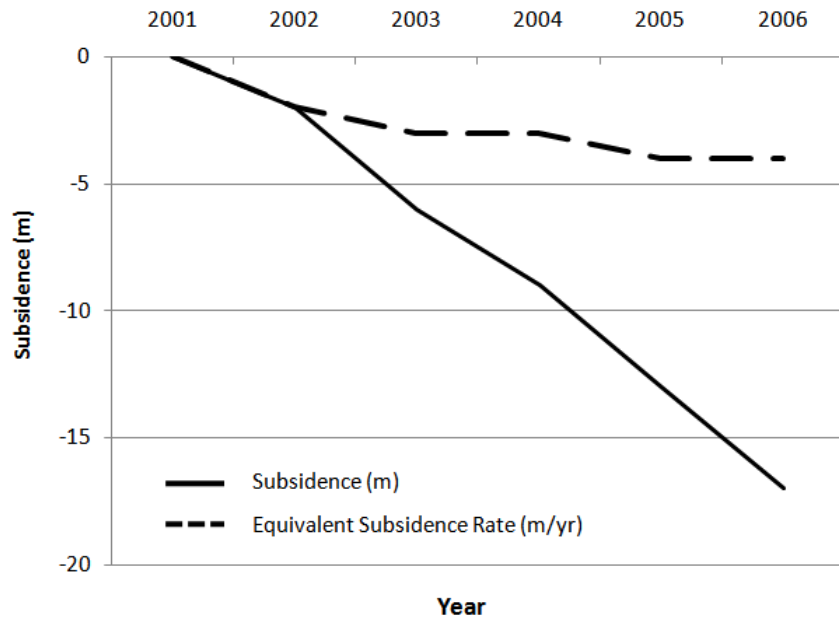


Figure 6.18: Development of subsidence between 2001 and 2006 calculated based on available DTMs,



Figure 6.19: Equivalent subsidence rate in the period 2003-2004 along the profile A-B calculated based on available DTMs (from the point A to the edge of pit's crest; temporal baseline of 318 days)

6.2. Argyle Diamond Mines

6.2.1. Case Study Overview

The Argyle diamond mine is located in the Kimberley region in the northeast of Western Australia about 550 kilometres southwest of Darwin (Figure 6.20). The Argyle diamond mine operation started in 1972 when the exploration program within the region began looking for possible deposits of diamond. The main Argyle mine pipe (AK1 pipe) was discovered in 1979 that led to the beginning of the Argyle Diamond Mine in December 1985. Argyle currently operates an open pit mine to recover diamonds from the AK1 lamproite pipe. Also, alluvial mining that commenced in 1983 is still continued.



Figure 6.20: Location of Argyle Diamond Mines (Google Inc., 2009)

In 2005, the Rio Tinto Board decided to start constructing an underground mine below the existing open pit. The objective of the project was to provide a demonstration of application of InSAR technique for determination of surface deformations (subsidence) induced by underground mining at the Argyle Diamond Mine. The InSAR processing and analysis included:

- Selection of suitable SAR images from the available archive data and planning of new SAR acquisitions to perform interferometric analysis,

- Processing of the acquired data to detect the radar line-of-sight deformation occurring at the mine site; using the 2-pass differential technique together with a Digital Elevation Model (DEM) generated from integration of the DTM provided by mine's surveying office and the DEM generated by SRTM mission,
- Initial interpretation of subsidence results and
- Recommendations for constructing a plan for monitoring surface deformation induced by future underground activities using the InSAR technique.

6.2.2. Data Selection

There are many SAR capable satellites both currently operating and planned in the future. Since satellites utilise active sensors they can only operate for approximately 10% of the time due to draining the batteries. This means that data is mostly only acquired when it has been specifically ordered. The search for available archive data, covering the Argyle's mining period, provided no results. Acquisition of new, planned SAR data was necessary. The planned SAR images have the advantage of being acquired with parameters suitable for interferometric processing; however it should be noted that even with using planned images not every pair of SAR images will result in a good interferograms and be the same as using historical data; issues such as large orbital separation (baseline) may still exist. Taking into account the satellite coverage and the required parameters for the Argyle Diamond Mine area, the Envisat satellite mission was selected to provide the required data.

Table 6.9 represents the selected dates and orbits of planned data to be used in this preliminary subsidence analysis over the Argyle Mine area. Table 6.10 shows possible pairs which can be produced using the planned data. As the objective was to provide a demonstration of the technique only the first pair (orbits 28234-28735 with 35 temporal and 92 metre spatial baseline) was purchased and processed. Other planned images were also acquired by satellite but not purchased and processed. These images are available in the Envisat data archive and can be obtained for any further analysis in the future. Also, more acquisitions can be planned and acquired in the future if any subsidence monitoring program is developed.

Table 6.9: Planned SAR images

Date	Orbit
25/07/2007	28234
29/08/2007	28735
07/11/2007	29737
12/12/2007	30238

Table 6.10: Possible pairs for interferogram generation using the available SAR images

Date	Day Diff	Baseline Diff (m)	Orbit
25/07/2007	35	92	28234
29/08/2007			28735
25/07/2007	140	122	28234
12/12/2007			30238
25/07/2007	105	145	28234
7/11/2007			29737
29/08/2007	105	214	28735
12/12/2007			30238
29/08/2007	70	53	28735
7/11/2007			29737
7/11/2007	35	267	29737
12/12/2007			30238

Due to the lack of historical SAR images covering the area of the Argyle Mine, it was decided to use 2-pass InSAR technique. In such a case, the DEM of area is required to derive the differential phase. A 90-m DEM provided by the SRTM mission has been used as the base terrain model. Since the SRTM mission was completed in year 2000 more recent elevation data was needed. A high resolution DEM has been created by integrating SRTM DEM and the recent DTM provided by mine's surveying office. This high resolution DEM has been used in the differential interferometry processing and also for generation of the layover mask. Detailed analysis of using current DEM for Argyle Diamond Mines was previously discussed in Chapter 5 (see section 5.2.2).

6.2.3. Layover Analysis

The Envisat satellite, on its ascending orbit, views the Argyle pit obliquely under an angle of 23° . The geometry is illustrated below in Figure 6.21. It shows that the Envisat satellite is viewing the pit from the West, meaning that the Eastern wall of the pit must be excluded from the analysis due to layover.

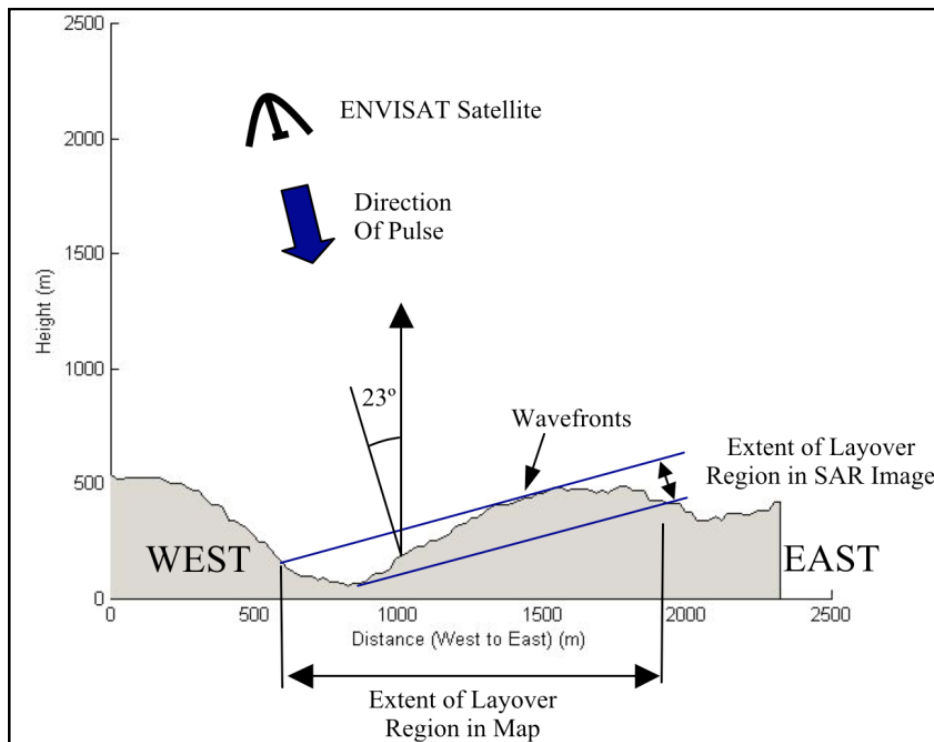


Figure 6.21: Height profile across the pit indicating the layover scenario

The appearance of the pit in the slant-range SAR image is shown in Figure 6.22. In this image, Envisat is viewing the geometry from the left of the illustration so the Western wall of the pit is very clear on the left of the image. Indeed, the benches are apparent as a series of parallel lines extending down into the pit bottom. To the immediate right of the benches is the main layover area (the bright S shaped area). The layover mask, shown, echoes this shape perfectly so the DEM is clearly correct for this scene. The results of terrain-correcting image (ortho-image) are shown in Figure 6.23. The shape of the pit has changed dramatically, as well as, the layover region. The layover area, although small in the SAR image, eliminates a large part of the pit from analysis.

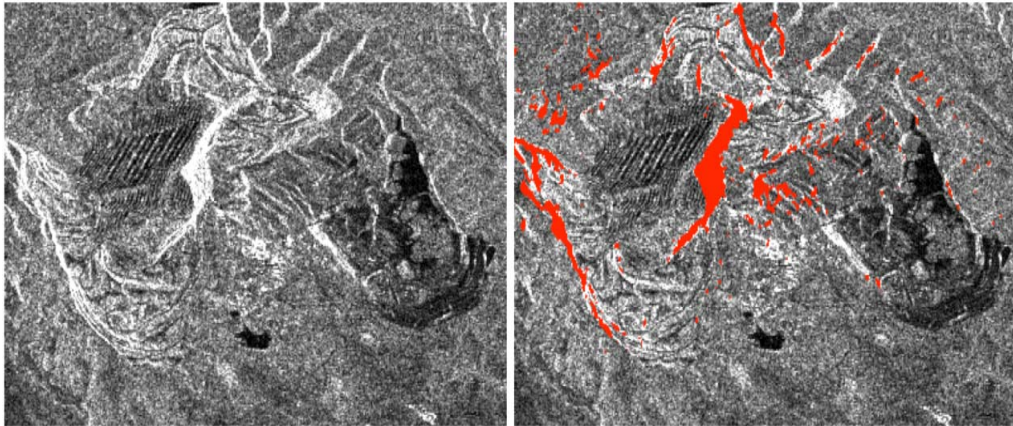


Figure 6.22: A slant range SAR image of Argyle (left) and with layover areas highlighted in red (right)

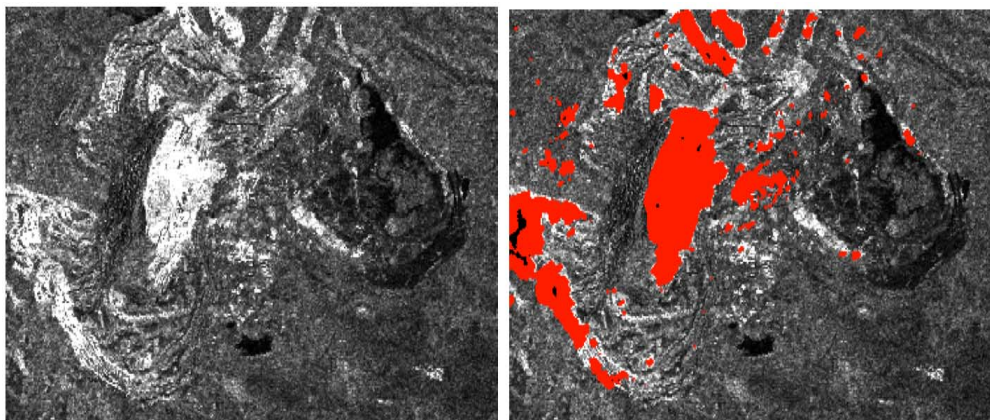


Figure 6.23: A geocoded SAR image of Argyle (left) and with layover area highlighted in red (right)

6.2.4. Data Processing and Result

The interferometric processing has been performed using the InSAR toolbox together with precise orbits (Scharroo et al., 1998) from the Delft Technical University. Phase unwrapping has been performed using the Snaphu software from Stanford University (Chen and Zebker, 2001).

The deformation map for the pair 28234-28735 between 25th of July and 29th of August 2007 is shown in Figure 6.24. The temporal baseline of the interferogram is 35 days, which means that any deformation shown took place in this time period. The deformation field over the research area was created with application of the layover mask. In order to eliminate local distortions, a global polynomial was best fitted to the result detected by InSAR. The best fit of the polynomial was characterised by: power = 2; mean error = $1.78e^{-5}$ and RMS = 0.00407. Figure 6.25

represents the interpolated deformation results in a contour form inside and around the pit.

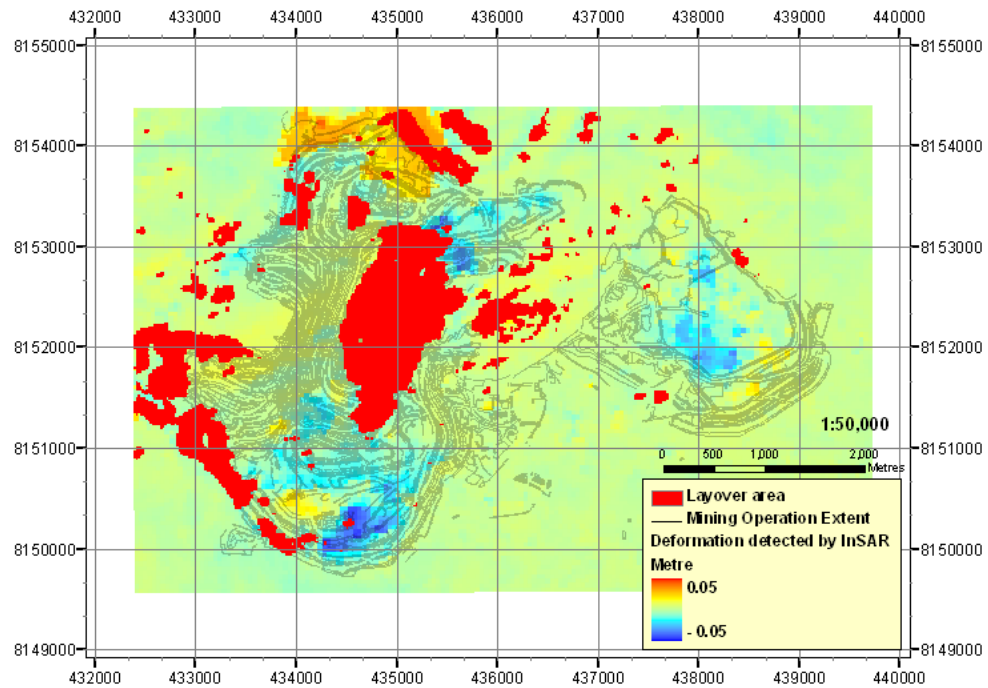
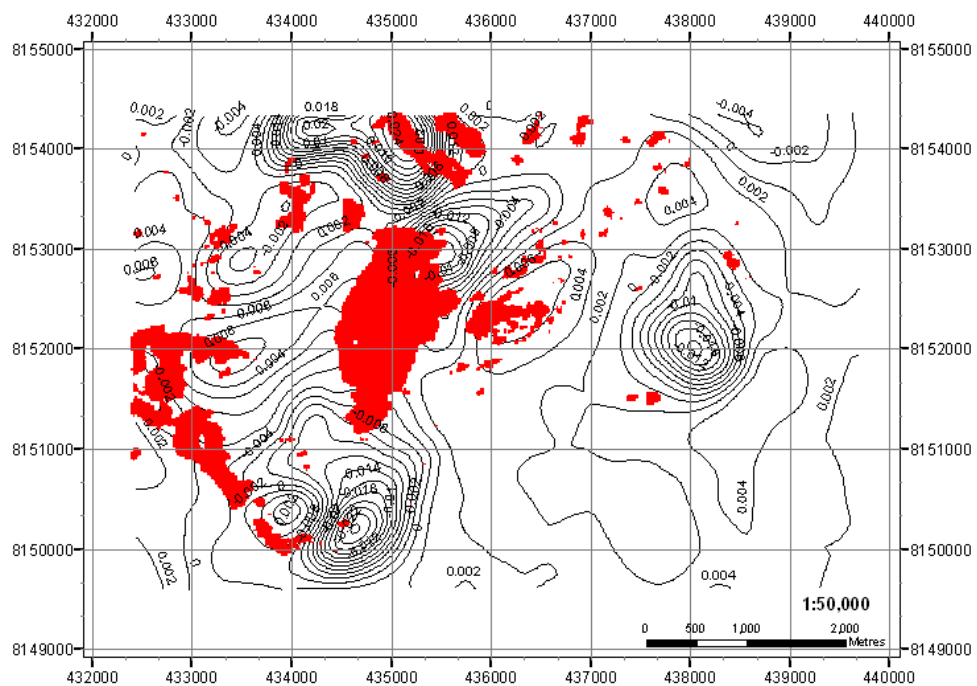


Figure 6.24: Deformation detected by InSAR for pairs with temporal baseline 35 days



studies should take into account the ambiguity issue as its existence is very likely in this case study.

Main deformed fields can be recognised around the lake banks, north of the pit, over the dumping area, south of the pit, tailing pool and in the north-east part of the pit. This might be the result of extraction activities inside the pit, dumping materials or settling of the materials in dump and tailing areas. Any further interpretation and result validation required more field data. However, it is clear that pit walls, in particular the west wall, were almost stable during the period between two SAR acquisitions (35 days apart).

As the result of this project, the WASM research team developed the methodology for the future analysis in the Argyle Diamond Mines. This includes both ascending and descending satellite tracks in order to reduce the resultant layover mask, a timetable of SAR image acquisitions with regards to development schedule of the Argyle underground operation and suggestion for future deformation monitoring plan involving InSAR technique

6.3. Ridgeway Underground Gold Mine – ALOS

6.3.1. Case Study Overview

As part of Cadia valley operations owned by Newcrest Mining Limited, the Ridgeway mine is one of the largest underground operations in Australia located in the Orange district, Central Western New South Wales. The first gold and copper deposit in the area was discovered in 1992 leading to commencing Cadia Hill open pit in 1998. Another deposit was discovered in 1996 approximately 500 metres below the surface and six years later, in 2002, the Ridgeway underground operation officially commenced when its 4 mtpa treatment plant was opened.

The Ridgeway underground mine uses the sub-level caving mining method, however the mine is in the process of transitioning to a block caving mining method in order to extract the ore beneath the existing mine. This project is called Ridgeway Deeps which is expected to commence in 2010.



Figure 6.26: Location of Ridgeway underground operation (Google Inc., 2009)

The mine is accessed by a decline and a sub-level caving method is used to extract deposit. Mining commenced at the top of the ore body and extraction levels are developed every 25 metres. Due to the caving process, the Ridgeway operation is characterised by extensive surface subsidence which was considered being studied using SAR interferometry (Figure 6.27).



Figure 6.27: Ridgeway and Cadia hill operations and location of subsidence cater above caving zone (Newcrest Mining Limited, 2009)

This section presents results obtained from a preliminary study on the Ridgeway operation using ALOS data. This was part of a proposed research project to Newcrest Mining Limited for developing a long-term subsidence monitoring plan using InSAR over their mining operations utilising caving methods. The expected project outcomes are as follows:

- Development of comprehensive planning procedures for SAR data acquisitions that involve:
 - ✓ Determination of the best sensor to be used,
 - ✓ Determination of the best orbital and geometric parameters,
 - ✓ Determination of the optimal monitoring frequency.
- Development of an accurate algorithm allowing determination of layover masks.
- Optimisation of the data processing procedures.
- Results tuning and validation by usage of active transponders.
- Further validation of InSAR results through comparison with data gathered using the classical surveying techniques.
- Development of algorithms allowing for resolution of ambiguity that may be present in InSAR results.
- Definition of file formats, for results of processing, which may be easily utilised by other mine software packages.
- Generation of deformation maps representing distribution of terrain subsidence in space and time.

6.3.2. Data Selection

In order to test data with longer wavelength and also considering highly vegetated areas over the Ridgeway operation, it was decided to use ALOS data for this project. Focusing on Ridgeway subsidence crater, nine images selected from historical data covering almost 2 years (the period between May 2006 and February 2008) were purchased and processed (Table 6.11).

Table 6.11: Geometric and Temporal baseline for selected pairs

Date	Day Diff	Baseline Diff (m)
02/11/2007 18/12/2007	46	93
02/11/2007 02/02/2008	92	588
18/12/2007 02/02/2008	46	492
04/01/2008 19/02/2008	46	91
01/01/2007 04/01/2008	368	1065
21/05/2006 06/07/2006	46	-348

6.3.3. Data Processing and Results

The interferometric processing has been performed using the InSAR toolbox the Snaphu software from Stanford University for phase unwrapping (Chen and Zebker, 2001). The study was focused on subsidence crater directly above caving zone and bank area around. Figure 6.28 compares amplitude images generated for the first processed pair (02/11/07 – 18/12/07). A change to whole surrounding (bank) area is obvious which can be related to potential collapse on the edge of the crater. This was later confirmed by processing more pairs.

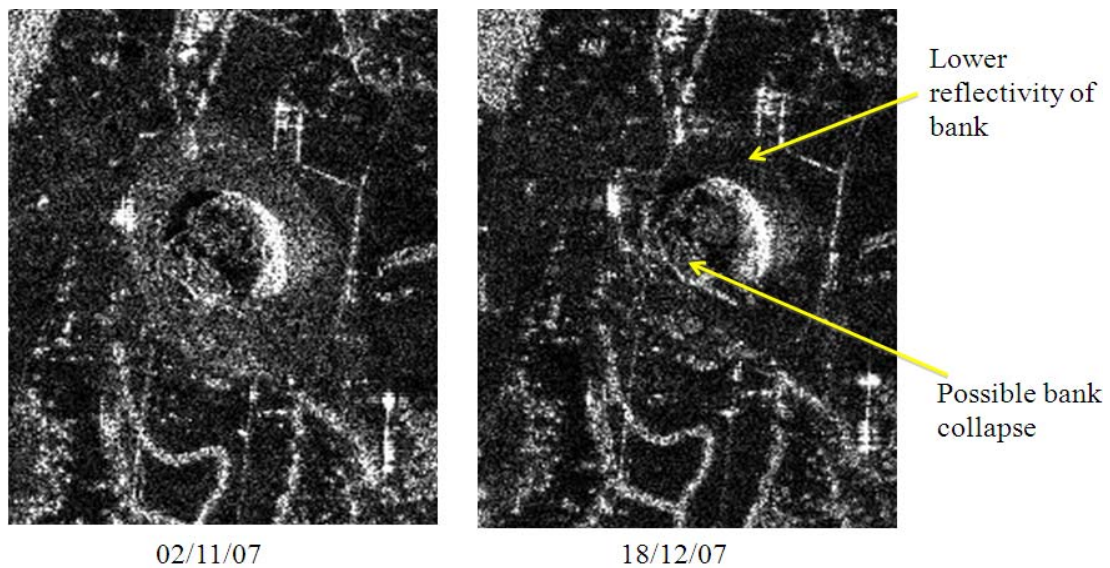


Figure 6.28: Amplitude images generated for the first processed pair, describing subsidence crater and surrounding area

Figure 6.29 shows result for pair between (02/11/07 – 18/12/07) representing possible subsidence of a few centimetres over the bank. The main problem that affected the result quality was an incoherency issue which was detected over the crater and bank area. It can be assumed that whole bank has collapsed; however the incoherency issue is not only limited to the area affected by subsidence and exists over the whole image. Later and by processing more pairs, it was found that incoherency is the main problem affecting all processed pairs which can be related to the type of vegetation over the area.

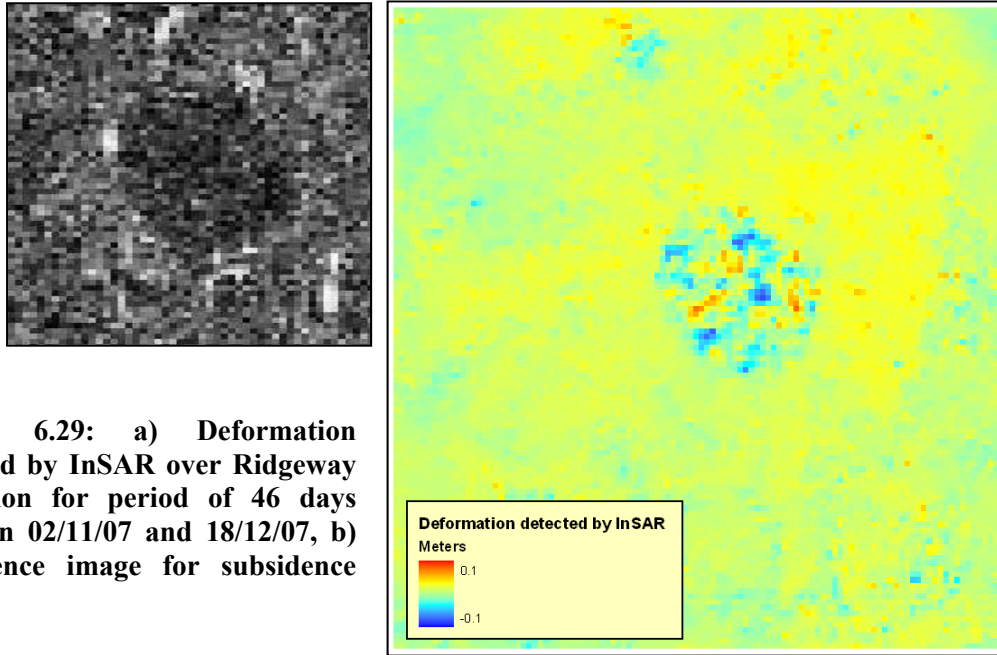


Figure 6.29: a) Deformation detected by InSAR over Ridgeway operation for period of 46 days between 02/11/07 and 18/12/07, b) Coherence image for subsidence crater

After processing the second pair (images between 18/12/07 and 02/02/08), further collapse on the left edge of the crater was detected (Figure 6.30). Similar to the first pair, incoherency is the main problem affecting results. As shown by Figure 6.31 most of the crater and bank to the right is incoherent and no evidence of subsidence is detected outside of incoherent area for this pair.

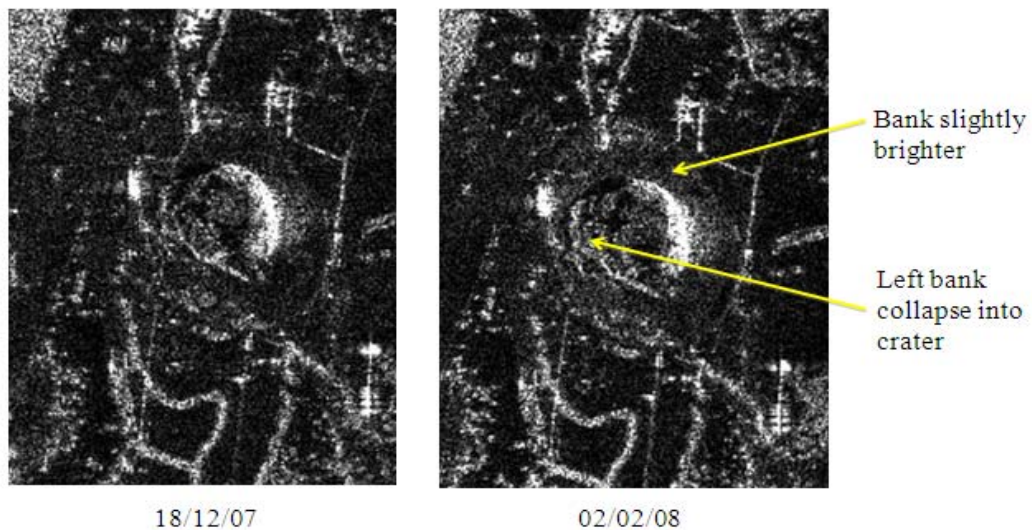


Figure 6.30: Amplitude images generated for images 18/12/07 and 02/02/08, describing subsidence crater and surrounding area

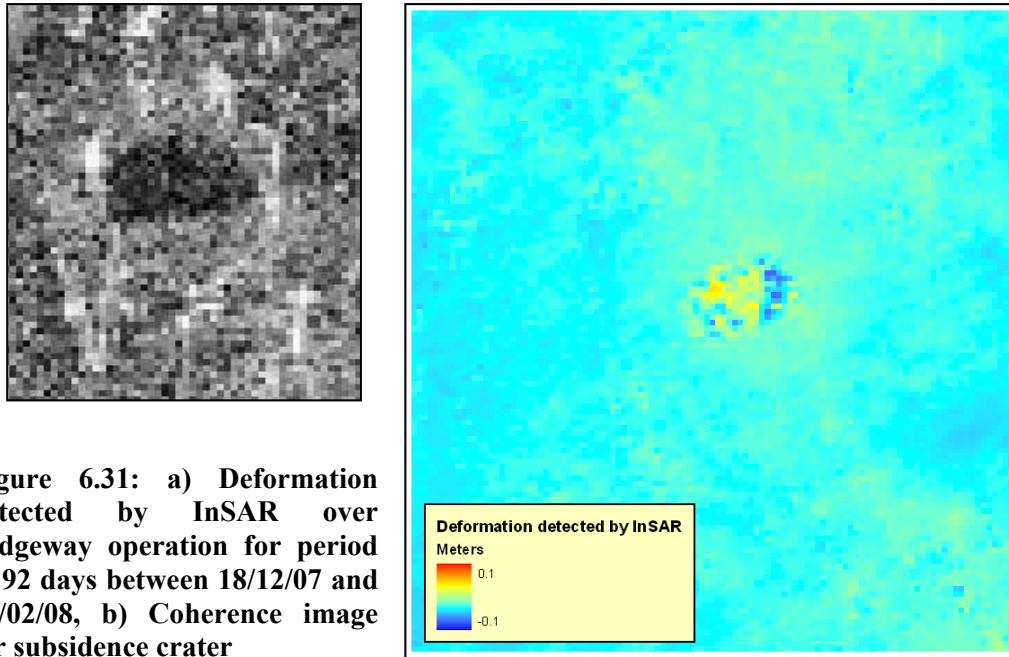


Figure 6.31: a) Deformation detected by InSAR over Ridgeway operation for period of 92 days between 18/12/07 and 02/02/08, b) Coherence image for subsidence crater

Processing third pair confirms that the left edge of crater collapsed during the period between two acquisitions. Despite the type of vegetation and considering no vegetation cover inside the crater, rapid changes in geometry due to collapse could be the main source for incoherency inside the crater. Figure 6.32 confirms this as overall coherence is worse than other pairs however better coherence on North bank is detectable. As represented by Figure 6.33 possible subsidence of a few mm to North and South of bank is detected by InSAR considering that the remaining area is incoherent.

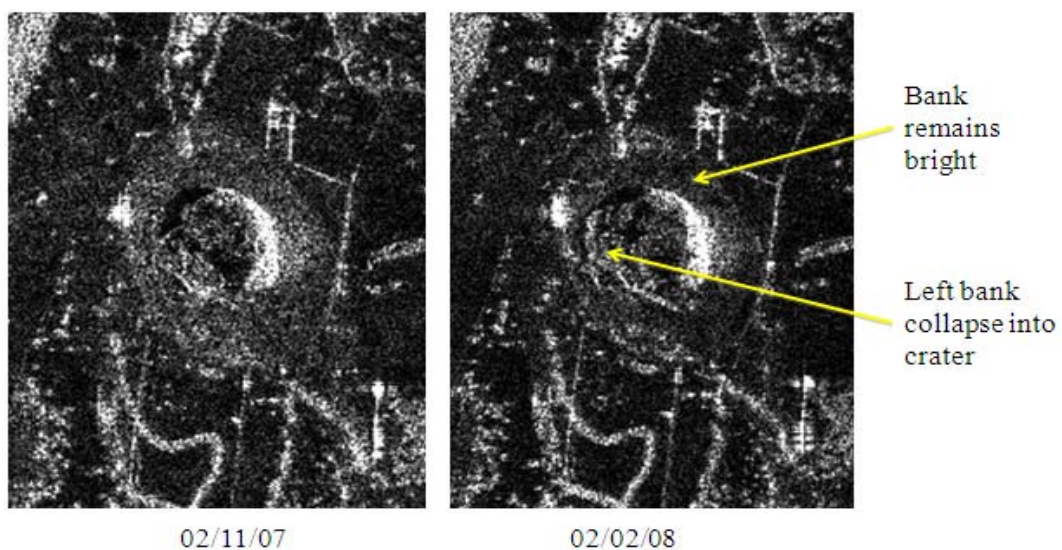


Figure 6.32: Amplitude images generated for images 02/11/07 and 02/02/08, describing subsidence crater and surrounding area

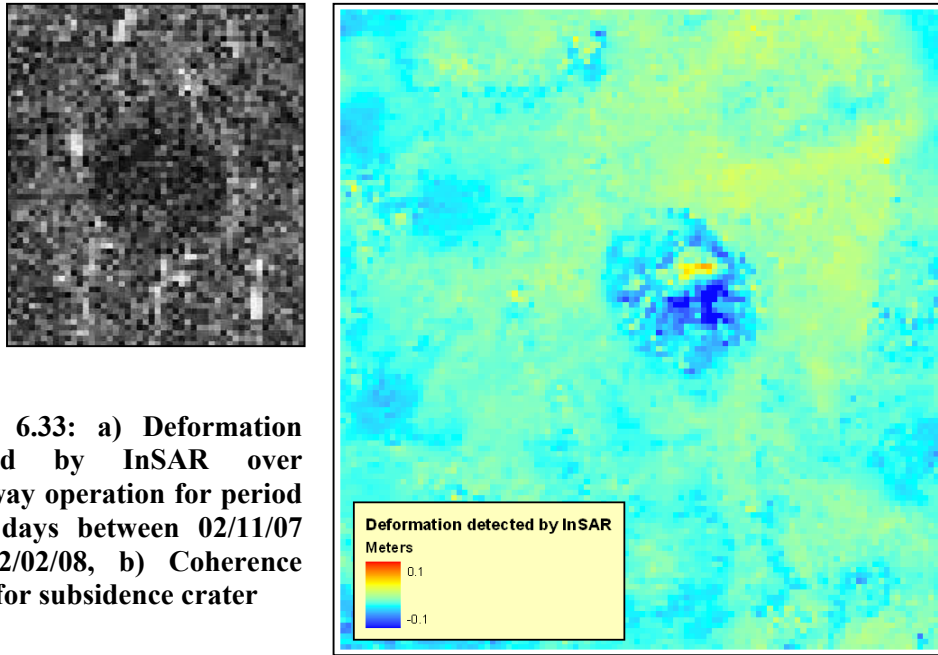


Figure 6.33: a) Deformation detected by InSAR over Ridgeway operation for period of 46 days between 02/11/07 and 02/02/08, b) Coherence image for subsidence crater

As a conclusion after processing most recent pairs, widespread subsidence from Nov.-Dec. 07 is detectable extending beyond the crater area. From Dec. 07 till Feb. 08, subsidence was mainly confined to the crater, with localised collapse from the bank. Results for images Nov. 07-Feb. 08 are also consistent with results from two other pairs.

Studies continued with processing other pairs. This time focus was to study deformation all over the area including the Ridgeway operation and also the Cadia Hill open pit and waste dumps. A map showing final deformation and coherence for each pair is presented in Figure 6.34, 6.35 and 6.36. As illustrated, incoherency is the most obvious issue that highly affected results.

Considering deformation inside and around the subsidence crater, results confirm previous results obtained by processing first three pairs. Also some deformations were represented over Cadia Hill, Cadia extended and waste dump. These deformations can be related to mining activity in these areas, however due to problem of incoherency and unknown contribution of height ambiguity, amount of detected deformation cannot be reliable enough. Unfortunately no filed data was available for any topographic analysis or to validate obtained results.

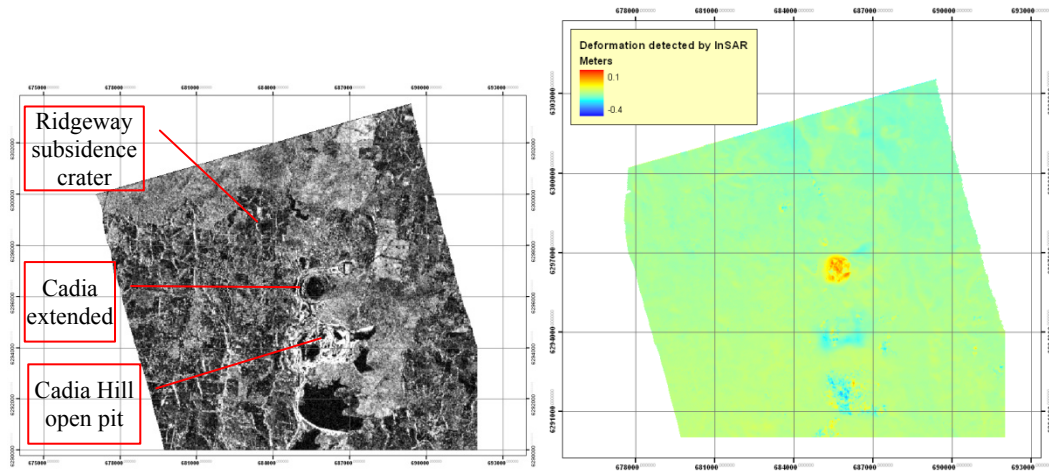


Figure 6.34: Coherence and deformation images produced by InSAR toolbox over Ridgeway and Cadia hill operations for period of 46 days between 21/05/06 and 06/07/08

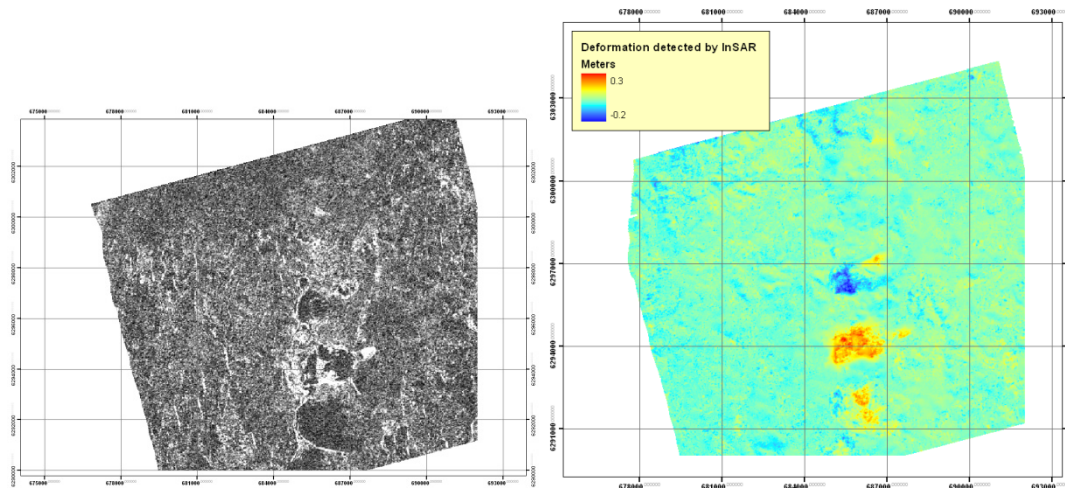


Figure 6.35: Coherence and deformation images produced by InSAR toolbox over Ridgeway and Cadia hill operations for period of 368 days between 01/01/07 and 04/01/08

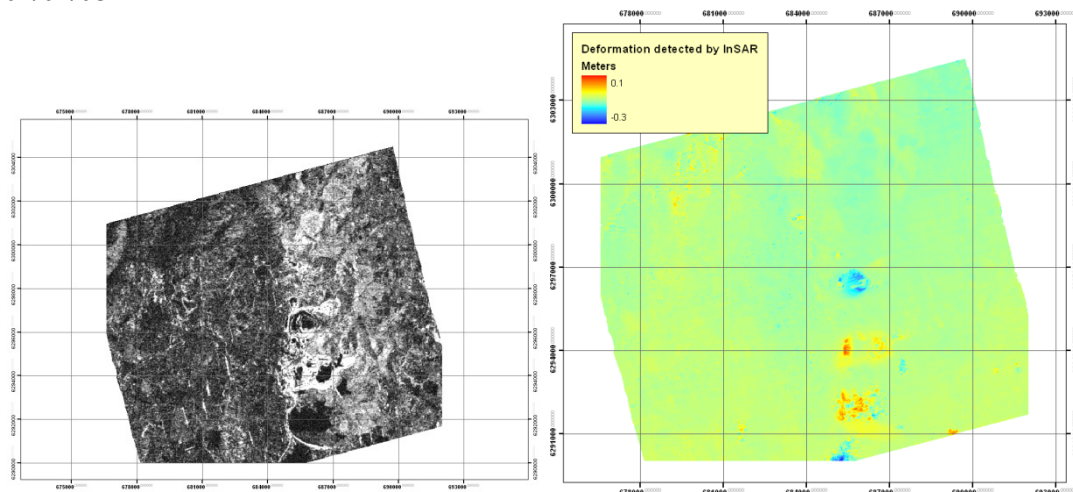


Figure 6.36: Coherence and deformation images produced by InSAR toolbox over Ridgeway and Cadia hill operations for period of 46 days between 04/01/08 and 19/02/08

6.4. Ridgeway Underground Gold Mine – TerraSAR-X

The author was granted permission for planning and processing three TerraSAR-X spotlight sensor acquisitions. These three images were planned to be acquired during Oct. 2008, starting from 03/10/08 with 11 days temporal baseline between them. The main reason for testing TerraSAR-X data was to study the possibility of taking advantage of its capability to produce high resolution images (1m×1m) which was thought to be helpful to avoid an ambiguity issue and also comparison between results produced using TerraSAR-X and ALOS data over the Ridgeway operation.

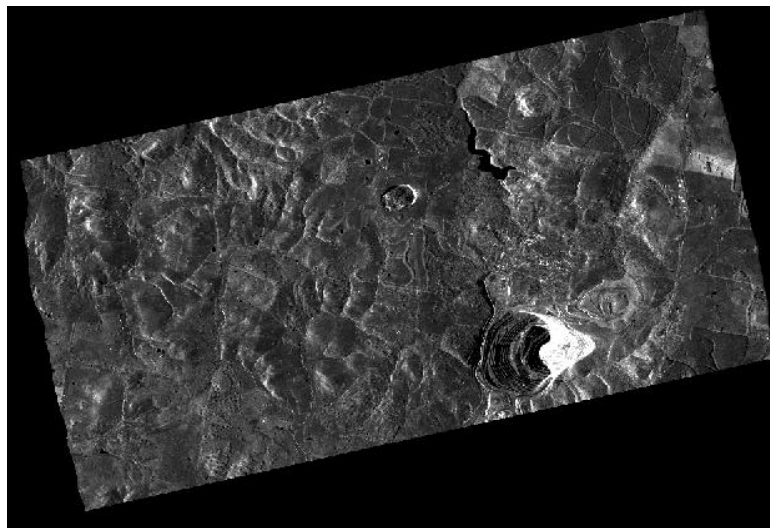


Figure 6.37: Amplitude images generated for TerraSAR-X image 03/10/08

Processing data showed that despite the fact that TerraSAR-X is able to deliver high resolution images (Figure 6.37), the coherence was very low for most of the image, showing that X-band is very much affected by the vegetation. The baseline for the first pair was about 51 m (perpendicular baseline) so baseline decorrelation should be low. Unfortunately, the crater area was too low in coherence to produce any reliable result. It was later confirmed by the data provider that based on their experience even the slightest vegetation (even grass) highly decorrelates the X-band SAR. Role of vegetation as an incoherency issue was also confirmed as the coherence falls sharply as soon as any vegetation is present at the mine edge. One possible solution would be considering a PS-InSAR technique (permanent scatterers); Shed, buildings and fences retain coherence and can be used to measure phase shift. However PS technique requires a large number of acquisitions and due to

lack of available data it was impossible to use PS-InSAR for the Ridgeway operation.

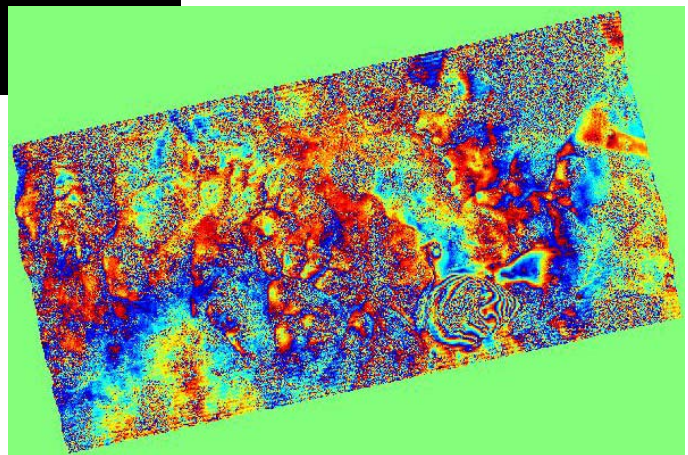
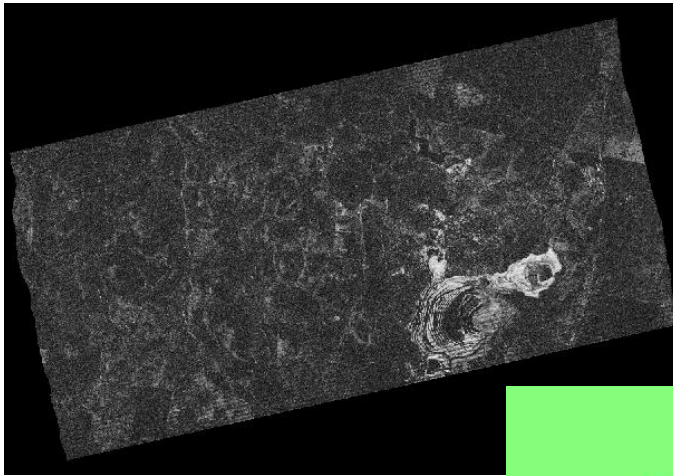


Figure 6.38: Coherence and deformation images produced by InSAR toolbox using TerraSAR-X data over Ridgeway and Cadia hill operations for period of 11 days between 03/10/08 and 14/10/08

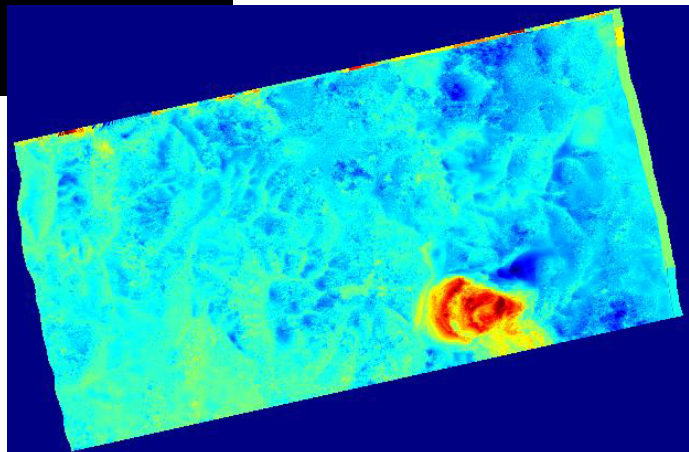
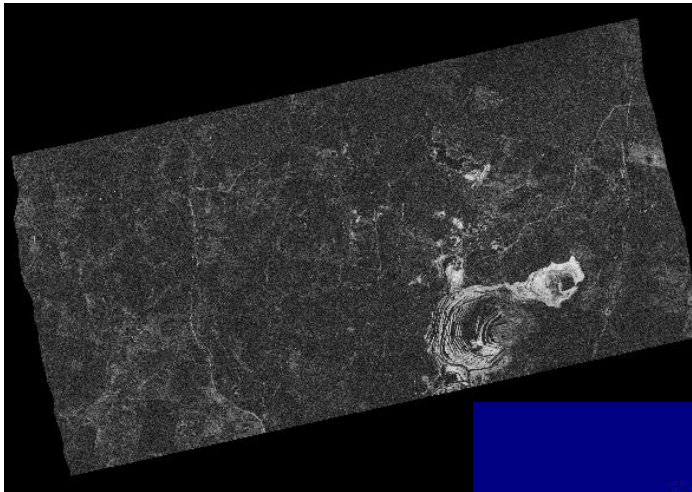


Figure 6.39: Coherence and deformation images produced by InSAR toolbox using TerraSAR-X data over Ridgeway and Cadia hill operations for period of 11 days between 14/10/08 and 25/10/08

6.5. Discussion and Summary

The studies showed that involving the developed tools can significantly improve and ease the processing steps as well as providing better understanding of limitation of the technique and also detection of areas where InSAR results are poor due to the presence of these limitations. The InSAR toolbox environment eases the definition of input data, editing processing parameters, rerunning any step, result validation, result interpretation, importing results into a given format and preparing reports; the InSAR toolbox functionalities are totally comparable with commercial software or in many cases exceed their capabilities.

In terms of data quality and availability, having a small number of available archived SAR acquisitions was the main issue affecting all case studies and that was mainly due to the lack of satellite coverage over Australia. For instance, in the case of the Perseverance operation, only 10 ERS-2 SAR images were available for the selected period. Considering the fact that not all possible pairs result in an interferogram, basically due to images decorrelation due to temporal/surface changes or large orbital separation (baseline), and also ERS-2 gyro malfunctions, from 45 possible pairs for the Perseverance operation only 2 pairs were sufficiently coregistered to be used for further analysis. Also in this case study, the geometry of the available data was almost the worst possible for the application. All of the available data was acquired from the satellite descending orbits, meaning that the radar was viewing in the (near) east to west direction. This caused the west wall of the pit to be in an area of layover, which extended some distance past the edge of the pit. Since the search for available archive data provided no results in the case of the Argyle case study, data acquisition planning was necessary. Using planned acquisitions makes it possible to obtain data with more suitable parameters, however even using such an approach not every pair of SAR images will result in good interferograms and same as the case of historical data, issues such as large orbital separation may still exist. For the Ridgway operation, the main issue was the data quality; In this case the type of vegetation over the area caused incoherency problem in both cases of ALOS and TerraSAR-X applications and largely affected all processed pairs.

With regards to data processing, main issues were layover and height ambiguity, though layover and ambiguity issues are always present in almost any SAR interferometry applications; nonetheless they are more of a concern in InSAR mining applications due to the small scale, highly dynamic nature of mine deformations. Research shows that using the developed distortion and deformation tools can be much more important and helpful to detect and access levels of influence of these issues.

In the case of the Perseverance open pit, much of the pit and in particular the Western side of the pit was affected by layover. For the Argyle case study; the layover area eliminates a large part of the pit from analysis, as well as east side of the crater induced by Ridgeway underground operation. For countries such as Australia, where most mining sites are located in inhabited areas, lack of satellite coverage and consequent unavailability of data acquired by different look angle, path or wavelength makes it even more difficult to deal with geometrical distortions including layover and ambiguity issues; for such cases therefore it is critical to define precise extent of the area affected by these distortions. This is where tools such as the distortions tool or deformation rate tool developed by this thesis can be helpful. It was recognised that such analyses provide basis for further adjustment of extend of poorly described areas by InSAR.

Regarding the ambiguity issue, deformation rate tool represented that for the Perseverance operation only 35% of the area, mostly outside of the boundaries of the pit and large deformation area, can be accurately detected by InSAR. The analysis of historical topographic surveys characterised the subsidence induced by inside the crater zone formed above the underground mining by large vertical and horizontal movements (few metres per year) leading to the development of significant discontinuities on the surface. A comprehensive analysis of ground deformation dynamics, based on topographical surveys showed that the rate of deformation causes such a level of ambiguity which cannot be resolved by InSAR. In the cases of Argyle and Ridgeway operations, it was not possible to validate results with respect to the ambiguity issue, due to the lack of validation data (field data). Other surveying techniques such as laser altimetry can also be used in order to analyse or resolve an

ambiguity issue. However, considering the fact that monitoring deformation is not seen as a crucial component of mine production process, the cost of utilising such techniques practically precludes their application.

As mentioned above, the other main issue affecting the studies was the unavailability of enough field data to validate InSAR results. For a typical mining site most of the classical survey stations previously installed inside the deformation area will be lost or fall into the inaccessible area; moreover, for areas outside the main deformation region, there is usually no classical survey stations installed since deformation monitoring over such areas does not directly affect mine production. In the case of the Perseverance operation, available classical survey data covers only small portions of the deformation region; the comparative analysis of the InSAR results and classical GPS surveys suggest little agreement in their common area of coverage. However, considering the density of observations over a specific area, InSAR results can be better justified. Unfortunately, no field data was available for any topographic analysis or to validate obtained results for Argyle and Ridgeway sites.

The performance of the InSAR toolbox can be evaluated taking different aspects into consideration: in terms of speed, it must be said that the time spent to complete the process steps is highly depended on the processing capacity of the machine and the operating system on which tools will be run, however python and raspberry scripts are quite fast and well-written to provide the most efficient framework; they do not required additional time to communicate or to be called. As a rough estimation, the time required to process data using InSAR toolbox is slightly less than DORIS and RIO-Pack.

It must be noted that the above mentioned time is only the time required for completing processing steps and does not include time needed to define input data or edit processing parameters or rerun a particular step; considering these aspects, InSAR toolbox proposes much faster, stable, sophisticated and user-friendly environment compare to all open-source InSAR processing software.

As a conclusion, the studies show that InSAR offers many potential advantages. The main advantage of the technique is the possibility of monitoring surface movement in the mining areas that are inaccessible due to their instability and cannot be monitored safely using the conventional monitoring techniques. Moreover, it provides continuous results which can be easily integrated into various processes and data analysis environments used in other mining studies carried out in different periods of mine life and also after mining. The research aimed to propose a mining-oriented InSAR methodology and also its integration in developing applied tools; considering numerous parameters that have impact on the accuracy and effectiveness of the InSAR results, research shows that it could be necessary and advantageous to have such a methodology and toolbox.

6.6. Chapter Summary

This chapter has discussed results generated using the InSAR toolbox. The methodology and tools were used for small-scale deformation detection in three different case studies in Australia: Perseverance (Leinster nickel mining operation), Argyle (diamond mine) located in Western Australia and Ridgeway (gold mine) in NSW. Studies planned to use data acquired by four different satellites (ERS-2, Envisat, ALOS and TerraSAR-X); it was due to the different nature of projects and also in order to test the methodology and tools using different sets of SAR data. Several issues arose during the period of studies including unavailability or poor topographical data for generating required elevation models and lack of classical survey data that limited result validation process. Nevertheless, the problem of lacking satellite coverage and the consequent issue of unavailability of suitable SAR acquisitions was found to be the main problem.

Chapter 7

Conclusions and Recommendations

Chapter 7

Conclusions and Recommendations

7.1. Summary

Surface subsidence is a source of risk for people, equipment and environments. It may also disrupt mining scheduling and increase the cost of mine safety and production and is always of major concern to the mining industry. Therefore, a comprehensive knowledge of the mechanisms associated with rock strata deformation is crucial for any mining activity. To provide accurate assessment of the surface subsidence and in particular the level of its impact on mine production and environment, it is necessary to develop and install comprehensive subsidence monitoring systems. Current techniques for monitoring surface deformation are usually based on classical surveys principles, In general, current techniques have disadvantages that limit their applicability; they follow point-by-point data collection techniques, they are relatively time-consuming and costly, they usually cover only a small area, they are not applicable for the monitoring of inaccessible areas and also they are not able to provide continuous data.

As a complementary or alternative technique, the thesis discussed the applicability of SAR interferometry for monitoring mining induced deformations. InSAR is a remote sensing technique that makes use of Synthetic Aperture Radar (SAR) observations to acquire topographic information. In spite of the wide application of the technique for monitoring of large-scale deformations of the Earth's crust, specific modifications are necessary for utilising the technology in a mining context. Limitations, such as a difficulty to resolve deformation for a high gradient slope, a difficulty to retrieve subsidence for localised highly dynamic ground movements and the unavailability of SAR images with the desired specifications, restrict the potential to monitor high rate, localised mine subsidence on a day-to-day basis.

Taking InSAR limitations into consideration, the optimal methodology was developed to be employed as a guideline for future InSAR applications in monitoring mine subsidence. Also, GIS-based methodologies and tools were developed and integrated into conventional InSAR techniques to improve and facilitate the general process. The applied methodology includes the following highlights:

- Improvement of current InSAR capability and providing insight about application of InSAR technique for monitoring of mining induced surface subsidence. The layover and ambiguity issues were recognised and the methodology for their determination developed.
- Proposing a guideline to be used in mining related InSAR application, and
- Integrating the InSAR processing chain into GIS environment by introducing various GIS-based tools and procedures.

The research introduced a set of new GIS-based developed tools and methodologies to be integrated into conventional InSAR techniques to improve and facilitate InSAR applications in mining, covering three main stages of pre-processing, data processing and post-processing. Research was aimed to address InSAR limitations associated with mining related applications and also to provide practical solutions to deal with them. The InSAR module was developed as a toolset inside ArcToolbox of ArcGIS desktop as one of the most popular GIS software used by the mining industry. The objectives of producing such tools can be summarized into three main aspects:

1. Providing a mining-oriented methodology for InSAR,
2. Providing a simple and user-friendly environment to run InSAR processing steps,
3. Integrating InSAR and GIS in order to propose an optimum data processing methodology.

Following a review of SAR interferometry development, stages of its evolution and applications, the thesis discussed principles of SAR imagery, SAR interferometry and limitations of the technique including limitations due to phase noises (e.g. atmospheric effect, temporal decorrelation...) and geometry related

limitations (geometric distortion and height ambiguity). General InSAR processing steps were also discussed in detail.

The introduced tools cover three main stages of pre-processing, data processing and post-processing for the InSAR application in mining. From programming languages supported by ArcGIS geoprocessing framework, the Python programming language was selected for developing designed tools and body of the InSAR data processing toolbox. The source code for Raspberry, an open-source Matlab script for SAR interferometry, developed by Dr Andrew Sowter from IESSG, was also used as the main reference for developing tools introduced by this research. InSAR toolbox contains two types of tools, scripts and models. Scripts are programs designed to perform specific task or glue different steps of a process; models are combinations of the scripts and ArcGIS tools that includes a chain of processes.

In the pre-processing stage of InSAR analysis, various tools and procedures useful for data selection, data preparation and data review steps, were discussed; however the emphasis was on discussion of layover and deformation rate issues. Layover is known as the most commonly seen distortion in SAR imagery over areas with severe terrain variations. The distortion tool was introduced to identify the precise extent of the area affected by layover. As part of a layover analysis, effect of using an accurate and up to date topographical model was also studied. It was shown that integrating a current DEM with widely used global DEMs such as SRTM could significantly improve results generated by the distortion tool.

The maximum detectable deformation gradient by InSAR is one fringe per pixel which means the deformation rate cannot exceed the dimensionless ratio of the pixel size to half of the wavelength. Therefore, conducting a deformation rate analysis before starting any data processing would help to estimate how much InSAR results are affected by ambiguity and more importantly, for which parts of the area InSAR results are valid. The deformation rate tool uses available elevation data (e.g. DTMs) to calculate deformation rate between neighbouring pixels for the period between SAR acquisitions and then compare it with acceptable limit defined by satellite wavelength to define extent of the area affected by height ambiguity problems. However, it should be notified that the deformation rate tool provides very rough

estimation as it uses a simple interpolation to calculate deformation occurred in the period between two SAR acquisitions.

The data selection process means finding an optimum set of images balancing data availability and data suitability; this process is very critical, particularly, in the case of regions with less satellite coverage such as the mining areas of Australia. By adopting a practical approach, the thesis discusses a set of crucial questions necessary to be answered for developing an optimum data acquisition policy. These include questions regarding expected rate and extent of deformation, vegetation coverage, expected level of distortion, suitable geometrical and temporal baselines, suitable wavelength, satellites coverage, possibility for planning acquisitions etc.

In data processing stage, body of the InSAR toolbox and also details for each process and sub-process were presented. The data processing module in InSAR toolbox includes following steps:

1. Reading master and slave header information and also reading and processing additional information such as precise orbit data.
2. Extracting complex SAR data and dumping it into binary files.
3. Preparation of available DEM resulting in simulation of an interferogram containing phase references obtained from the DEM.
4. Image coregistration (coarse coregistration and fine coregistration).
5. Subtracting master and slave phase components generating a complex interferogram.
6. Creation of differential interferogram and removing topography component.
7. Phase unwrapping (Using Snaphu software developed by Stanford Radar Interferometry Research Group).
8. Converting phase values to height and result georeferencing.

In the post-processing stage, value-added tools, already available in GIS packages, were also introduced; the trend tool for removing phase trends imposed as a result of orbital error, geostatistical analysis for result interpolation and georeferencing or project raster tool for precise georeferencing and coordinate transformation.

Following the presentation of developed tools and procedures, results obtained from applying the described methodology in three case studies (located in Australia) were presented. These studies were planned to use data acquired by four different satellites (ERS-2, Envisat, ALOS and TerraSAR-X). The problem of lacking satellite coverage and the consequent issue of unavailability of suitable SAR acquisitions was found to be the main problem in all case studies.

Underground mining operations beneath the Perseverance open pit in Leister Western Australia was the primary case study of the thesis. The long-term objective of the project was to provide help with tuning of a finite element model representing deformation of rock mass and with the analysis required for planning and design of the next mining phase. The main problem was a very small number of available archived SAR acquisitions. The geometry of the available data was also almost the worst possible for the application. Analysis conducted with help of the deformation rate tool showed that only 35% of the area, mostly outside of the boundaries of the pit and large deformation area can be accurately detected by InSAR. The analysis of historical topographic surveys which was used to extract subsidence data spanning the period between 2001 and 2006, also confirmed the presence of an ambiguity issue. According to topographical analysis the subsidence inside the crater zone was characterised by large vertical and horizontal movements (few metres per year) leading to the development of significant discontinuities on the surface and also height ambiguity issue. Nonetheless, InSAR was able to deliver a 20m×20m deformation map for the acceptable area.

Following the InSAR data processing stage, the comparative analysis of the InSAR results and classical GPS surveys suggest a rough agreement between both results in their common area of coverage. The average difference and standard deviation of differences were detected to be 2 mm and ± 3 mm respectively. However, considering the density of observations over a specific area, InSAR results can be better justified.

The Argyle diamond mine located in the Kimberley region in the northeast of Western Australia was the second discussed case study. The objective of the project was to provide a demonstration of application of an InSAR technique for determination of surface deformations (subsidence) induced by recently commenced underground operation at the Argyle Diamond Mine. Only one pair of Envisat data was processed. Subsidence rate over the area of study was detected to be generally small. The validation analysis and so ambiguity issue analysis was impossible. Main deformed fields were recognised around the lake banks, north of the pit, over the dumping area, south of the pit, tailing pool and in the north-east part of the pit. It was also clear that pit walls, in particular west wall, were almost stable during the period between two processed SAR acquisitions.

The Ridgeway underground operation located in NSW, characterised by extensive surface subsidence, was selected as the third case study. This time ALOS and TerraSAR-X images were used for the analysis. The main problem affecting the result quality was an incoherency issue which was partially due to crater collapse, but particularly due to the type of vegetation over the area as incoherency exists almost over whole the image. In conclusion after processing ALOS data, widespread subsidence from Nov. - Dec. 07 was detectable extending beyond subsidence crater area. From Dec. 07 till Feb. 08, subsidence was mainly confined to crater, with localised collapse from the bank. Processing ALOS data represented that left edge of subsidence crater collapsed during the period of acquisitions. Also some deformations were detected over Cadia Hill, Cadia extended and waste dump. These deformations can be due to mining activity in these areas, however incoherency and unknown contribution of height ambiguity, limited reliability of detected amount of deformation. Unfortunately no field data was collected for any topographic analysis or to validate obtained results.

Ridgeway studies continued with processing limited number of available TerraSAR-X data. High resolution images (1m×1m pixels) by spotlight sensor were thought to be helpful in order to avoid an ambiguity issue; however very low coherency over most of the image highly affected result. Unfortunately, the crater area was too low in coherence to produce any reliable results. It showed that despite the fact that X-band sensors are able to provide high resolution images, however X-

band images are very sensitive to vegetation and even the slightest vegetation (short grass coverage) highly decorrelates the X-band SAR.

7.2. Results and Developed Tools

7.2.1. InSAR and Mining

Analysis of rock strata deformation requires high accuracy input data and the new remote sensing technologies may resolve this dilemma. The studies by this research confirm the advantages of using InSAR technique:

- InSAR does not require any field instrumentation and consequently allows for monitoring of surface movement in the mining areas that are inaccessible due to their instability and cannot be monitored safely using the conventional monitoring techniques.
- InSAR uses radar signals and so it is able to work under different atmospheric conditions and is also able to detect localised surface subsidence with accuracy less than a centimetre.
- Utilisation of the InSAR technique may significantly reduce the costs of the monitoring and interpretation process.

However, there are some critical limitations, which must be taken into consideration:

- InSAR is only able to provide the line-of sight component of the three-dimensional displacement vector. It may be possible to extract two components of the deformation vector by processing both ascending and descending images.
 - Radar-scattering characteristic within each pixel must not change over the period between two acquisitions. Otherwise, the phase component caused by the interaction of the signal and the ground cannot be removed. If radar-scattering characteristics within each pixel strongly change, it causes the temporal decorrelation which is one the main limitations of InSAR.
-

- Vegetation, wind effects, soil moisture, snowfall and human activities such as mining are the most commonly seen reasons for temporal decorrelation.
- Large, rapid displacements cannot be detected with InSAR. Displacement gradient between adjacent pixels must be less than half of the radar wavelength; otherwise the phase difference will be ambiguous.

Satellite coverage delivering selected specification and data availability are main challenges for case studies located in areas with less satellite coverage. For instance, Western Australia is very rich in terms of mining activities, however the mostly vast uninhabited areas in WA are not a primary target of satellite missions, hence the archived data is scarce and without any continuity. Nonetheless, considering the increasing number of satellites capable to provide data for SAR interferometry, this problem is going to be solved in the near future. Availability of more SAR images provides the opportunity to test for different SAR interferometry techniques such as the Persistence Scatterers that required numerous SAR images. Availability of more images with both ascending and descending geometry also means avoiding geometrical distortion such as shadows and layover.

The initial SAR missions (ERS1-2, Radarsat-1, Envisat, etc.) provided a spatial resolution of approximately 25m×25m. By improving satellite navigation systems and also introducing new imaging technologies, future missions will be able to deliver significantly higher scanning resolutions. Higher resolution (smaller pixel size) is critical for accurately detecting small-scale, highly dynamic deformations since it would be possible to produce better estimation for phase unwrapping, which significantly decreases the impact of ambiguity issues.

In addition to the subsidence analysis the research delivered important insight about application of InSAR for monitoring of surface subsidence in the area of existing open pit mine with deep and steep slopes. The results showed that layover is an almost certain occurrence in SAR images of open mines. However, with the chance to choose an incidence angle and prospect for the radar observation, and with knowledge of the terrain and the location of possible deformation, it would be

possible to optimise acquisition of SAR images to minimise the layover and maximise the samples in the area of interest. Therefore, in processing the stream of an InSAR mining application, the most emphasis must be put on data selection and data planning steps since it is possible to avoid or limit the effects of layover, ambiguity or data incoherency and provide more accurate and reliable results through selection of suitable wavelength, path and configuration.

The other main issue is data validation, considering a typical mining site, with expanding deformation region, most of the classical survey stations, initially set up to detect deformation, either will be lost or falling into the inaccessible area. For areas outside of main deformation region, there is usually no classical survey stations installed. So, one of the main objectives of using InSAR in mining applications is to monitor areas where previous instrumentation was lost or areas were not previously instrumented. However, it is also obvious that in most cases there is not enough data for validating InSAR results and particularly detecting extents of areas affected by the ambiguity issue. Other surveying techniques such as laser altimetry can be considered as a resolution of InSAR ambiguity issue. Considering the fact that monitoring deformation is not seen as a crucial component of everyday mine production process, the cost of utilising such techniques practically precludes their application.

As seen during the data processing step, the quality and accuracy of results provided by InSAR is dependent on different parameters, mainly:

- Satellite coverage of areas of study that defines configuration of acquisitions and quality of acquired data,
- Geometry of the target area (pit, subsidence crater, high or low gradient terrain...),
- Presence of objects causing incoherency (vegetation, water...) and
- Characteristics of the target deformation itself.

The cost analysis of the case studies can be discussed with regards to three main components: cost of data, cost of software and cost of processing. It should be noted in terms of data cost that all data providers have an intention to support research

projects, hence most of the required data was purchased at a discounted rate; However in order to provide a realistic view of cost of data for an InSAR application, Table 7.1 lists the price of SLC SAR images for different SAR missions for each non-research projects.

Table 7.1: Price list for SLC SAR images

Mission	Price for Archived SLC SAR Image (€)	Additional cost for planning acquisitions (€)
ERS-1 and 2	500	100
Envisat	600	200
ALOS	500	-
Radarsat-1	2760 to 3170*	100
Radarsat-2	2540	85
TerraSAR-X	6750**	25% surcharge

* This is the price for each pair of SAR images depending on number of ordered pairs

** 50% discount for data older than 6 months and 30% discount for data older one year are applicable
Price for TerraSAR-X is from price list by Infoterra, all rest prices are based on price list by Euroimage

The cost of available software varies from nothing to several thousand dollars. Most of available software are open-source and can be downloaded from the developers' websites installed and used for free. Such software are sometimes even more powerful than commercial ones with the possibility to be modified by users; however as previously mentioned, they are complicated with no support services, not easy to use and usually designed to be used by experts. In other hand, few commercial software are also available that can be purchased and used. Though these software offer more user-friendly environments, they are very expensive and are not flexible enough. The research proves that the InSAR toolbox can fill this gap by providing open-source, easy to use scripts and tools for InSAR data processing.

It is not possible to give an accurate estimate regarding the cost of processing, as it varies depending on the experience of the person or team who processed the data and the services which they provide. Considering all the above, it is obvious that comparing with the cost of utilising conventional mine deformation surveying and monitoring techniques, InSAR is able to deliver continuous, accurate results covering large extents at significantly lower costs.

In general, InSAR can be considered as a quick technique that is able to provide results in a short period of time. Delay due to data acquisition by satellite is the only

main parameter that can be a source of delay; In case of having all required images in hand, all processing steps can be performed in a short period of time, for instance in less than a week, on average, for presented case studies (Only data processing part). Obviously, data processing time varies depending on the number of pairs to be processed.

7.2.2. InSAR Toolbox

The performance of the InSAR toolbox can be evaluated taking different aspects into consideration: in terms of speed, it must be said that time spent to complete the processing steps is highly dependent on the processing capacity of the machine and the operating system on which tools will be run, however python and raspberry scripts are quite fast and well written to provide most efficient framework; they do not required additional time to communicate or to be called.

As a rough estimation, the time required to process data using the InSAR toolbox is slightly less than DORIS and RIO-Pack. It must be noted that the mentioned processing time only includes the time required for completing processing steps and does not include the time needed to define input data, edit processing parameters or rerun a particular step. Considering these processes, the InSAR toolbox proposes a faster, more stable, sophisticated and user-friendly environment in comparison to all open-source InSAR processing software.

In terms of the price, InSAR toolbox and all necessary packages to run its tools (Python and all its packages, GDAL, Snaphu, cygwin, GeoEco toolbox, etc) are free and open-source. They can be downloaded and installed with no significant cost. Nonetheless, Matlab and ArcGIS are commercial software and proper licences must be purchased to be able to use them; however these software are very popular and can be found in many mining companies. Moreover, significant discounts are offered by both ESRI and MathWorks (developer companies) for academics and students. It is also necessary to be reminded that with future modification of the toolbox and translating all Matlab scripts to Python, there would be no need to purchase a licence for Matlab.

GIS functionalities integrated into InSAR processing methodology can be very useful in preparing InSAR results for further applications by mining companies. Accurate, continuous results generated by InSAR are not only useful for detecting and monitoring deformation but they can also be a comprehensive source of information for future mine planning and mine management projects; for instance such data can be easily used in Finite Elements (FE) analysis usually performed as part of the mine planning process in order to analyse rock mass behaviour in response to mining activities. As seen by case studies, using GIS capabilities and developed tools, it would be easy to view and work with results with no need for any additional software which is the case in most of the open-source and even commercial software. Using the InSAR toolbox makes it possible to prepare results in different formats such as maps, images, diagrams, sections and etc, compare results generated applying different parameters, transfer results to different local and global coordinate systems and also import data into almost any required formats readable by a given mine planning software or any other software.

Despite the many advantages of the InSAR toolbox, some problems still exist, for example: the installation process of the toolbox is rather complicated due to several small software packages to be installed; preparing an efficient installer and also a clear installation guide was attempted. The other main problem is the lack of error or progress messages produced by the tools. This was mainly due to the necessity of running the Matlab engine in the background that causes some difficulty in piping its messages to Python and ArcGIS environment; however this problem does not affect data processing since the main error messages will be shown with no problem. These problems will be solved in future modifications of the toolbox. In particular, moving from Matlab-Python to an entirely Python framework will be very helpful in eliminating such issues.

The research shows that using the InSAR toolbox can significantly ease InSAR processing steps in all three main stages (pre-processing, data processing and post-processing). Using the InSAR toolbox can improve quality of the results; it also provides a set of tools for more accurate interpretation of the results suggesting less effect of InSAR limitations. The InSAR toolbox provides faster and easier options for the definition of input data, editing processing parameter, rerun different steps,

result validation, result comparison, result interpretation, importing results into a given format and also the preparation of reports; With the aim of a GIS-based environment, InSAR toolbox functionalities are totally comparable with commercial software or in many cases exceed their capabilities.

7.3. Recommendations for Future Research Projects

Future research can be extended in two directions: Development of a new set of tools for improving image processing stages, or development of the new methodologies introducing new instruments or data (acquired by new missions) to the analysis. Regarding a new set of GIS-based tools, the first step following the research presented in this thesis would be to entirely transfer Matlab-Python based scripts of InSAR toolbox to a set of Python based tools. Using such an approach, there is no more need to run Matlab in the background. This should lead to smoother running of processing steps, possible free software (eliminating cost of purchase Matlab license) and provisions of easier options to modify scripts in order to integrate pre-developed ArcGIS tools. Using Scipy and Numpy libraries, Matlab scripts can easily be translated to Python. All data and tools are accessible by request from WASM to be used by other researchers who wish to further expand research in this area.

High gradient and small scale mining induced deformation calls for further detailed study of available phase unwrapping techniques and possible development of new unwrapping techniques considering mining induced deformation characteristics. Further research can be designed in order to test and quantify rates of success of unwrapping techniques. One possible methodology would be to study the rate of success of different unwrapping techniques on an imaginary subsidence domain through calculating and quantifying level of ambiguity (area of correctly unwrapped value of subsidence over area of domain). The effect of using different satellite wavelengths must be also taken into consideration. However development of new unwrapping techniques requires a high level of pure mathematical knowledge.

In some cases, the SAR interferometry technique suffers from the problem that suitable targets do not exist or are not visible enough to allow accurate processing. If

the natural targets are not available the artificial targets (transponders) could be introduced. Such approaches should allow for an accurate georeferencing of SAR scenes and consequently for increase of the accuracy of subsidence monitoring. Implementing an array of transponders is suggested, with some in a stable zone not subject to deformation, and some in an active zone affected by mine subsidence. Stability and movement of transponders should be monitored using GPS and/or classical surveying methods. This approach should help with identifying any problems due to ambiguity and phase unwrapping as well as validating the InSAR results.

As a general conclusion, the InSAR method of subsidence monitoring uses a rapidly developing technology that offers many potential advantages. The InSAR capability of performing many thousands of accurate measurements over small areas, and GIS's ability to handle, analyse and model spatial data, offers much more detailed analysis of the deformation mechanism at a significantly less cost and higher accuracy. The method can also be utilised to detect and predict mining induced deformation as an alternative or complementary method of classical survey techniques, as well as, providing valuable data for tuning rock strata deformation models. However, the numerous parameters that impact the accuracy and effectiveness of the InSAR indicates that the technique should be considered as experimental if applied to monitoring high rate surface subsidence.

Chapter 8

References

Chapter 8

References

Aronoff, S. (1982). *Geographic Information Systems: a management perspective*. Ottawa, Canada, WDL Publications.

Ashkenazi, V., A. H. Dodson, et al. (1980). "Remote measurement of ground movements by surveying techniques." *Civil Eng. Survey* 5(4): 15–22.

Balmer, R. (1999). *The SRTM mission—a worldwide 30 m resolution DEM from SAR interferometry in 11 days*. 47th Photogrammetric Week '99. Wichmann Verlag, Heidelberg.

Baran, I. (2004). *Advanced satellite radar interferometry for small-scale surface deformation detection*. Western Australian School of Mines. Kalgoorlie, Curtin University of Technology: 178.

Baran, I., M. Stewart, et al. (2003). "A modification to the Goldstein radar interferogram filter." *IEEE Transactions on Geoscience and Remote Sensing* 41(2): 2114-2118.

Bell, F. G. and L. J. Donnelly (2006). *Mining and its impact on the Environment*. London, Taylor & Francis.

Brady, B. H. G. and E. T. Brown (1993). *Rock mechanics for underground mining*. London, Chapman & Hall.

Brown, E. T. (2003). *Block caving geomechanics*. Queensland, Julius Kruttschnitt Mineral Research Centre.

Buderi, R. (1996). *The invention that changed the world: How a small group of radar pioneers won the Second World War and launched a technological revolution*, Simon & Schuster.

Buderi, R. and W. Aspray (1996). "The story of radar." *Science* 274(5285).

Bürgmann, R., P. A. Rosen, et al. (2000). "Synthetic Aperture Radar Interferometry to measure earth's surface topography and its deformation." *Annual Review of Earth and Planetary Sciences* 28(1): 169-209.

Burrough, P. A. (1986). *Principles of Geographical Information Systems for land resources assessment*. Oxford; New York, Oxford University Press.

- Carnece, C. and C. Delacourt (2000). "Three years of mining subsidence monitored by SAR interferometry, Gardanne, France" *Journal of Applied Geophysics*, 43: 43-54.
- Carnece, C., D. Massonnet, et al. (1996). "Two examples of the use of SAR interferometry on displacement fields of small spatial extent." *Geophysical Research Letters* 23(24): 3579-3582.
- Chandler, J. H. and R. Moore (1989). "Analytical photogrammetry: a method for monitoring slope instability." *Journal of Engineering Geology Quart.* 1.(22): 97-110.
- Chang, H. C. (2008). *Differential Interferometric Synthetic Aperture Radar for land deformation monitoring*. School of Surveying and Spatial Information Systems. Sydney, The University of New South Wales: 183.
- Change, H. C., L. Ge, et al. (2004). Application of repeat-pass DInSAR and GIS for underground mine subsidence monitoring. *IEEE Geoscience & Remote Sensing Symposium. (IGARSS)*. Anchorage, Alaska. V: 2815-2818.
- Chen, C. W. and H. A. Zebker (2000a). "Network approaches to two-dimensional phase unwrapping: intractability and two new algorithms." *Journal of the Optical Society of America* 17(3): 401-414.
- Chen, C. W. and H. A. Zebker (2000b). Two-dimensional phase unwrapping with statistical models for nonlinear optimization. *Geoscience and Remote Sensing Symposium*, Honolulu, Hawaii, 24-28 July 2000, IEEE International.
- Chen, C. W. and H. A. Zebker (2001). "Two-dimensional phase unwrapping with use of statistical models for cost functions in non-linear optimisation." *Journal of the Optical Society of America* 18: 338-351.
- Chen, C. W. and H. A. Zebker (2002). "Phase unwrapping for large SAR interferograms: statistical segmentation and generalized network models." *IEEE Transactions on Geoscience and Remote Sensing* 40(8): 1709-1719.
- CSIRO. (2008). "Light detection and ranging (LiDAR)- Fact Sheet." Retrieved 18 Oct. 2008 from <http://www.csiro.au/resources/LightDetectionLidar.html>
- Curlander, J. C. and R. N. McDonough (1991). *Synthetic Aperture Radar - Systems and signal processing*. New York, John Wiley & Sons, Inc.
- Davis, B. E. (2001). *GIS: a visual approach* (2th Edition). Albany, N.Y., Delmar Thomson Learning.
- Ding, L. X., L. Ge, et al. (2004). Atmospheric effects on InSAR measurements in southern china and Australia: a comparative study. 20th ISPRS Congress, Istanbul,
-

Turkey, 12-23 July 2004, International Society for Photogrammetry and Remote Sensing (ISPRS).

Dixon, T. (1995). SAR interferometry and surface-change detection. Miami, University of Miami, Technical Report TR 95-003: 97.

Ecological Australia (2004). The Impacts of longwall mining in the upper Georges River Catchments, Ecological Australia Pty Ltd.

Elachi, C., W. E. Brown, et al. (1982). "Shuttle imaging radar experiment." *science* 218(4576): 996-1003.

ESRI. (2009). "ESRI Online GIS Dictionary." Retrieved 30 Oct. 2009 from <http://support.esri.com/index.cfm?fa=knowledgebase.gisDictionary.gateway>

Eurimage. (2009). "Eurimage products and services guide: Envisat." Retrieved 19 Oct. 2009 from <http://www.eurimage.com>

European Space Agency (ESA). (2001). "ERS mission homepage, European Space Agency (ESA) homepage." Retrieved 26 Aug. 2006 from: <http://earth.esa.int>

Farr, T. G., S. Hensley, et al. (2000). The shuttle radar topography mission. CEOS SAR Workshop, CNES, Toulouse, 26-29 October 1999, ESA SP-450.

Ferretti, A., G. Savio, et al. (2007). "Submillimeter accuracy of InSAR time series: experimental validation." *IEEE Transactions on Geoscience and Remote Sensing* 45: 1142-1153.

Fielding, E., R. Blom, et al. (1998). "Rapid subsidence over oil fields measured by SAR interferometry." *Geophysical Research Letters* 25: 3215-3218.

Fischer, M., H. J. Scholten, et al. (1996). *Spatial analytical perspectives on GIS*. London, Bristol, PA, Taylor & Francis.

Forrester, D. J. and T. R. C. Aston (1987). "A review of mining subsidence instrumentation and its potential application for seabed monitoring." *Mining Science and Technology* 4: 225-240.

Franceschetti, G. and R. Lanari (1999). *Synthetic aperture radar processing*. Boca Raton, CRC Press.

Furuta, R., M. Shimada, et al. (2005). Interferometric capabilities of ALOS PALSAR and its utilization. Fringe2005. Frascati, Italy.

Furuta, R., M. Shimada, et al. (2005). Interferometric capabilities of ALOS PALSAR and its utilization. Fringe 2005 Workshop. 28 Nov.- 2 Dec. Frascati, Italy.

- Gabriel, A. K. and R. M. Goldstein (1988). "Crossed orbit Interferometry: Theory and experimental results from SIR-B." *International Journal of Remote Sensing* 9: 857-872.
- Gabriel, A. K., R. M. Goldstein, et al. (1989). "Mapping small elevation changes over large areas: differential radar interferometry." *Journal of Geophysical Research* 94: 9183-9191.
- Galloway, D., K. Hudnut, et al. (1998). "Detection of aquifer system compaction and land subsidence using interferometric synthetic aperture radar, Antelope Valley, Mojave Desert, California." *Water Resour. Res.* 34: 2573-2585.
- Ge, L., H. Chang, et al. (2003a). Differential Radar Interferometry for mine subsidence monitoring. 11th International Symposium on Deformation measurements, Santorini, Greece, 25-28 May 2003.
- Ge, L., H. C. Chang, et al. (2003b). The integration of GPS, radar interferometry and GIS for ground deformation monitoring. Symposium on GPS/GNSS. Tokyo, Japan.
- Ge, L., M. H. Change, et al. (2004). Monitoring ground subsidence due to underground mining using integrated space geodetic techniques, Australian Coal Association Research Program (ACARP).
- Gilbride, L. J., K. S. Free, et al. (2005). Modeling block cave subsidence at the MolyCorp, Inc., Questa Mine – A case study. Proc. 40th US Symposium on Rock Mechanics: 05-881.
- Gili, J. A., J. Corominas, et al. (2000). "Using Global Positioning System techniques in landslide monitoring." *Engineering Geology* 55 (2000): 167-192.
- Google Inc. (2009). Google Map. Retrieved 15 Nov. 2009 from <http://map.google.com>.
- Goldstein, R., H. Engelhardt, et al. (1993). "Satellite radar interferometry for monitoring ice sheet motion: application to an Antarctic ice stream." *Science* 262: 1525-1530.
- Goldstein, R. M. and R. L. Carpenter (1963). "Rotation of Venus: Period estimated from radar measurements." *Science* 139(3558): 910-911.
- Goldstein, R. M. and W. F. Gillmore (1963). "Radar observations of Mars." *Science* 141(3586): 1171 - 1172.
- Graham, L. C. (1974). "Synthetic Interferometer Radar for topographic mapping." *Proceedings of the IEEE* 62: 763-768.
-

Groundprobe. (2009). "Case study: Kemess South Mine" Retrieved 30 Oct. 2009 from

http://www.groundprobe.com/docs/Slope_Stability_Kemmess_GroundProbe.pdf

Gulla, G., P. G. Nicoletti, et al. (1988). A portable device for measuring displacements along fractures. 5th International Symposium on Landslides, Lausanne. 1: 423-426.

Hamrin, H. (2001). Underground mining methods and applications. Underground mining methods: Engineering fundamentals and international case histories. W. A. Hustrulid and R. L. Bullock. Littleton, Colorado, SME: 3-14.

Hanssen, R. F. (2001). Radar interferometry: data interpretation and error analysis. Dordrecht, Kluwer Academic.

Harries, N.J. and Roberts, H. (2007). "The use of slope stability radar (SSR) in managing slope instability hazards". First Canada-U.S. Rock Mechanics Symposium Proceedings, Vancouver 1: 53–59.

Hartl, P., K. H. Thiel, et al. (1994). "Application of SAR interferometry with ERS-1 in the Antarctic." Earth Observation Quarterly. Quarterly 43: 1-4.

Hartman, H. L. (1992). SME Mining Engineering Handbook. New York, Society of Mining, Metallurgical, and Petroleum Engineers.

Harvey, C. (1992). SME Mining Engineering Handbook. Baltimore: Port City Press, Society of Mining, Metallurgy and Exploration.

Henderson, F. M. and A. J. Lewis (1998). Principles and applications of imaging radar. Manual of remote sensing. Somerset, NJ (United States), John Wiley and Sons, Inc.

HLURB (2007). GIS cook book. Quezon City, Philippines, Housing and Land Use Regulatory Board (HLURB).

Hoek, E. (1974). "Progressive caving induced by mining an inclined orebody." IMM Section A: A133-A139.

Holla L. and B. E. (2000). Mine subsidence in the Southern Coalfield, NSW, Australia, Mineral Resources New South Wales.

Hovanessian, S. A. (1980). Synthetic Array and Imaging Radars. Washington DC, USA, Artech House.

IEEE website. (2009). Retrieved 10 Dec. 2009 from <http://www.ieee.org>.

- Ikehara, M. (1994). "Global Positioning System surveying to monitor land subsidence in Sacramento Valley, California, USA." *Journal of Hydrological Sciences* 39(5): 417-429.
- Jarosz, A. (2009). Lecture notes for the unit: Advance Mine Surveying 341. Western Australian School of Mines. Kalgoorlie, Curtin University of Technology.
- Jarosz, A. and D. Wanke (2004a). Detection and monitoring of mining deformations using InSAR technology. The 12th Australian Remote Sensing and Photogrammetry Conference, Freemantle, Australia.
- Jarosz, A. and D. Wanke (2004b). Use of InSAR for Monitoring of Mining Deformations, Western Mining Corporation (WMC), CN: 4600008314.
- Jarosz, A. and H. Zahiri (2007). Integration of InSAR and GIS for monitoring of subsidence induced by block-cave Mining. International Federation of Surveyors (FIG) Working Week. Hong Kong, May 2007.
- Kampes, B. and S. Usai (1999). Doris: the Delft Object-oriented Radar Interferometric Software. 2nd International Symposium on Operationalization of Remote Sensing, Enschede, Netherlands.
- Klees, R. and D. Massonnet (1999). "Deformation measurement using SAR interferometry: potential and limitations." *Geologie en Mijnbouw* 77: 161-176.
- Kratzsch, H. (1983). *Mining Subsidence Engineering*. Berlin, Springer-Verlag.
- Lanari, R., P. Lundgren, et al. (1998). "Dynamic deformation of Etna volcano observed by satellite radar interferometry." *Geophysical Research Letters* 25: 1541-1544.
- Laubscher, D.H. (2000) *Block caving manual*. Prepared for International Caving Study. JKMRC and Itasca Consulting, Group, Brisbane.
- Leick, A. (1990). *GPS Satellite Surveying*. New York, USA, John Wiley & Sons.
- Li, F. and R. M. Goldstein (1990). "Studies of multi-baseline space borne Interferometric Synthetic Aperture Radars." *IEEE Transactions on Geoscience and Remote Sensing* 28(1): 88-97.
- Li, Z. W., X. L. Ding, et al. (2002). Study of atmospheric effects on satellite Synthetic Aperture Radar (SAR) measurements in tropical regions FIG XXII International Congress, Washington, D.C. USA, 19-26 April 2002, International Federation of Surveyors.
-

- Lu, Z., O. Kwoun, et al. (2007). "Interferometric Synthetic Aperture Radar (InSAR): Its Past, Present and Future." *Photogrammetric engineering & Remote sensing* March 2007: 217-221.
- Maptek (2009). " Safe, accurate scanning by I-Site at La Coipa in Chile" Retrieved 30 Oct. 2009 from http://www.maptek.com/products/i-site/i-site_case_studies.html.
- Martensson, U. (2000). "Introduction to Geographical Information Systems." Retrieved 30 Oct. 2009 from http://www.lst.se/strategis/english/English_index.htm
- Massonnet, D. (1994). Giving an operational status to SAR Interferometry. ERS-1 Pilot Project Workshop. European Space Agency, Toledo, Spain.
- Massonnet, D., P. Briole, et al. (1995). "Deflation of Mount Etna monitored by space borne radar interferometry." *Nature* 375: 567-570.
- Massonnet, D. and K. L. Fiegl (1998). "Radar Interferometry and its application to changes in the Earth's surface." *Reviews of Geophysics* 36(4): 441-500.
- Massonnet, D., T. Holzer, et al. (1997). "Land subsidence caused by the East Mesa Geothermal Field, California, observed using SAR interferometry." *Geophysical Research Letters* 24: 901-904.
- Massonnet, D., M. Rossi, et al. (1993). "The displacement field of the Landers earthquake mapped by radar interferometry." *Nature* 364: 138-142.
- Melsheimer, C., W. Alpers, et al. (1996). Investigation of multifrequency/multipolarization radar signatures of rain cells, derived from SIR-C/X-SAR data. International Geoscience and Remote Sensing Symposium, Piscataway, N.J, IEEE Press.
- MSE (2007). Introduction to Longwall Mining and Subsidence, Mine Subsidence Engineering Consultants, Chatswood - NSW: 12.
- Nesbitt, A. (2003). Subsidence monitoring West Cliff Colliery Longwall 5A4. APAS (Association of Public Authority Surveyors). Wollongong, Australia, Association of Public Authority Surveyors.
- NewcrestMininigLimited. (2009). Retrieved October 14, 2009, from www.newcrest.com.au
- Numpy website. (2009). "Scipy" Retrieved 10 Dec. 2009 from <http://numpy.scipy.org>.
- Oka, N. (1998). "Application of photogrammetry to the field observation of failed slopes." *Journal of Engineering Geology* 50: 85-100.
-

Owen, K. C. (1981). Block caving at Premier Mine: Design and Operation of Caving and Sublevel Stopping Mines. New York, Society of Mining Engineering, AIME.

Ozemoy, V. M., D. R. Smith, et al. (1981). "Evaluating computerized Geographic Information Systems using decision analysis." *Interfaces* 11(5): 92-99.

Perski, Z. and D. Jura (1999). "ERS SAR Interferometry for land subsidence detection in coal mining areas" *Earth Observation Quarterly* 63: 25-29.

Perski, Z. (2003). InSAR and POLinSAR for land subsidence monitoring – a user perspective. Proceedings of POLinSAR workshop, Frascati, 6p.

Perski, Z. Hanssen, R. A. Wojcik, et al. (2009). "Insar analyses of terrain deformation near the Wieliczka salt mine, Poland" *Engineering Geology* 106(1-2): 58-67

Power, D., J. Youden, et al. (2006). InSAR applications for highway transportation projects - Publication No. FHWA-CFL/TD-06-002, US Federal Highway Administration.

Raucoules, D., C. Maisons, et al. (2003). "Accurate monitoring of slow ground deformation by ERS radar interferometry - the case of Vauvert (France) ", *Remote Sensing of Environment*, 88(4): 468–478

Rosen, P., S. Hensley, et al. (2000). "Synthetic Aperture Radar Interferometry." *Proceedings of the IEEE* 88(3): 333-382.

Rosen, P. A., S. Hensley, et al. (1996). "Surface deformation and coherence measurements of Kilauea Volcano, Hawaii, from SIR C radar interferometry." *Journal of Geophysical Research* 101 (E10) (23): 109-126.

Sandwell, D., D. Myer, et al. (2007). "Accuracy and resolution of ALOS interferometry: Vector deformation maps of the father's day intrusion at Kilauea." *IEEE Transactions on Geoscience and Remote Sensing* 46 (1): 3524-3534.

Scharroo, R., P. N. A. M. Visser, et al. (1998). "Precise orbit determination and gravity field improvement for the ERS satellites." *Journal of Geophysical Research* 103(C4): 8113-8127.

Schofield, W. and M. Breach (2007). *Engineering surveying*. Oxford, Butterworth-Heinemann.

Schreier, G. (1993). *SAR Geocoding: data and systems*. Karlsruhe, Wichmann Verlag.

Scipy website. (2009). "Scipy" Retrieved 10 Dec. 2009 from <http://www.scipy.org>.

Singh, K., N. Stussi, et al. (1997). Baseline estimation in interferometric SAR. Third ERS Symposium on Space at the service of our Environment, Florence, Italy, 14-21 March 1997, European Space Agency.

Singh, U. K., O. Stephansson, et al. (1993). "Simulation of progressive failure in Hanging-wall and footwall for mining with sublevel caving." *Transactions-Institution of Mining and Metallurgy* 102: 188-194.

Smith, T. R., S. Menon, et al. (1987). "Requirements and principals for implementation and construction of large-scale geographical information systems." *International Journal of Geographical Information Systems* 1: 13-31.

Soliman, M. (1998). *Environmental Hydrology*, CRC Press LLC.

Solomon, S. C., V. R. Baker, et al. (2003). "Plan for living on a restless planet sets NASA's solid earth agenda." *Eos, Transactions American Geophysical Union* 84(45): 485-491.

Sowter, A. (2009). "Orthorectification and interpretation of differential InSAR data over mountainous areas: A case study of the May 2008 Sichuan earthquake." accepted for publication by *International Journal of Remote Sensing*.

Stevens, N. F. and G. Wadge (2004). "Towards operational repeat-pass SAR interferometry at active volcanoes." *Natural Hazards* 33: 47-76.

Stow, R. J. and P. Wright (1997). Mining subsidence land survey by SAR interferometry. 3th ERS symposium on space at the service of our environment Florence, Italy, March 1997, European Space Agency.

Strozzi, T., P. Farina, et al. (2005). "Survey and monitoring of landslide displacements by means of L-band satellite SAR interferometry." *Landslides* 2(3): 193-201.

Thumm, M. (2009). "Historical German contributions to physics and applications of electromagnetic oscillations and waves." Retrieved 19 Oct. 2009 from <http://www.radarworld.org/history.pdf>.

Trimble website. (2009). "Products A-Z" Retrieved 30 Oct. 2009 from <http://www.trimble.com/productsaz.shtml>.

Turton, D. and D. Jonas (2003). Airborne Laser Scanning - Cost Effective Spatial Data. Map Asia Conference 2003. Kuala Lumpur, Malaysia, 13 ~ 15 October 2003: AD1.

USGS (2007). Shuttle Radar Topography Mission, 3 Arc second scenes SRTM, Global Land Cover Facility, University of Maryland, College Park, Maryland, Feb. 2000.

Villegas, T. (2008). Numerical Analyses of the Hangingwall at the Kiirunavaara Mine. Department of Civil and Environmental Engineering. Sweden, Luleå University of Technology: 109.

Wadge, G. (2003). "A strategy for the observation of volcanism on Earth from space." *Philosophical transactions - Royal Society. Mathematical, physical and engineering sciences* 361: 145-156.

Wasowski, J., F. Bovenga, et al. (2007). "Satellite Interferometry Reveals Spatial Patterns of Subsidence in the Ancient Wieliczka Salt Mine (UNESCO Heritage Site, Poland)" *Proceedings of FRINGE 2007 Workshop. 26-30 Novembre, Frascati, Italy.*

Wegmuller, U., T. Strozzi, et al. (2000). Monitoring of mining induced surface deformation in the Ruhrgebiet (Germany) with SAR interferometry. *Geoscience and Remote Sensing Symposium. IEEE International.*

Wegmuller, U., V. Spreckels, et al. (2005). Monitoring of mining induced surface deformation using L-band SAR interferometry. *Geoscience and Remote Sensing Symposium, Seoul, Korea, 25-29 July 2005, IEEE International.*

Wiley, C. A. (1965). "Pulse Doppler radar methods and apparatus" United States Patent, No. 3, 196, 436, Filed, August 1965.

Whittaker B. N. and D. J. Reddish (1989). *Subsidence: occurrence, prediction, and control.* New York, Elsevier.

Zahiri, H. and E. Baafi (2008). *Geographical Information Systems and mining impacts: A predictive methodology for mapping potential mining induces rock falls.* KG, Saarbrücken, Germany, VDM Verlag Dr. Muller Aktiengesellschaft & Co.

Zahiri, H., D. R. Palamara, et al. (2006). "A GIS-based Weights-of-Evidence model for mapping cliff instabilities associated with mine subsidence." *Environmental Geology* 51(3): 377-386.

Zebker, H. A. and R. M. Goldstein (1986). "Topographic mapping from interferometric synthetic aperture radar observations." *Journal of Geophysical Research* 91(B5): 4993-4999.

Zebker H. A., P. A. Rosen, et al. (1994). "On the derivation of coseismic displacement fields using differential radar interferometry: The Landers earthquake" *Journal of Geophysical Research* 99:19617-19634

Zebker, H. and K. Chen (2005). "Accurate Estimation of Correlation in InSAR Observations" *IEEE Geoscience and Remote Sensing Letters* 2(2):124 – 127
